The Center of Attention: the Locus Coeruleus' Role in Dopamine Dynamics

Avi Matarasso

A dissertation

submitted in partial fulfillment of the

requirements for the degree of

Doctor of Philosophy

University of Washington

2025

Reading Committee:

Michael R. Bruchas, Chair

Larry Zwiefel

Andre Berndt

Program Authorized to Offer Degree:

Bioengineering

University of Washington

Abstract

The Center of Attention: the Locus Coeruleus' Role in Dopamine Dynamics

Avi Matarasso

Chair of the Supervisory Committee:

Michael R. Bruchas

Department of Pharmacology

Arousal is essential for survival, and maladaptive arousal processing leads to inability to focus, anxiety-like behavior, and dysregulated affective states which implicate the locus coeruleus. The locus coeruleus (LC) is a major source of norepinephrine (NE) in the brain that projects to distinct brain regions which modularly influence arousal, anxiety, learning, and exploration, among other behavioral states. Recent timely studies have implicated dopamine (DA) as also co-released from the LC, yet definitive measures of release across regions, stimulus paradigms, and behaviors typically associated with the LC-NE system remain controversial.

In this thesis, I utilize recently developed tools to establish catecholamine dynamics and more specifically the boundaries of LC-DA release, in appetitive and aversive behaviors. In **Chapter 1**, I review the current understanding of LC-evoked DA

release and NE and DA release downstream of LC in a variety of behaviors. Next, I characterize the limitations of modern neuromodulator detection tools (**Chapter 2**). In **Chapter 3**, I establish baseline NE and DA dynamics in response to a variety of aversive, appetitive, and neutral stimuli in basolateral amygdala (BLA) and hippocampus (CA1). In **Chapter 4**, I address limitations in the biosensors used in detection of catecholamines. Then, I characterize evoked dopamine from LC terminals in CA1 and BLA. Lastly, I demonstrate that the LC releases DA during aversive and appetitive stimuli. In **Chapter 5**, I discuss the findings of this thesis in relationship with existing literature and outline future work that would meaningfully build on my dissertation work. My dissertation work expands our understanding of the LC's role in releasing DA and provides context for how maladaptive LC activity may affect DA signaling in aversive and appetitive conditions.

Table of Contents

Acknowledgements

The past 6 years completing this work have been some of the most exciting, frustrating, tiring, rewarding years of my life. Between the pandemic, personal hardship, and housing instability, there were moments where I was truly unsure how I was going to get through graduate school. I found my vulnerability was always met with support, understanding, and care. I will always appreciate those moments.

This dissertation work would not be possible without the personalized mentorship and support of the lab and especially Dr. Michael Bruchas. Michael's uncompromising passion and excitement for this work reinvigorated me when I hit dead ends, and his insight and endless ideas always encouraged me to find solutions to technical problems. I will always remember and appreciate Michael's niche interests that surprised me, such as Ecuadorian dark chocolate or the pepperoni that curls up when cooked in hot pizza ovens.

I would also like to thank Dr. Sean Piantadosi for his mentorship and friendship. His contributions to experimental design and conceptual background were essential in completing this work. His enthusiasm and patience really helped me through the challenging days in completing this work.

I am so thankful for Elena Seaholm, Itzel Rodriguez Reyes, and Ashritha Cheeyandira who propelled this work forward, drove me crazy with their antics, and made graduate school fun for me. I have deeply enjoyed mentoring (and sometimes therapizing) them and learning from them as a mentor. A special shout out to my unofficial mentee Cat Zamorano who really helped me feel back at home in South Florida in gloomy Seattle.

This work would have been impossible without the help of my lab manager Dr. Azra Suko, who would always chat over a cup of espresso and made sure viruses were ready when we needed them. Lab technicians were essential throughout this work in ensuring our mouse colony was in order and animals were ready for experiments. I'm so grateful for Taylor Hobbs, Carina Pizzano, Akshay Rana, Valerie Lau, and Bailey Wells.

Each member of the Bruchas lab has deeply impact on me. Each postdoc in the lab has been extremely helpful in designing experiments, interpreting data, reassuring me in critical moments, and being excited about new data I showed along the way. A special thank you to my dear friends and fellow Bruchas lab cohort members Carrie Stine and Anthony English. I'm so glad we went through grad school together. Thanks to Dr. Kasey Girven for being the best benchmate and friend. I feel extremely lucky for learning from and working with you all. I could not have asked for a better work environment, and my standards for coworkers are now impossible because of you all.

I want to also thank Michael Rappleye, Guangfu Wu, and Yue Cao, who were contributors to the content in Chapter 2. Michael developed μMASS and dMASS sensors the mentorship of Dr. Andre Berndt. Guangfu developed the aptamer-gFet aptamer devices and Yue spearheaded the PDMS component of the project.

Thank you to my thesis committee, Drs. Larry Zwiefel, Sheri Mizumori, Andre Berndt, and Azadeh Yazdan for the discussion, feedback, and guidance which have all bolstered the strength of this work.

I would not be where I am today without my first lab experiences which piqued my interest in developing my own project. Thank you to Drs. Kevin Otto, Hong Gan, and Janis Daly, as well as the supportive mentors and labmates in each of these experiences.

I will always appreciate my parents for the hard work they put in to ensure I could be successful. Thank you to my dad for showing me how we can use humor to get through hardship, and to my mom for showing me care is not mutually exclusive from being a hard worker. I appreciate you both for instilling in me the values that I live by. I'm glad I was able to become a doctor like you all wanted!

I am so thankful for the friends I have made during this time, and they were also crucial in helping me through this time. Will, you are an icon and an inspiration for me, and I'm so glad we found each other when we did. Carina, my fashion consultant, I seriously don't know how I would have made it through the instability without your support. Jonathan, thank you for the nights cooking and cracking each other up. To Diana, I'm glad I found another loud and warm Floridian. Thank you for your patience and sweetness and for helping me get through these last few months. I am so thankful for my small community of stable geniuses I have kept in touch with from UF. Angela, Kierstin, and Ryan, thank you for reminding me who I am through the years.

To the dancefloors and the friends I made, the catharsis I found through you has been a source of joy and freedom I needed to make it through this time. Leon, Dom, Karina, Nat, Mika, Shareef, Jordan, and so many more, I have loved to dance and frolic the early morning existential planes with you all.

Chapter 1. Introduction

1.1 Maladaptive attention processing in the 21st century

Arousal and attention are essential for our survival. When we walk through the beautiful old growth forests in the Pacific Northwest, and we stumble across a bear walking, our attention is piqued. We are focused on the bear and how it is behaving, the direction it's moving, and what we may have to do to survive. We are thinking back to old stories we have been told in Boy scouts, or on camping trips with friends. In preparation for confrontation, we may think, "Is that bear black or brown? Does the color even represent how they look? Do I yell and get big or do I run?" Prey animals possess instincts that mirror these thoughts. When you stumble upon a rabbit in the residential streets of Seattle, they will often stop as you get closer, frozen in fear and determining how they should respond.

To survive in a dangerous environment, an individual must be able to act flexibly and in a goal-directed manner (Barrett et al., 2004; Engle, 2002). Their responsive actions depend on available attention and executive control. Impaired attention would force us to be more reactive to environmental stimuli, and not as goal-directed in our response. But what happens when we are under environmental duress? When individuals are exposed to stress-inducing situations, one study found they perform significantly worse on tests of controlled attention for three days. Selective and sustained attention were diminished in the survival environment after exposure to environmental duress (Leach & Ansell, 2008). What happens when individuals inadvertently expose themselves to environmental duress multiple times every day through social media?

In the past 30 years, technological developments have captivated people around the world and completely changed how humans direct our attention. Modern platforms like Tik-Tok and Instagram serve as alternative news sources with no filters. The public is exposed to a nonstop flow of information including raw images and videos of atrocities around the world, such as the merciless genocide in Gaza, police brutality in U.S. cities, or the realities of a mass pandemic killing over a million people in the US alone. Whether users seek out this content to stay informed or it is simply suggested to them via social media, individuals may be inadvertently traumatizing themselves. One *in silico* study suggested that media exposure to mass traumatic events can increase PTSD prevalence in a community (Abdalla et al., 2021), and growing internet addiction may exacerbate the effect of traumatic events inducing PTSD (Cheng & Li, 2014).

In 2016, media consumption researchers found that people were spending six and a half hours online per day, with two and a half hours spent on mobile devices (*Digital vs Traditional Media Consumption*, n.d.). Most of that time, around 2 hours per day, was spent on social networks and services, around two hours per day, and this time increased by 34 minutes from 2012 to 2016. Social network use in the U.S. and Europe has a negative correlation with academic performance (measured by grade point average) (Barton et al., 2021; Jacobsen & Forste, 2011; Karpinski et al., 2013). On top of this time using social media, people watch television for two hours per day and are using a second screen while they are watching television. This trend increased drastically from 2012 to 2016 – up from 47% to 65% of people reporting second-screen behavior. The worsening of internet addiction and divided attention forebodes a young generation condemned to

dysregulation of controlled attention, seeking to escape the real world, and only finding more trauma online.

As many people in 2025 worry about the rising threat of federal funding cuts, economic instability, and overt fascism on our ability to work and live, the feedback loop of maladaptive attention processing to negative news may become a trap of anxiety and doom. Across the nation, people must strive to build the networks and skills to meet the needs of our communities and not live in trauma. We should not be reactive; we need to build systems that allow us to act flexibly and in a goal-directed manner, together against oppressive systems. Are we doomed to be frozen in fear, like a rabbit in the streets, or will we get big and yell back at the bear in front of us?

1.2 Locus Coeruleus and Ventral Tegmental Area

A more recent social media trend is the “dopamine detox,” or abstaining from social media use and other stimuli that bring us instant gratification. While this oversimplifies the complexity of neural circuits involved in reward and attention, this trend aims to mitigate maladaptive processing of reward through delayed gratification and regulated attention.

Norepinephrine (NE) and dopamine (DA) are two neuromodulators critically involved in regulating attention and reward processing. In the central nervous system, norepinephrine is primarily sourced from a small nucleus called the locus coeruleus (LC) (Aston-Jones & Cohen, 2005; Poe et al., 2020). The LC is activated by stress and stress-related neuropeptides (Itoi & Sugimoto, 2010; McCall, n.d.; Poe et al., 2020). Quick bursts of LC activity, known as phasic firing, are associated with high arousal (Sara & Bouret, 2012) and attention and heighten performance in tasks (Aston-Jones & Cohen, 2005).

The LC also exhibits phasic firing in response to salient aversive stimuli (Chen & Sara, 2007a; Hirata & Aston-Jones, 1994). Typical LC noradrenergic (LC-NE) neuron firing rates are 5-10 Hz during high arousal states like stress, although phasic bursts of 2-3 spikes can occur at up to 20 Hz (Devilbiss & Waterhouse, 2011a). Slower, sustained firing of LC neurons is known as tonic firing, and is associated with stress and prolonged engagement in higher attention tasks and occurs at 3 – 5 Hz (Devilbiss & Waterhouse, 2011a; Grimm et al., 2024; McCall, n.d.-a). At lower arousal states like sleep, the LC is typically firing at 1-3hz. Tonic firing of LC neurons leading to NE release is adaptive for stressful situations and cognitive flexibility, but chronic exposure to stress may lead to dysfunctional neuromodulator release (Curtis et al., 2012; Itoi & Sugimoto, 2010; McCall, n.d.-a; McCall et al., 2017a).

The LC projects bilaterally to the major source of DA in the brain, the ventral tegmental area (VTA) (Deutch et al., 1986; Guiard et al., 2008; Mejias-Aponte et al., 2009). The VTA also has long and influential projections throughout the brain. VTA neurons have much heterogeneity compared to LC, with about twice as many DA neurons as glutamatergic neurons and GABA-ergic interneurons (Grace & Onn, 1989; Kauer, 2004). DA neurons in VTA have long been accepted as implicated in reward and valence, although some reports also suggest their activity is more correlated to salient stimuli than positive valence (Kutlu et al., 2021). VTA-DA neurons typically fire around 4-6hz, while VTA-GABA neuron activity is around 10 hz (Cohen et al., 2012; Steffensen et al., 1998). During punishment, GABAergic neurons will increase activity, spiking as high as 60hz, decreasing DA neuron activity to a lower firing rate. During reward, dopamine neurons fire as high as 15 hz, and GABAergic neurons fire at around 60 hz. Chronic use of

addictive substances can alter reward processing in the VTA (Kauer, 2004). The LC-NE system has been shown to also be altered in long-term use of addictive substances (Nestler & Aghajanian, 1997). Dysfunction of the LC-NE system has also been characteristic of many neuropsychiatric disorders such as anxiety, ADHD, PTSD, Alzheimer's disease, and Parkinson's disease (Poe et al., 2020).

1.3 Noradrenergic receptors

LC-NE terminals are often either synaptic apposition surrounded by glia or close to synapses (Liprando et al., 2004). Because of a lack of gap junctions, LC-NE terminals release neuromodulators outside of the synaptic cleft through volume transmission, and so most NE travels through extracellular fluid to reach post-synaptic cells. Perisynaptic GABAergic and glutamatergic terminals are also regulated through adrenoceptors (Mejias-Aponte, 2016). There are several subtypes of adrenoceptors that have different functions depending on their locations. For the purposes of this review, we will simplify receptor functions based on their relationship with relevant monoamine neurons.

All noradrenergic receptors are part of a class of proteins called G protein-coupled receptors (GPCRs), which are membrane-bound and transduce extracellular chemicals into neural activity (Christopoulos, 2002; Rosenbaum et al., 2009). α_1 adrenoceptors couple with G_q proteins, which activate phospholipase C and in turn increase IP3 and DAG concentration. The IP3 leads to calcium release from the endoplasmic reticulum. This G_q protein cascade is predominantly excitatory, but can be inhibitory when α_1 is expressed presynaptically through a protein kinase C signaling pathway (Mouradian et al., 1991). β adrenoceptors couple often with G_s proteins, which convert ATP to cAMP

and initiate an excitatory effect on neurons, and β_2 receptors may also couple to G_i proteins (Barnes, 1995; Perez, 2020). α_2 adrenoreceptors, on the other hand, couple with G_i proteins and are predominantly pre-synaptic. G_i initiates an inhibitory cascade through downregulation of cAMP (Perez, 2020). α_2 adrenoreceptors are often pre-synaptic autoreceptors, which modulate activity of the pre-synaptic neuron when NE levels are too high in the synapse (Devilbiss & Waterhouse, 2000).

Adrenoceptors modulate noradrenergic signaling but are also located on other types of neurons and affect their activity. In-situ hybridization (ISH) has revealed α-1b, but not β nor α_2, was detected in VTA, with 2-fold higher expression in VTA than in substantia nigra (SN) (Greene et al., 2005; Nicholas et al., 1993b, 1993a). Although ISH data suggest only α_1 adrenoceptors were present in VTA, autoradiography suggests that the LC has 3x as many α_2 binding sites as VTA (Boyajian & Loughlin, 1987). Immunohistochemistry has revealed some expression of α_2 in SN and VTA, and minimal expression on DA neurons in SN (4%) and slightly more in VTA (14%) (Rosin et al., 1993). These studies suggest the dopaminergic system has some variety of adrenoceptors on its neurons and implies the LC may modulate VTA-DA neurons.

1.4 Lesions and genetic knockouts effect on dopamine release

The rate limiting step in producing NE in LC neurons occurs before DA is synthesized. Tyrosine hydroxylase synthesizes DOPA from Tyrosine, and this step is the rate-limiting step in synthesizing NE (Udenfriend & Dairman, 1971). DOPA is converted to DA in the presence of DOPA decarboxylase, and dopamine beta hydroxylase (Dbh) catalyzes NE synthesis from DA. Because the enzyme Dbh is readily accessible in

noradrenergic neurons, and localized in vesicles, somata, and proximal processes of neurons in the LC (Brimijoin, 1974; Cimarusti et al., 1979a), it has previously been assumed that no DA is stored or released from LC terminals. Here, I will highlight previous studies showing noradrenergic induction of DA release.

LC and VTA lesions have helped reveal the influence of neuromodulator sources on other regions in the brain as well as neuromodulator release. Selective lesioning of LC increases VTA-DA neuron activity, and VTA-DA neuron lesioning increases LC-NE neuron activity(Grenhoff et al., 1993; Guiard, El Mansari, & Blier, 2008), which supports old data suggesting there are LC-VTA bilateral projections (Deutch et al., 1986; Mejias-Aponte et al., 2009). Downstream of LC, lesions (6-OHDA, DSP-4) decrease basal, nomifensine, and amphetamine-induced DA release in nucleus accumbens (NAc), mPFC, and CN (Lategan et al., 1990, 1992; Masana et al., 2011). LC lesioning also decreased DA release induced by nomifensine, a dopamine reuptake inhibitor, in mPFC (Masana et al., 2011).

In contrast to these studies, another study showed dorsal noradrenergic bundle (dNAB, which includes the LC) 6-OHDA lesions did not decrease DA dialysate in OCC and parietal cortex, but these lesions did abolish reboxetine-induced increases in DA release and did increase DA in mPFC (Valentini et al., 2004). As reboxetine is a norepinephrine reuptake inhibitor, this suggests that dNAB might not release DA across all projections, but NET in dNAB neurons might be clearing DA from the synapse. Similarly, in the hippocampus, some studies have found that noradrenergic lesioning decreased NE, but not DA (Guiard et al., 2008; Lategan et al., 1992), while another found both NE and DA are decreased significantly (Kempadoo et al., 2016a).

Genetic manipulations have less often been employed in understanding the effect of *Dbh* on DA release. When *Dbh* is knocked out, there are significantly fewer basal DA levels in NAc, Caudate Putamen (CP), but not PFC (Schank et al., 2006), which could also be due to intact 'noradrenergic' fibers without Dbh maintaining DA in PFC through NET or some other mechanism. This explanation would not discount other studies showing a decrease in DA levels in PFC when LC fibers are lesioned (Devoto et al., 2005; Lategan et al., 1990, 1992; Valentini et al., 2004). The decrease in basal DA in NAc and CP is contrary to the hypothesis that NE neurons provide a general inhibition of VTA-DA neurons, but perhaps local 'noradrenergic' DA released after ablation of *Dbh* provides some inhibition of VTA-DA output in CP and NAc. Generally, loss of noradrenergic signaling seems to increase VTA signaling through disinhibition of VTA-DA neurons, potentially through less NE influence on VTA-GABA interneurons.

1.5 Noradrenergic receptors mediate DA release

While electrical stimulation and lesions of LC and DBH may reveal necessity of LC in DA release, receptor pharmacology may demonstrate sufficiency in eliciting DA release from noradrenergic GPCR signaling. As mentioned in the previous section, GPCR cascades affect neural activity. Past studies used GPCR signaling to understand neural circuit function through pharmacology mediation of neuromodulator release. One region of focus for noradrenergic sourced dopamine has been in the cortex. For example, D2 antagonism increased DA and NE in prefrontal cortex (PFC), but not in occipital cortex (OCC), implying there is less detectable dopaminergic innervation in OCC (Devoto et al., 2004). Because there is less DA innervation in OCC and an α_2 antagonist increased both

DA and NE, α_2 receptors sufficiently regulate release of noradrenergic sourced dopamine (Devoto et al., 2003, 2005).

Although clonidine (locally and systemically injected, α_2 agonist) reduced NE and DA levels in mPFC, mice with noradrenergic lesioning had no change in DA levels, displaying the necessity of α_2 in regulating noradrenergic DA release (Devoto et al., 2005, 2019). NET reuptake inhibitor and α_2 antagonist each increased DA levels, but had no effect when noradrenergic fibers were denervated, and together they increased basal NE levels by 2100% and DA by 600%, which was much more than either alone (Devoto et al., 2019). Taken together, these data suggest that α_2 autoreceptors mediate the release of noradrenergic DA from NET in mPFC.

While these pharmacology experiments suggest noradrenergic fibers could be a source of DA, the experiments do not have a combination of projection-specific manipulations and strong enough temporal resolution to determine the direct source of DA. Perhaps LC-NE neurons are upregulating DA through other circuit mechanisms involving DA neurons.

In the hippocampus, specifically CA1, several studies have explored NET's potential to release DA. NET inhibitor and α_2 antagonist, but not D_2 antagonist, increased DA levels in hippocampus(Borgkvist et al., 2011; Valentini et al., 2004). In dorsal CA1, D_1-dependent amphetamine enhancement of glutamate signal is blocked by loss of TH in LC, but not by loss of TH in VTA. This effect is also blocked by NET inhibition, but not by DAT inhibition, and can be rescued by application of D_1 agonist implying that NET is required for the D_1-dependent response (Smith & Greene, 2012a). The authors proposed that amphetamine causes dysfunction of VMAT2 and MAO production, leading to NET

reverse transport of DA to the synapse. All these studies support the hypothesis that noradrenergic neurons in CA1 release DA through NET.

1.6 The Locus Coeruleus' role in DA release

Given the modular nature of LC activation and that the LC is activated differentially in response to salient stimuli and anxiogenic processing, aversive stimuli, and during appetitive behaviors (Borodovitsyna et al., 2018a; Chandler et al., 2019a; Chen & Sara, 2007b; Curtis et al., 2012; de Medeiros et al., 2005a; McCall et al., 2017a; Poe et al., 2020; Silveira et al., 1993a; Uematsu et al., 2017a), understanding DA release from LC requires examining multiple brain regions with distinct functional roles. We can use the differential activation across regions during aversive and appetitive behaviors to explore the roles of DA and NE in these regions, and the relationship that the LC specifically has in DA release in these regions.

A region well known for its role in processing aversive and appetitive stimuli is the amygdala. Early research into the amygdala recognized its role in emotion, as ablating the amygdala led to tameness and extinction of conditioned avoidance (Weiskrantz, 1956). The amygdala is most known for its involvement in fear learning and implicit emotional memory (Davis & Whalen, 2001; Phelps & LeDoux, 2005). In these types of seminal conditioned fear studies, animals were exposed to a neutral conditioned stimulus, often a tone, with an aversive unconditioned stimulus (US), a shock. In the BLA, associations are formed between the unconditioned stimulus and the environment in which the animal experiences the US (Davis & Whalen, 2001; Fanselow & LeDoux, 1999; Kapp et al., 1992; Maren, 2001; Walker & Davis, 2002). Our lab has previously found

tonic optical stimulation of LC terminals in BLA to be necessary and sufficient in producing anxiety-like behavior (Llorca-Torralba et al., 2019a; McCall et al., 2017a). While it was originally believed that LC stimulation and exposure to footshock inhibit BLA neurons (Chen & Sara, 2007b), our lab also found through multi-unit recording that some BLA cells are inhibited and some excited by LC stimulation (McCall et al., 2017a, p. 20).

There is a dearth of studies on LC release of DA in BLA, but there are many studies on the LC-NE and VTA-DA systems' role in BLA. Both LC and VTA have strong projections to BLA (McCall et al., 2017a; W. Tang et al., 2020). The DAergic system is involved in fear processing and reward seeking in BLA, so it is likely also contributing DA while LC is active during these same processes. VTA-BLA projections are excited by salient stimuli and regulate fear extinction (de Oliveira et al., 2011; Oliveira et al., 2009; Shi et al., 2017; W. Tang et al., 2020). While LC-BLA activation increases anxiety-like behavior, VTA-BLA activation is sufficient for decreasing anxiety-like behavior (Morel et al., 2022).

Another region that LC and VTA activity affects is the hippocampus. While primarily releasing NE, more recent studies have suggested LC-sourced DA plays a role in learning and memory in hippocampus, independent of the VTA (Kempadoo et al., 2016b; Smith & Greene, 2012b; Takeuchi et al., 2016a). The dorsal hippocampus (dCA1) is typically involved in spatial processing and contextual learning (de Lavilléon et al., 2015; Dupret et al., 2010a; Gasbarri et al., 1996; Kentros et al., 2004). There are dense noradrenergic fiber projections in the dorsal hippocampus, specifically CA1, but there is much less dopaminergic innervation (Broussard et al., 2016; Gálvez-Márquez et al., 2022; Kempadoo et al., 2016a; Takeuchi et al., 2016b; Tsetsenis et al., 2021).

Because dorsal hippocampus-dependent memory persistence is mediated by D_1Rs (Bethus et al., 2010; O'Carroll et al., 2006), it was assumed that the VTA had strong projections to the hippocampus (Bethus et al., 2010; Gasbarri et al., 1996; Lisman & Grace, 2005a). Despite this, CA1 has weak VTA-DA innervation (J. Tang & Dani, 2009), and further evidence that midbrain dopamine has significant effects on hippocampal synaptic plasticity, memory, and learning (Broussard et al., 2016; Kempadoo et al., 2016b; McNamara et al., 2014; Rossato et al., 2009; Smith & Greene, 2012b; J. Tang & Dani, 2009). Data from recent studies suggest that DA in the VTA to CA1 circuit regulates persisting contextual memory (Broussard et al., 2016b; Lisman & Grace, 2005a) and learning (Sayegh et al., 2024; Tsetsenis et al., 2021), independent of LC. But other studies suggest that dense LC-CA1 innervations mediate DA release that is sufficient to enhance novelty-associated spatial learning (Gálvez-Márquez et al., 2022; Kempadoo et al., 2016; Takeuchi et al., 2016). The LC-CA1 studies relied on supraphysiological optogenetic LC stimulation to show that DA is released from LC terminals. Particularly, pharmacological blockade of behavioral effects have been shown at high concentrations of D_1 and β antagonists, and D_1-β heteromers have been found to form in HEK cells (Kobayashi et al., 2022), causing concern for how these allosteric modulatory effects might be involved in these behaviors.

More recent studies show a decrease in DA release while inhibiting the LC (Gálvez-Márquez et al., 2022), and another shows DA release in response to chemogenetic activation of LC (Wilmot et al., 2024). These studies, while helpful in understanding LC-evoked release of DA, do not account for potential release of DA from LC at subsecond resolution, and do not clearly establish the LC's necessity in releasing

DA in natural behavior or in response to stimuli. Thus, there remains substantial controversy over the multiple sources of DA in dCA1 and what physiological conditions regulate this release.

1.7 Genetically-encoded neural indicators

Data described above suggest noradrenergic receptors and the LC play a role in DA release. Most of these experiments use pharmacology to affect GPCR activity and elicit the release of DA. In combination with chemical lesions and behavior, microdialysis data reveal the potential for noradrenergic sourced DA release. These data do not preclude the influence of other neural circuits, especially at the longer time-scales that microdialysis requires for sample collection and detection. Further, systemic injection of pharmacological agents has effects throughout the brain. Fast scanning cyclic voltammetry provided an alternative with high temporal resolution, but not strong enough selectivity to detect norepinephrine and dopamine separately without pharmacological intervention (Park et al., 2009, 2010). In order to adequately isolate the release of DA from the LC in response to stimuli or behavior, the sensing technique must meet specific criteria:

1. Adequate selectivity of DA over NE
2. Subsecond temporal resolution
3. Cell-type or Projection-specific manipulations

Whether DA can be released under physiological conditions was difficult to investigate with the tools of the time. With the advent of genetically encoded neural indicators such as GRABNE and dLight (Feng et al., 2019a; Patriarchi et al., 2018a), we

can detect dopamine with greater selectivity than voltammetry, at subsecond temporal resolution, which was not possible with microdialysis, and following projection-specific manipulations. In the next chapter, I will elaborate more on these tools, and my contribution to characterizing their functionality.

Chapter 2: Technology development for sensing neuromodulators

2.1 Introduction

Neuromodulators play a crucial role in behavior, affect, and plasticity. Understanding these chemicals' involvement in behavior requires accurate and precise detection with high spatial and temporal resolution. While technologies to detect these neuromodulators have existed since the early 20th century, they have increasingly advanced in their temporal and spatial resolution. In the previous section preceding I described recently developed biosensors. In this introduction, I will introduce the tools that preceded these sensors and their limitations.

In the 1980s, HPLC started being used for neurotransmitter detection in tissue samples. HPLC is very selective in detecting neurotransmitters, but lacks the temporal specificity that many of the other tools we have access to, on the range of several minutes to over ten minutes (Guiard & Gotti, 2024). Because dialysate takes time to collect, HPLC is less useful for neurotransmitter detection during behavior, but it has been used to detect the presence of neuromodulators in tissue evoked by pharmacology and, more recently, optogenetics (Kempadoo et al., 2016a). Microdialysis was established in 1960s. Microdialysis probes separate perfusion media from tissue using porous membranes for selective diffusion of neuromodulators. One advantage of microdialysis is that this technique can detect electrically inactive transmitters (Z. Wu et al., 2022). Microdialysis when paired with high performance liquid chromatography (HPLC) detects exact concentrations of both exogenous substances and endogenous molecules. Microdialysis suffers from low temporal resolution, on the timescale of tens of minutes for collecting samples, with some cutting edge studies getting collection as low as 1 minute (Gu et al.,

2015). Dialysate collection is limited by low spatial resolution as well, with probes being as small as 100 μm in diameter. Implanting microdialysis probes is invasive, and can lead to gliosis in immune response (Z. Wu et al., 2022). Another shortfall of microdialysis is that neuropeptides, which are much smaller than other neuromodulators and have strong effects on behavior and neural circuits, have much lower yield (<5%) in detection (Wotjak et al., 2008).

Another commonly used technique introduced in 1976 is fast-scanning cyclic voltammetry (FSCV), which is used for measuring electrically-active chemicals in tissues (Adams, 1976). Cyclic high voltage ramps (100 V/s) scan the surface of a carbon-paste electrode to oxidize and reduce electroactive chemicals. Detected peaks in current are characteristic of specific molecular analytes. FSCV is less invasive than microdialysis – probes are less than 10 μm in diameter (Z. Wu et al., 2022), and have much better temporal resolution than microdialysis, sampling in the subsecond range. While there are some advantages, FSCV cannot distinguish structurally similar molecules with similar electrochemical properties, which is crucial for some neuromodulators like norepinephrine and dopamine (Z. Wu et al., 2022).

As previously mentioned, norepinephrine and dopamine act on GPCRs. Recently developed genetically-encoded neural indicators have risen to prominence for neuromodulator detection due to their advantages over previous detection techniques. These sensors were developed by modifying GPCRs to include a fluorescent protein bound to the intracellular loops of the receptor, expressed in either a pan-neuronal or cell-type specific manner. When the targeted ligand binds to the modified receptor, the GPCR undergoes a conformational change leading to a positive change in fluorescence. These

sensors have been optimized so that the change in fluorescence is strong enough to be detected via optical fiber while maintaining a strong enough affinity at the receptor level for binding the target molecule (Feng et al., 2019a; Patriarchi et al., 2018a; Z. Wu et al., 2022). While these sensors have relatively high selectivity and cell-type specificity, they are limited in their kinetics depending on the sensor and ligand, often in the sub-second range (Z. Wu et al., 2022). Characterization of these sensors has been limited to HEK cells and cultured neurons (Feng et al., 2019a, 2024; Patriarchi et al., 2018a). Some properties of the sensors I will use in this chapter are enumerated in **Table 2.1**.

Another method of neuromodulator monitoring is using aptamer-based technology. Aptamers are sequences of nucleic acids that selectively bind target molecules. Coupled with microtransistors, aptamers hold promise as a highly selective option for neurochemical monitoring (Dhiman et al., 2017). Recent studies have shown the potential for serotonin monitoring *in vivo* with aptamer-based probes (Zhao et al., 2021). With future developments to minimize impedance and increasing stability, aptamer-based probes have strong potential for multiplexed, chronic *in vivo* detection of neuromodulators. In collaboration with the Zhang lab, we have characterized graphene microtransistors with aptamers to detect dopamine. Graphene has a high carrier mobility and shows promise in chronic implantation due to biocompatibility and chemical inertness (Gao et al., 2016; *Sensing at the Surface of Graphene Field‐Effect Transistors - Fu - 2017 - Advanced Materials - Wiley Online Library*, n.d.).

In this chapter, I test and characterize several new sensors and neuromodulator detection systems in collaboration with bioengineers. I expand on previous characterization of these sensors by looking at their expression and functionality under 2-

photon imaging. These experiments provide a foundation to understand how these sensors work *in vivo* under more controlled conditions. I also look at the immune response to chronic aptamer probe implantation as well as the differences along the depth of the implantation with and without a protective polymer coating. I characterize recently developed sensors in *ex vivo* slice experiments, with concentration response curves of ligands of interest for each sensor.

2.2 Methods

2.2.1 Animals

Adult (20-35 g) male or female DBH-Cre or TH-Cre mice and Cre (-) littermate control mice were used for in vivo experiments after backcrossing to C57BL/6J mice for at least 10 generations. Mice were group housed, given access to food pellets and water ad libitum, and maintained on a 12:12-hour dark/light cycle (lights off at 7:00 a.m.). Animals were held in a sound attenuated holding room facility in the lab starting at least one week prior to surgery, as well as post-surgery and throughout the duration of behavioral assays to minimize stress from transportation and disruption from foot traffic. All mice were handled and, where appropriate, connected to fiber optics two times a day for one week prior to behavioral experimental testing. All experimental procedures were approved by the Animal Care and Use Committee of Washington University and the Animal Care and Use Committee of University of Washington and conformed to NIH guidelines.

2.2.2 Stereotaxic surgery

Surgeries were performed under 2% isoflurane anesthesia (Piramal Healthcare, Maharashtra, India). All injections in NAc and dCA1 were performed using a Hamilton blunt syringe (Reno, NV). For concentration response curves, 500nL of AAV5-ef1a-dMASS (designed by Drs. Michael Rappleye and Andre Berndt, prepared by Dr. Azra Suko, Seattle, WA) were injected with a Hamilton blunt syringe (Reno, NV) into the dCA1 (AP: 1.9, ML: -1.4, DV: -1.65) of Dbh-cre mice, or a mixture of 500nL of AAV5-ef1a-μMASS (designed by Drs. Michael Rappleye and Andre Berndt, prepared by Dr. Azra Suko, Seattle, WA) and AAV5-hSyn-DIO-ChrimsonR-tdtmto was injected into the NAc of *Penk*-cre mice (coordinates in mm: AP + 1.34, ML 1.10, DV:-4.3). After injections, fiber optic ferrules (Doric) were chronically implanted above either the BLA, dCA1, and vCA1, and dental cement (Lang Dental, Wheeling, IL) or C&B Metabond were used to secure the implants. Mice were allowed to recover and viruses to express for a minimum of 5 weeks. For detecting NE and DA dynamics in *ex-vivo* slice experiments, Dbh-cre mice were injected with 500-700nL of GRABNE or GRABDA into dorsal CA1 (AP: 1.9, ML: -1.4, DV: -1.65).

2.2.3 GFET devices and Immunohistochemistry

Aptamer-gFET devices (about 390 μm wide, 77 μm thick; prepared by Zhang lab, University of Connecticut) were implanted in the dorsal striatum (ML: 2.0, AP: 0, DV: -5.0) of mice for 1 and 6 weeks (**Fig. 2.1A**). To determine the immune response to the implanted devices, we stained tissue at both time points for astrocytes and activated microglia. We used consistent confocal microscope settings to quantify the immune

response for astrocytes and microglia at the 1 week time point and at the 6 week time point. A region of interest (ROI) analysis was done in the imaging analysis software Fiji. First, an ROI was drawn around the device. The intensity of the immune response was recorded in 10 μm increments from the device.

For polydimethylsiloxane (PDMS) coated devices, the Zhang lab prepared the gFET samples with and without PDMS coating. Devices were implanted for 24 hours, and then tissue was extracted and sliced axially in preparation for immunohistochemistry. To determine the immune response to the implanted devices, we stained tissue at both time points for astrocytes and activated microglia. The primary antibodies used were anti-GFAP guinea pig (SySy, 1:500 dilution) and anti-Iba1 rabbit (Abcam, 1:500 dilution), and the secondary antibodies used were Alexa Fluor 555 goat anti-guinea pig (Life Technologies, 1:1000 dilution) and AlexaFluor 488 goat anti-rabbit (Invitrogen, 1:1000 dilution). We used the same confocal microscope settings to determine how the immune response for astrocytes and microglia changed at the 1-week time point compared to the 6-week time point. All procedures were approved by the Animal Care and Use Committee of the University of Washington and conformed to US National Institutes of Health guidelines.

2.2.4 Ex vivo slice preparation

Mice were briefly anesthetized with isofluorane. Mice were perfused with cold N-methyl-d-glucamine (NMDG)–substituted artificial cerebrospinal fluid (aCSF) containing 93 mM NMDG, 2.5 mM KCl, 1.25 mM NaH2PO4, 30 mM NaHCO3, 20 mM Hepes, 25 mM glucose, 5 mM ascorbic acid, 2 mM thiourea, 3 mM Na-pyruvate, 12 mM N-acetyl-l-

cysteine, 10 mM MgSO4, and 0.5 mM CaCl2. After perfusion, brains were extracted. Coronal sections of the hippocampus were cut to a slice thickness of 250 μm using a vibrating Leica VT1000S microtome in a bath of cold, oxygenated NMDG solution. The slices were then placed in hot NMDG aCSF solution (32-34 degrees C) for 10min. Then slices were placed in a room temperature holding chamber filled with HEPES solution consisting of: 92 mM NaCl, 2.5 mM KCl, 1.2 mM NaH2PO4, 30 mM NaHCO3, 20 mM Hepes, 25 mM glucose, 2 mM CaCl2, 2 mM MgCl2 (pH adjusted to 7.3 to 7.4 with NaOH). The samples were kept in the HEPES solution for at least 30min prior to 2-photon imaging, and were covered to minimize photobleaching. For both HEPES and NMDG osmolality was confirmed to be between 300-310 mOsm/kg, and pH was confirmed to be between 7.3-7.4.

2.2.5 2-photon slice imaging, optogenetic stimulation, and pharmacology

Flow rate of ACSF or drug was maintained at 2mL/min. Temperature of flowing ACSF was controlled at 31-34°C by the temperature controller TC-324C before any slice was added to the bath. An anchor was used to keep the brain slice stable while ACSF or ACSF and drug was washed on. A vacuum pump ensured a steady 2mL/s of flow. An Olympus 4x UPlanFL N lens was used to localize expression, and then an Olympus 20x XLPLN25XWMP lens 2mm working distance for water immersion, and we acquired images with Olympus FV31S-SW software. The 2-photon scope used was an FVMPE-RS Olympus 2p scope powered by a Mai Tai Ti-sapphire laser with dispersion compensation running at 920nm. Individual frames were acquired at 0.92hz using a Galvano scanner with a resolution of 512px x 512px.

For optogenetic stimulation of brain slices, a red LED (615 nm, CoolLED) controlled by a master-9 stimulator was programmed for either 5hz or 20hz stimulation for 3s or 30s. All opioid ligands were prepared with thiorphan (1 μM) and bestatin (10 μM) to minimize peptide degradation. Solutions were oxygenated for at least 5min prior to slices being placed in the apparatus.

2.2.6 Region of Interest analysis of 2-photon imaging sessions

For all analysis of 2-photon imaging sessions, I created a custom code for analyzing ROIs in 2-photon imaging files. First, the user draws a mask for each session where the slice is expressing sensor, then allows the user to confirm the mask looks good over the image. A 3s rolling average of the images is applied to smooth noise in the signal, and then an average of the ROI is found for each image sample. $\Delta F/F$ is calculated for each session:

$$\Delta F/F = \frac{F - F_0}{F_0}$$

$$where\ F\ is\ the\ timeseries\ of\ the\ avg\ ROI, and\ F_0\ is\ the\ mean\ of\ a\ 20s\ baseline$$

For comparisons of before and after optogenetic stimulation, a 3s average of the time series right before stimulation starts is compared to right after stimulation ends.

2.2.7 Statistical analysis

2.3 Results

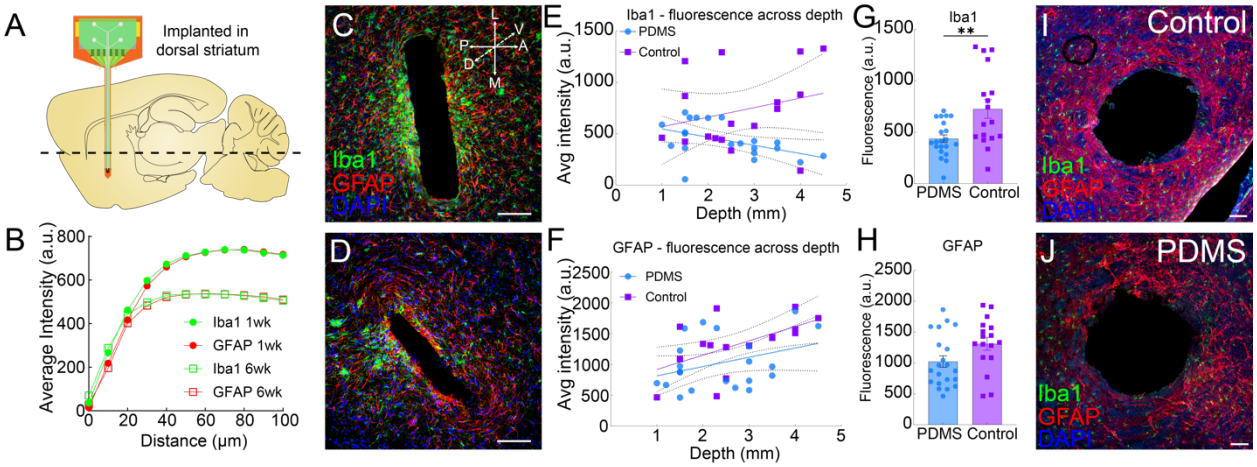

Figure 2.1. Immune response to GFET device implantation decreases over time, and decreases with depth using PDMS

(**A**) Schematic of gFET device implantation in the striatum. (**B**) Representative changes in intensity within ROI as distance from device increases for both Iba1 (red) and GFAP (green) at 1 week (closed circle) and 6 weeks (open square). N=1 for 1wk and 6wk. (**C–D**) Representative confocal fluorescence images of horizontal striatal slices show immunohistochemical staining for DAPI (blue), astrocytes (GFAP, red), and activated microglia (Iba1, green) and overall lesion from gFET device implantation after 1 week (**C**) and 6 weeks (**D**). (**E-F**) Linear regression of immune response for microglia (**E**) and astrocytes (**F**) across the sample's depth. **E-H**, n=3 exp,3 control. The slopes are not significantly different (**E**, p=0.0597, **F**, p=0.52), and the intercept of Iba1 is significant (p=0.004). Iba1: PDMS r^2= 0.21, Control r^2=0.07. GFAP: PDMS r^2= 0.12, Control r^2= 0.33. (**G**) There is a significant decrease in the Iba1 response (p=0.007), and (**H**) nonsignificant decrease in GFAP (p=0.051). (**I-J**) Representative confocal fluorescence images of horizontal striatal slices show immunohistochemical staining for DAPI (blue), astrocytes (GFAP, red), and activated microglia (Iba1, green) in (**I**) control group and (**J**) PDMS group. All histological and confocal settings were kept consistent across groups, 20x. (Scale bars, 100 μm.).

A major concern in research and in clinic with implantable devices is device failure due to heightened impedance after immune response. In collaboration with Dr. Zhang's lab at University of Connecticut, we developed aptamer devices that sense dopamine *in vivo*. To test the immune response, we measured astrocyte and microglia accumulation around the gFET device to see how the immune response changed over time and with the protective silicone layer PDMS. The first 20 μm distance from the implant had a

consistent glial response over 1 and 6 weeks (**Fig 2.1B**). After 30 µm, the immune response plateaued in the 6 week group (**Fig 2.1D**), and both microglia and astrocytes have greater expression in the 1 week (**Fig 2.1C**) group past this point. These data suggest microglia and astrocyte response to device implantation decreases over time.

To better understand complications with the depth of implant, I next looked at how astrocytes and microglia response changed with depth. I also wanted to understand the impact of a protective layer, PDMS, and so I repeated the experiment with PDMS coated gFET devices. GFAP's slope had a significant deviation from zero in control mice (**Fig 2.1F**, linear regression, p=0.016), indicating that astrocytes increased with depth when targeting the dorsal striatum. We also saw a significant deviation in the slope in the Iba1 PDMS linear regression (**Fig 2.1E**), which suggests the PDMS decreases the microglia

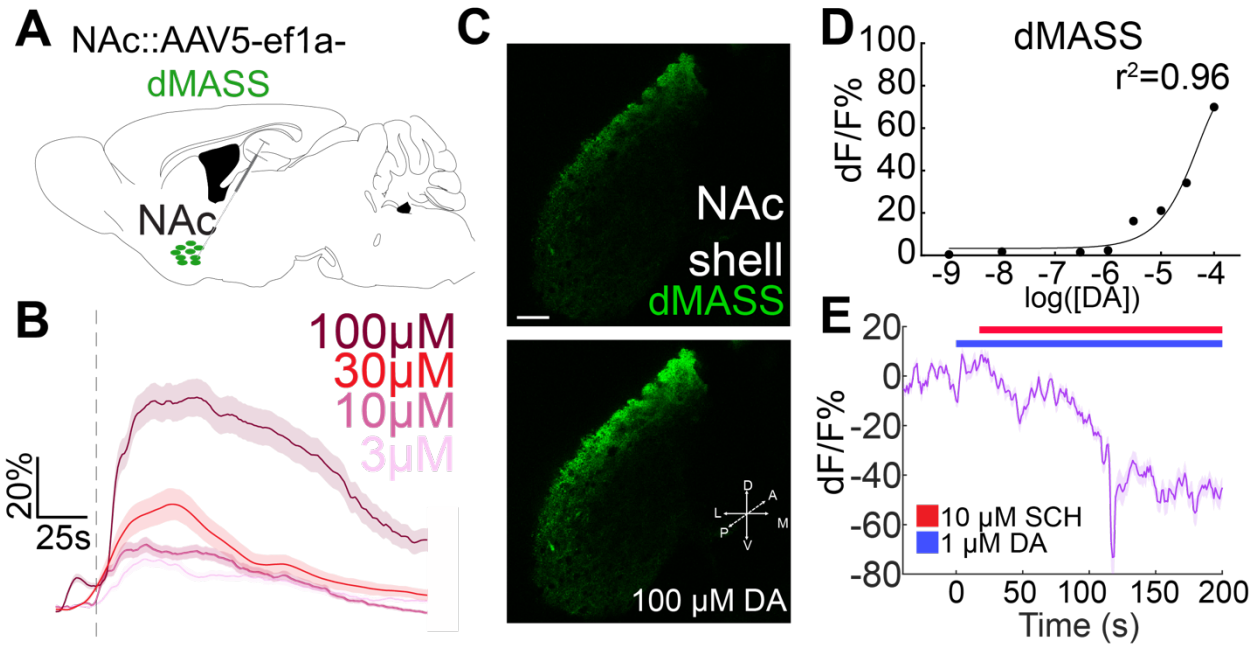

Figure 2.2. dMASS responds reliably to DA in *ex vivo* 2-photon imaging
(**A**) Surgery schematic of dopamine sensor dLight3A expression in NAc shell. (**B**) Averages of *ex vivo* slices responding to DA washes from 3µM to 100µM for 15s. (**C**) Representative 2-photon images of NAc shell before (top) and after (bottom) responding to 100µM DA. (**D**) dLight concentration response curve, r^2= 0.96, n=1. (**E**) dLight response to 1 µM wash for 15s, followed by SCH23390 wash (Scale bars, 100 µm.). F_0 was calculated with 20s baseline before applying ligand.

response was decreasing with the depth of the implantation. As the transistor detection surface is at the tip of the probe, reducing the immune response deeper in the brain is especially important. While there was nonsignificant decrease in the astrocytes (**Fig 2.1H,** p=0.051), there was a significant decrease in the microglia response (**Fig 2.1G**, p=0.007). As more therapeutic devices are studied and brought to clinic, understanding how to extend the longevity and biocompatibility of these devices is crucial to implantable devices to pass regulations.

Recently developed genetically-encoded biosensors have already revolutionized how neuromodulator studies are conducted. I tested dMASS to determine its efficacy in *ex vivo* slice pharmacology experiments. I expressed the dopamine sensor dMASS (AAV5-ef1a-dMASS) in the NAc (Rappleye et al., 2023). Under 2-photon imaging, I developed a concentration response curve for dMASS washing on 1 nM to 100 μM concentrations of DA (**Fig 2.2B**), and I fit a well-fit concentration response curve (**Fig 2.2D**, r^2=0.96). Although the goodness of fit is high, the concentration response curve is incomplete, presumably due to low sample size. As a positive control, we washed on 1 μM of DA for 15 s, then washed on 10 μM D_1 antagonist SCH23390 for 180s and saw a great reduction in dMASS signal.

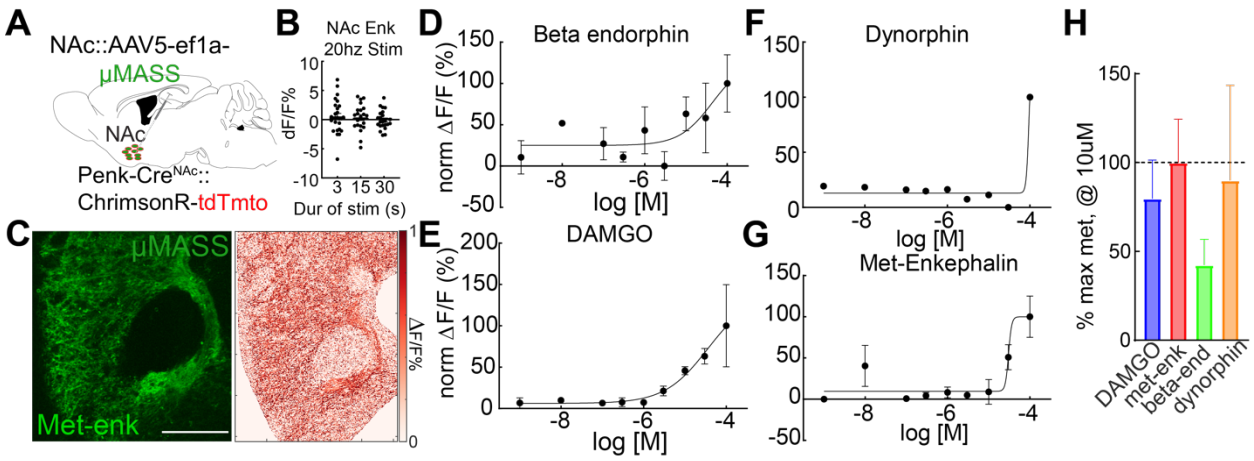

Figure 2.3. μMASS responds promiscuously in response to opioid ligands in *ex vivo* 2-photon imaging

(**A**) Surgery schematic of mu-opioid sensor μMASS expression in NAc shell. ChrimsonR expression in NAc. (**B**) Stimulation of NAc enkephalin terminals. (**C**) Representative 2-photon images of NAc shell with met-enkephalin washed on (left) and a heat map showing normalized change in fluorescence responding to 100μM met-enkephalin. (**D-G**) μMASS concentration response curves for (**D**) beta-endorphin, r^2= 0.39, n=2. (**E**) DAMGO, r^2= 0.76, n=2. (**F**) dynorphin, r^2= 0.96, n=1. (**G**) met-enkephalin r^2= 0.73, n=2. (**H**) The fluorescence response for each ligand at 10 μM, normalized to the response at 10 μM met-enkephalin wash for each ligand. Scale bars=100 μm.

Another sensor I tested was μMASS (AAV5-ef1a-μMASS), expressing it in the NAc of Penk-Cre mice with the red-shifted channelrhodopsin, Chrimson (**Fig 2.3A**). When I stimulated enkephalin neurons in NAc at 20hz for 3, 15, and 30s, I saw no significant differences from zero (**Fig 2.3B**, one-sample t test; 3s, p=0.33, 15s, p=0.47, 30s, p=0.91). In response to 100μM met-enkephalin, there is clear changes in fluorescence across the ROI analyzed (**Fig 2.3C**). I washed a range (1 nM to 100 μM) of endogenous opioids and DAMGO on slices expressing the sensor to prepare concentration response curves for beta endorphin, dynorphin, DAMGO, and met-enkephalin (**Fig 2.3D-G**). The response curve for sensors was right-shifted compared to HEK cells. The beta-endorphin concentration response curve was not well-fit (**Fig 2.3D**, r^2=0.39), and the EC50 was estimated as 43μM. The dynorphin concentration response curve was well-fit, though the

model reliability was limited due to sparse data (**Fig 2.3F**, r^2=0.96). The dynorphin EC50 was estimated as 94μM. The met-enkephalin response curve was moderately-well fit, and the EC50 was 30 μM (**Fig 2.3G**, r^2=0.73). The DAMGO response curve was moderately-well fit to the concentration response curve, and the EC50 was 36 μM (**Fig 2.3G**, r^2=0.76). I normalized all responses at the max responding at 10 μM to met-enkephalin to compare responsiveness across ligand and found that μMASS responded indiscriminately to opioid ligands. As opioid sensors are developed, selectivity for endogenous opioids will continue to be a challenge that needs to be addressed.

Catecholamine sensors, like opioid receptors, also suffer from selectivity issues (López et al., 2024a). To investigate selectivity of these sensors more in depth, I washed 1 nM to 100 μM NE on $GRAB_{NE}$ expressing slices in the dorsal CA1 (**Fig 2.4B**). The EC50 of $GRAB_{NE}$ response is 42 μM NE. I repeated the process with DA washes on dLight, and the EC50 of dLight to DA was 41 μM DA. Because $GRAB_{DA}$ was the most selective DA sensor we used (**Table 2.1**), I prepared concentration response curves for DA and NE

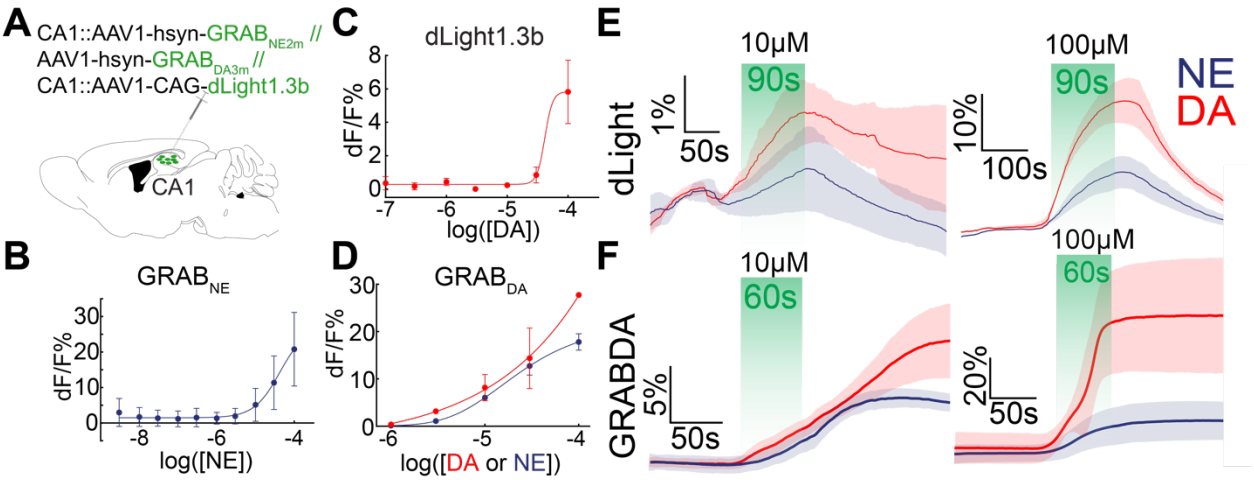

Figure 2.4. $GRAB_{NE}$ and $GRAB_{DA}$ respond reliably to DA in *ex vivo* 2-photon imaging
(**A**) Surgery schematic for 2-photon characterization of GRAB sensors *ex vivo.* (**B**) $GRAB_{NE}$ concentration response curve to NE, r^2=0.66, n=3-7. (**C**) dLight1.3b concentration response curve to DA, r^2=0.92, n=2. (**D**) $GRAB_{DA}$ concentration response curve to DA (r^2=0.90, n=2) and NE (r^2=0.97, n=2). (**E-F**) Averaged (**E**) dLight and (**F**) GRABDA washes of NE (blue) and DA (red) at 10 μM (left) and 10 μM (right).

washes, and found $GRAB_{DA}$'s EC50 values to be 61 μM DA and 21 μM NE. This yields a fold difference of 2.9 DA to NE. These results suggest that $GRAB_{DA}$ is less selective in slice than suggested in HEK cells and cultured neurons (Feng et al., 2024; Patriarchi et al., 2018a; Sun et al., 2020).

2.4 Discussion

Here we characterize several different tools for sensing neuromodulators and neuropeptides *in vivo* and *ex vivo*, and address some of their limitations. Neuromodulator detection techniques have struggled from limitations in temporal and spatial resolution, selectivity, and immune response. Catecholamines and opioids have long-term effects on behavior and neural circuit activity (Bunney et al., 1973; Nestler & Aghajanian, 1997; O'Brien et al., 1977; Wise & Rompre, 1989), but now have developed the tools to strongly observe neural dynamics at subsecond temporal resolution and with behavioral relevance. At the same time, electrical implantable devices are moving to the clinic and understanding the immune response is crucial for long-term success and efficacy of implantation (Kozai et al., 2015). In this chapter, I contribute to the growing literature on immunoreactivity to devices and provide data suggesting PDMS may serve as a potential protective layer to minimize gliosis. I also characterize recently developed mu opioid and catecholamine sensors and address their selectivity in live brain slices.

While device size is key for avoiding inflammatory tissue response (Kozai et al., 2012, 2015), gliosis is still a considerable concern at the scale of the gFET-aptamer device. We demonstrated that at the scale of this device, glial response, both astrocytes and activated microglia, decreases with time after implantation. We also found that when

we implanted PDMS-coated implants, we saw a significant decrease in microglial response compared to control implants. Astrocyte expression was decreased, but the difference was nonsignificant. Microglia respond more transiently to injury than astrocytes (Matejuk & Ransohoff, 2020), and astrocytes are the primary scavengers of microglial debris (T. Zhou et al., 2022), suggesting that astrocyte response likely diminishes after microglia. A significant inverse correlation was observed between microglial depth and response intensity while the slope of the depth affecting astrocyte response is not significantly non-zero suggest that microglial response is more affected by the depth or tissue composition than astrocytes. This was the first work I am aware of that looked at differences in depth in the brain with relation to immune response.

Though dMASS, GRAB sensors, and dLight were engineered independently, we observed a right-ward shift in the concentration response curves found in *ex vivo* slice experiments compared to curves seen in HEK cells and cultured neurons (Table 2.1). As the fold difference for the EC50s is 3 times greater for DA than NE, DA responds to $GRAB_{DA}$ at higher concentrations but is much brighter according to these experiments. In the literature, $GRAB_{DA}$ EC50 was found to be 120nM in cultured neurons and fold selectivity against NE to be 80-fold higher (Zhuo et al., 2024). Here we find the EC50 to be 61μM for DA and 21 μM for NE. Because the upper range of the DA curve was unstable, this result is inconclusive.

While a right-ward shift is what we would expect as we increase the variability of the system, as we do when moving from cultured neurons to *ex vivo*, these data are the first to show this effect in *ex vivo* samples. There are some limiting factors in this work. A helpful future control for 2-photon imaging wash experiments would define a saturating

wash duration, as 15s does not appear to be a saturating wash concentration in **Figure 2.2**. When I repeated washes on experiments with dLight expressing hippocampal slices, by 90s, we approach the saturating point for the fluorescence expressed in slice during 100μM washes. At lower concentrations like 10μM wash, it appears the saturating point is not reached at 90s (**Fig 2.4E**). For these reasons, these data are difficult to interpret. Certainly, μMASS is activated by off-target opioid ligands and $GRAB_{DA}$ and dLight are activated by both NE and DA. In more controlled conditions, it might be apparent there is a larger difference in the difference in responding that we would expect and do not see.

The promiscuity of opioids on receptors is a definitive challenge for these sensors. At the time of the experiments, μMASS was one of the only μ-OR sensors that had been reported on. All reported μ-OR sensors are not selective for μ-OR ligands, and respond nonselectively to off-target opioids (Dong et al., 2024; Kroning et al., 2021; Livingston et al., 2018). In its engineering, μMASS was calibrated to DAMGO, and in *ex vivo* slice experiments, μMASS responds most reliably at lower concentrations to DAMGO. With 15s washes and 100 μM washes, it has not reached its plateau in the concentration response curve. Off-target opioids activate the sensor, although they did not respond as precisely as DAMGO. Specifically, μOR target opioids DAMGO and beta-endorphin responded at a lower range of concentrations than met enkephalin and dynorphin. We found met enkephalin to be slightly more selective than DAMGO at the μMASS sensor, indicating a lack of selectivity for μ-OR selective agonists. Beta endorphin was not responding as brightly to washes at 10 μM as dynorphin or leu enkephalin. If similar control experiments as described previously were done in these slices, selectivity in slice could more confidently be determined.

2.5 Tables

Sensor	Color	GPCR backbone	Apparent affinity (EC_{50}, nM)	Apparent off-target affinity (EC_{50}, uM)	DA/NE Fold difference	τ_{ON} (ms)	τ_{OFF} (s)	Response max $\Delta F/F$
GRABNE2m	G	α-2R (human)	NE: 380[a]	DA: 20[a]	NE/DA: 52	100	1.4	NE: 3.8[a], 2.3[b]
GRABDA3m	G	D_1R (human)	DA: 89[a], 120[b]	NE: 8	80	69	0.56	DA: 10.0[a], 24.0[b]
GRAB-rDA2m	R	D_2R (red fire ant)	DA: 210[a], 140[b]	NE: 9.2	60	50	2.24	DA: 5.3[a], 6.6[b]
dLight1.3b	G	D_1R (Human)	DA: 870[a], 690[b]	NE: 59	70	10	0.1	DA: 3.7[a], 5.2[b]

Table 2.1. Sensor characteristics
Affinity of target ligand and off-target affinities and DA/NE fold increase is included. On and off kinetics defined by tau are included as well as $\Delta F/F$ response maximum.
[a]; in cultured cells, [b]; in cultured neurons

Chapter 3: NE and DA in CA1 and BLA during appetitive and aversive behaviors

3.1 Introduction

The amygdala and hippocampus are both critically involved in fear conditioning, and affective memory. Amygdala neurons encode valence of visual stimuli (J. Liu et al., 2021; Paton et al., 2006; Shan et al., 2023). The amygdala has heightened activity when processing fearful faces (Morris et al., 1998; Whalen et al., 1998) compared to happy faces. When the amygdala is impaired, perception of emotionally salient stimuli is diminished and cortical activity decreases (Anderson & Phelps, 2001; Vuilleumier et al., 2004). The amygdala modulates cortex leading to vigilance in response to perceived danger (Armony et al., 1997; Davis & Whalen, 2001). These studies reveal stimuli with negative emotional valence activate BLA, which then modulates cortical activity and heightens attention.

Physically salient aversive stimuli also activate BLA, in turn affecting behavior. For example, distinct BLA neurons increase activity (Sengupta et al., 2018) while others decrease activity (Buffalari & Grace, 2007) in response to shock. BLA is also directly involved in fear conditioning, as inhibition of BLA diminishes loss of conditioned fear from auditory and visual conditioned stimuli(Campeau & Davis, 1995; Sengupta et al., 2018). Still, BLA inhibition does not preclude conditioned mice from avoiding the context in which they received shocks (Vazdarjanova & McGaugh, 1998), so they may not associate the cues, but they still remember the context.

BLA is also involved in processing positive valence cues. Recent studies have shown VTA projections to BLA during pavlovian conditioning are necessary to associate

a reward with cue, and the VTA-BLA projection releases DA in response to retrieving reward (Sias et al., 2024). BLA neurons' activity (Ambroggi et al., 2008a; Paton et al., 2006; Tye & Janak, 2007; Uwano et al., 1995) and VTA-BLA^{DA} (Sias et al., 2023) increase in response to reward-associated cues and reward delivery. BLA projections to the NAc are necessary for reward seeking behavior (Ambroggi et al., 2008b; K. Zhou et al., 2022) through NAc-GABA neurons disinhibiting the VTA (K. Zhou et al., 2022). Taken together, subsets of BLA neurons are activated by contextual fear cues, anxiogenic situations, cues associated with reward, and salient stimuli.

Salient, associative stimuli do not exclusively activate BLA neurons. BLA neurons are also activated by salient sounds (J. Liu et al., 2021; Shukla & Chattarji, 2022; Uwano et al., 1995) and odors (Schoenbaum et al., 1999; Uwano et al., 1995) and stressful situations (Wang et al., 2019) without an association. Different sets of BLA neurons fire with exposure to different types of stimuli, and neurons that fire in response to an innate fear, like the fear of heights, have been shown to also develop conditioned response to the context in which they received shock, but not cued fear (J. Liu et al., 2021). These data support the theory that BLA neuron populations have distinct activity associated with the valence of stimuli, and some BLA neurons fire in response to stimuli.

Another region that has been explored with relationship to aversive and appetitive situations is the hippocampus. The hippocampus has long been the focus of many studies on spatial learning and memory in reward and fear studies (Anagnostaras et al., 1999; Bird & Burgess, 2008; de Lavilléon et al., 2015; Kaufman et al., 2020; Kentros et al., 2004; J. J. Kim et al., 1993; Li et al., 2003; Martig & Mizumori, 2011). Lesioning dorsal CA1 diminishes contextual fear conditioning, but has no effect on auditory cue conditioning

(Anagnostaras et al., 1999; Fanselow & LeDoux, 1999; J. J. Kim & Fanselow, 1992; Phillips & LeDoux, 1992). Hippocampal inactivation also impaired categorization of location and features in a visual learning task (J. Kim et al., 2018). These studies imply the hippocampus is involved with physical and visual spatial understanding, but few studies, if any, have explored any effect of visual salience alone on CA1 activity.

Nonvisual salient stimuli have effects on CA1 activity. Dorsal CA1 pyramidal neurons fire in response to aversive stimuli like tail shock and airpuff, scaling with salience and context and independent of location (Barth et al., 2023). dCA1 activity also increases with the valence of a reward-predictive cue, and does not respond to neutral cue until valence is assigned (Yun et al., 2023). Certain cells in dorsal CA1 selectively respond to reward throughout despite global remapping of place cells (Gauthier & Tank, 2018). CA1 lesions produced disinhibition of Pavlovian goal-seeking behavior (Ito et al., 2005). This suggests that the dCA1 has inhibitory control over appetitive behaviors.

Hippocampal inputs to basolateral amygdala (BLA) are important for conditioning to contextual conditioned stimuli (Maren & Fanselow, 1995; Phillips & LeDoux, 1992). The hippocampus is required for the expression of conditioned fear in the context of the unconditioned stimulus (J. J. Kim et al., 1993). Other studies suggest that amygdala detects salient stimuli and its activity influences hippocampal activity during recognition emotional, salient memory (Zheng et al., 2017).

Data in the past thirty years have shown that ventral and dorsal hippocampus have functionally distinct roles in behavior and memory (Fanselow & Dong, 2010; Hock & Bunsey, 1998; Maren & Holt, 2004; Trivedi & Coover, 2004). While dorsal CA1 activity is much more associated with spatial learning and episodic memory, vCA1 activity affects

anxiety-like behavior and motivation. Inactivating vCA1, but not dCA1, leads to passive avoidance of anxiogenic situations, reduced freezing to conditioned fear and contextual conditioned stimuli (CS) (Trivedi & Coover, 2004), and impairs acquisition of auditory fear conditioning (Maren & Holt, 2004). These data suggest vCA1 facilitates defensive behaviors like freezing and passive avoidance, although these anxiogenic effects are only observable in male mice (Wang et al., 2019). Another study shows c-Fos activation in dCA1, vCA1, not BLA, by a single exposure to predator-attack simulation (Zhong et al., 2023). dCA1 may be activated when mice engage in defensive behavior in response to an active attack that are obscured in oversimplified avoidance experiments.

vCA1 neurons respond more than dCA1 to salient features of events in both aversive and reward-predictive cues (Yun et al., 2023), and the encoding of these features are stable once learned (Biane et al., 2023). vCA1 neurons fire during anxiogenic behaviors (projecting to PFC) (Ciocchi et al., 2015; Padilla-Coreano et al., 2019) and during goal-directed behavior (projecting to the NAc) (Ciocchi et al., 2015; LeGates et al., 2018; Okuyama et al., 2016). vCA1 neurons projecting to BLA and lateral hypothalamus increase in activity to shock (Jimenez et al., 2020), but only vCA1 to LHA projections encode anxiety behavior (Jimenez et al., 2018).

The vCA1 also displays its own functional diversity across the region, as vCA1 has been found to have spatially separated cells that are molecularly and functionally distinct and respond to appetitive and aversive stimuli separately (Shpokayte et al., 2022). While the dCA1 stably represents value and representations of space, vCA1 activity is more associated with behavioral response.

Although BLA and CA1 neuron activity during fear and appetitive conditioning, spatial exploration, and salient stimuli, there are not many studies that explore the release of DA and NE in the hippocampus or in BLA in response to behaviors. We know vCA1 responds to salient features of events, and novel stimuli increases DA and NE in vCA1 (Titulaer et al., 2021). Similarly DA and NE are released in dCA1 in response to novel configuration of familiar items (Moreno-Castilla et al., 2017). Our lab has previously shown that LC stimulation releases NE in BLA and increases anxiogenic activity (McCall et al., 2017a) and others have shown stress induces NE release in BLA (Giustino et al., 2020). As mentioned, VTA-BLA projections release DA in response to retrieving reward (Sias et al., 2024), but NE in BLA during reward has not been shown. In this chapter, I build upon these studies relating noradrenergic and dopaminergic systems in appetitive and aversive conditions by exploring the release of NE and DA to these stimuli in BLA and across the hippocampus.

3.2 Methods

3.2.1 Animals

Adult (20-35 g) male or female DBH-Cre or TH-Cre mice and Cre (-) littermate control mice were used for in vivo experiments after backcrossing to C57BL/6J mice for at least 10 generations. Mice were group housed, given access to food pellets and water ad libitum, and maintained on a 12:12-hour dark/light cycle (lights off at 7:00 a.m.). Animals were held in a sound attenuated holding room facility in the lab starting at least one week prior to surgery, as well as post-surgery and throughout the duration of behavioral assays to minimize stress from transportation and disruption from foot traffic.

All mice were handled and, where appropriate, connected to fiber optics two times a day for one week prior to behavioral experimental testing. All experimental procedures were approved by the Animal Care and Use Committee of Washington University and the Animal Care and Use Committee of University of Washington and conformed to NIH guidelines.

3.2.2 Stereotaxic surgery

Surgeries were performed under 2% isoflurane anesthesia (Piramal Healthcare, Maharashtra, India). All injections in BLA, dCA1, and vCA1 were performed using a Hamilton blunt syringe (Reno, NV), while LC injections were performed using a Hamilton beveled syringe (Reno,NV). For recording initial neural dynamics in response to behaviors, either 500nL of AAV1-CAG-dLight1.3b or AAV1-hSyn-GRAB$_{NE2m}$ (both prepared in the UW NAPE center Viral Core, Seattle, WA) were injected into the BLA (AP: -1.4, ML: -3.15, DV: -4.8 to -4.55), dCA1 (AP: 1.9, ML: -1.4, DV: -1.65), or vCA1 (AP: -3.16, ML: -3.25, DV: -3.50 to -3.85) of Dbh-cre or Th-cre mice. After injections, fiber optic ferrules (Doric) were chronically implanted above either the BLA, dCA1, and vCA1, and dental cement (Lang Dental, Wheeling, IL) or C&B Metabond were used to secure the implants. BLA and dCA1 implants and injections were done within the same mice. vCA1 implants were done in different cohorts. Mice were allowed to recover and viruses to express for a minimum of 5 weeks. For detecting NE and DA dynamics in *ex-vivo* slice experiments, Dbh-cre mice were injected with 500-700nL of GRABNE or GRABDA into dorsal CA1 (AP: 1.9, ML: -1.4, DV: -1.65).

3.2.3 In vivo Fiber Photometry

An optic fiber was secured to implanted fibers on experimental mice with a ferrule sleeve (Doric, ZR_2.5). Two light-emitting diodes (LEDs) were driven by a real-time processor (TDT, either RZ5P or RZ10x) that recorded dynamics from optic fibers detecting biosensor activity expressed in the brain, with 531-Hz sinusoidal 470nm (465nm on the RZ5P) and 211-Hz sinusoidal 405nm light. The 470nm LED was used to record emitted light from green sensors ($GRAB_{NE}$, dLight, and $GRAB_{DA}$) while the 405nm LED served as an isosbestic control. In dual sensor recordings taken with the RZ10x, 311-Hz sinusoidal 535nm light was used to record red sensors ($GRAB_{rDA}$). LED power for each LED wavelength were measured at the tip and adjusted to 30μW before each day of recording.

3.2.4 Photometry analysis

A custom MATLAB script was developed for analysis of photometry recordings in the context of mouse behavior. For each photometry recording, a linear-least squares regression was used to find the projection of the isosbestic curve onto the 470 nm excitation photometry trace. The best fit isosbestic 405 nm excitation control signal was subtracted from the 470 nm excitation signal to remove artifacts from intracellular NE-dependent sensor fluorescence (Lerner et al., 2015). Baseline drift was evident in the signal due to slow photobleaching artifacts, particularly the first several minutes of each recording session, and the linear least squares subtraction of the isosbestic control signal eliminated the drift seen in the 470 nm excitation signal. After centering the signal around the first three minutes of the session, the photometry trace was z-scored relative to the

mean and standard deviation of the test session. The post-processed fiber photometry signal was analyzed by time-locking each onset of behavior or stimulus, centering the data, and averaging the signal.

3.2.5 Ambient light exposure

On testing days, we placed mice in a modular (17.8×15.2×18.4cm^3; Med Associates Inc.) arena where they were allowed to freely roam. Mice were not previously exposed to this arena before the experiment. Using a MEDPC program, we randomly had an ambient light turn on for 5s at a pseudorandom ITI of 65, 95, 125s, with an average of 100s, with a total of 19 possible exposures in each session. Fiber photometry was used to record $GRAB_{NE}$, $GRAB_{DA}$, or dLight signal throughout the experiment.

3.2.6 Odor exposure

Mice were placed in a polyethylene chamber (approximately 12 x 12 x 24 cm) within a fume hood to minimize odor release into room. A vacuum continuously pulled air from the chamber at a rate of 2L/min, and vacuumed air was passed through a carbon filter. Odors (2% 2MT or 2% peppermint oil) were delivered four times per session for 30s periods with an ITI of 180s.

3.2.7 Looming stimulus

Adult mice were put in a custom-made open clear acrylic box, (50cm x 50cm) within a sound-attenuated room maintained at 23°C. Ambient room lights were on throughout the session. The open box had white paper on all walls to limit outside stimuli. Mice were

allowed to roam the box for 11 minutes prior to stimulus presentation to habituate to the box. At 11 minutes and in 60s intervals, a looming posterboard blocking overhead lighting was held over the arena for 10s, reducing arena illumination from 400 lux to ~150 lux. This was repeated 5 times. Fiber photometry was recorded for multiple biosensors detecting neural dynamics.

3.2.8 Shock

Mice were placed in a modular arena and allowed to freely roam. After a baseline period of 180s in the arena, mice experienced the shock of a 0.5-0.7mA current run through the metal grating floor of the arena for 2s. There was a pseudorandom ITI of 20-90s, with 10 total shocks. Fiber photometry was recorded for multiple biosensors detecting neural dynamics.

3.2.9 Reward

Mice were initially food deprived to 90% of their body weight. Prior to testing, we put multiple sucrose pellets per mouse in their home cage to extinguish neophobia of this reward. On testing days, we placed mice in a modular (17.8×15.2×18.4cm^3; Med Associates Inc.) arena where they were allowed to freely roam. Using MEDPC program, we randomly delivered rewards at a pseudorandom ITI of 30, 60, 90, 120s, with an average of 90s, with a total of 18 possible rewards in each session. Fiber photometry was used to record $GRAB_{NE}$, $GRAB_{DA}$, or dLight signal.

3.2.10 Operant conditioning – FR1

Mice were trained on an operant conditioning paradigm with an FR-1 contingency. After poking their nose in the correct nose port one time, there was a two second delay before an ambient light turned on for 5s and then the reward is delivered. If they poked their nose in the incorrect nose port, then nothing happened. Mice were considered fully trained if they are poking for reward

3.3 Results

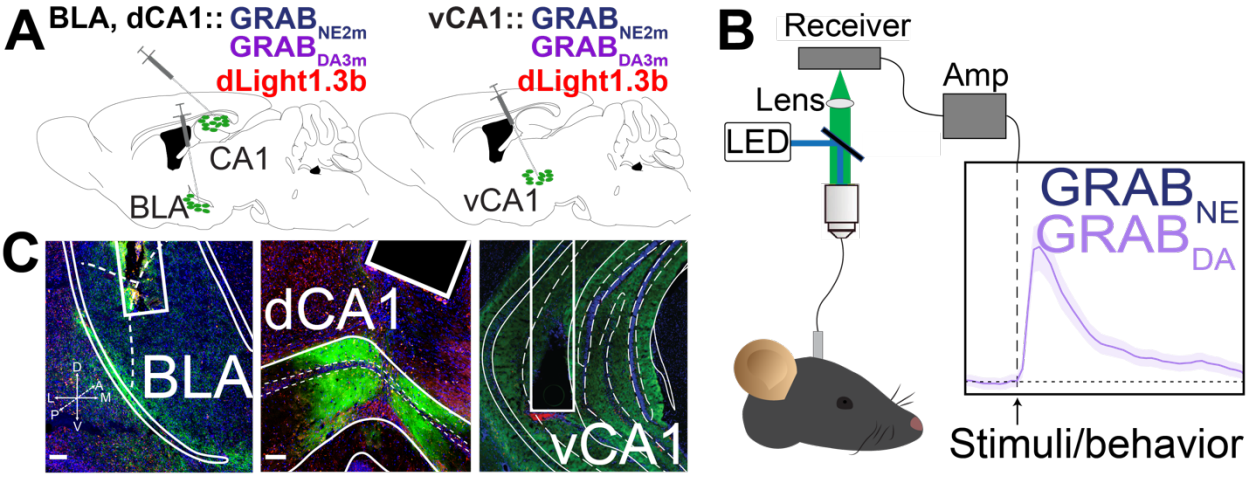

Figure 3.1 Experimental schematic and histology
(**A**) Surgery schematic for photometry experiments. (**B**) Schematic of recording photometry, depicting amplified fluorescence from biosensors. (**C**) Histology of GRABNE in BLA, dlight in CA1, and GRABNE in vCA1 expression with photometry fiber tract. Chrimson expression in LC terminals. Scale bars=100 µm.

We have previously reported that photostimulation of the LC releases NE in BLA using voltammetry (McCall et al., 2017b). To detect dynamics with the greatest selectivity, we expressed genetically-encoded neural sensors $GRAB_{NE2m}$, $GRAB_{DA3m}$, or dLight1.3b, virally delivered with human synapsin promoter in the BLA, dCA1, and vCA1 unilaterally (**Figure 3.1A**). After viral expression (**Figure 3.1C**), we recorded bulk fluorescence of the sensors from the BLA through photometry, amplified the signals, and time-locked them to when mice were exposed to stimuli (**Figure 3.1B**).

To understand dynamics responding to a neutral stimulus, I tested the NE and DA response to a low salience visual stimulus, a low ambient light turned on for 5s. After the first few exposures, the response to the light was diminished, so I limited the photometry traces to the first three exposures for each mouse. In response to the ambient light, there was a subtle increase in DA signal in BLA aligned with the onset of the light (**Fig 3.2A, left**). In dCA1, there was a ramping of DA signal throughout the duration of the light being on (**Fig 3.2A, right**). NE increases in both BLA and dCA1 were subtle.

NE and DA dynamics in response to a variety of stimuli have not been reported before, particularly at a subsecond time-scale. I exposed mice to a variety of stimuli, ranging in valence from neutral or aversive to appetitive. Mice rely heavily on their olfactory system for navigation and detection of food and predators, and olfactory input to amygdala is important for initiation of emotional responses (Ashwell, 2012). To greater understand catecholamine release in BLA and CA1 during odor exposure, we recorded the neural dynamics in response to a variety of odors (**Fig 3.1D**). In this experiment, I looked at either peppermint oil or 2MT. While peppermint oil is neutral at 2% concentration, 2MT is a synthetic predator odor and is highly aversive in mice (Bruzsik et al., 2021; J. Wu et al., 2020). In response to 30s of peppermint exposure, the NE and DA signal both rise in BLA (**Fig 3.2C**). In response to 2MT, the BLA-DA signal clearly increases, but the BLA-NE signal is not affected by the onset of 2MT (**Fig 3.2C**). In dCA1, we see an immediate increase in NE to peppermint and 2MT, and a more gradual increase in DA dynamics in response to both odorants (**Fig 3.2E**). In vCA1, there was clearly NE released in response to peppermint, but not a strong DA response to either 2MT or peppermint (**Fig 3.2F**). In both dorsal and ventral CA1, there was an immediate

increase in NE with the onset of 2MT odor, followed by a sharp decrease in NE signal below baseline, that returns to baseline after the odor is cleared from the chamber.

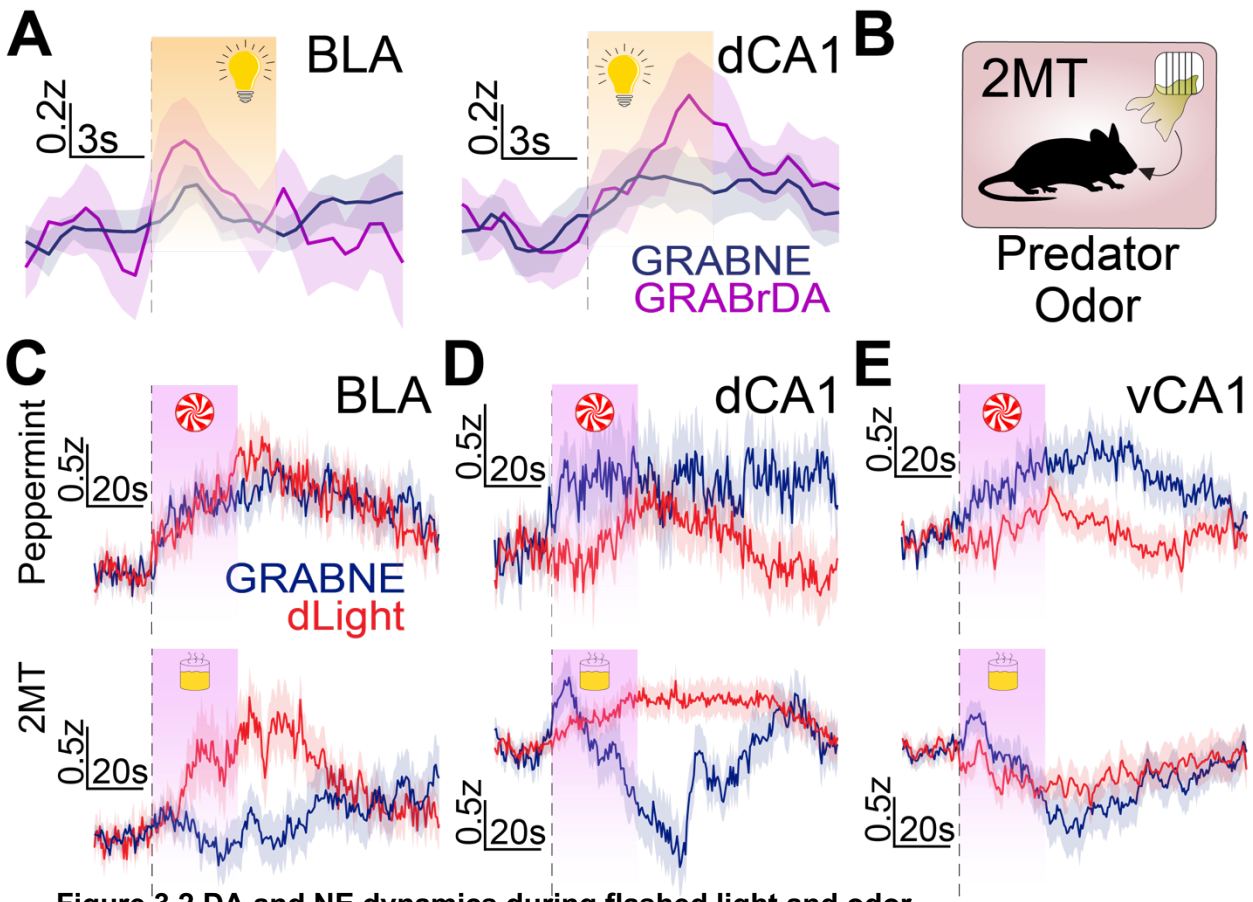

Figure 3.2 DA and NE dynamics during flashed light and odor
(**A**) Photometry trace in response to the first three exposures to 5s houselight in BLA (left, n=4) and dCA1 (right, n=4). (**B**) Schematic of 2MT odor entering the behavior box. (**C-E**) $GRAB_{NE}$ and dLight photometry traces in (**A**) BLA, (**B**) dCA1, (**C**) vCA1 in response to 30s of exposure to peppermint (top) and 2MT (bottom). Peppermint: BLA, n_{NE}=8, n_{DA}=5; dCA1, n_{NE}=5, n_{DA}=9; vCA1, n_{NE}= 6, n_{DA}=7. 2MT: BLA, n_{NE}=8, n_{DA}=6; dCA1, n_{NE}=5, n_{DA}=9; vCA1, n_{NE}= 6, n_{DA}=7.

The amygdala and hippocampus have long been studied in their relationship to internalizing and contextualizing aversive stimuli. I aimed to understand how NE and DA dynamics differ in response to anxiogenic and fear-inducing stimuli. To do so, I exposed mice to 10s of a looming posterboard to simulate a predator and 2s shocks (**Fig 3.3F**).

With each exposure to the looming stimulus, mice exhibited mild darting behavior, seen in their significant increase in velocity during stimulus presentation (**Fig 3.3D**). In BLA, GRABDA had a clear increase to the onset and offset of the looming stimuli, while NE had a much clearer increase with the onset of the stimulus (**Fig 3.3A, top**). In dCA1, only NE signal increased with the onset of the stimulus (**Fig 3.3B, top**). In vCA1, NE has a clear increase to the onset and offset of the looming stimulus, while the DA signal did not change much (**Fig 3.3C, top**).

First, mice were exposed to a 2s shock which served as a highly salient, aversive stimuli. In BLA, the $GRAB_{DA3m}$ response was greater than $GRAB_{NE2m}$ in response to shock, but $GRAB_{NE2m}$ had a slow decay for over 30s, which was dissimilar to the decay in $GRAB_{NE2m}$ signal in response to other stimuli (**Fig3.3A, bottom**). In CA1, $GRAB_{NE2m}$ and $GRAB_{DA3m}$ increased at the onset of the shock, with DA response lower than NE (**Fig 3.3B, bottom**). In vCA1, the NE and DA increase with shock duration, but $GRAB_{NE}$ signal is sustained after the offset of the shock (**Fig 3.3C, bottom**). In order to establish a fear response was present, we assessed freezing behavior and found mice exhibited significantly greater freezing behavior in the last five minutes of the shock session compared to the five-minute baseline (**Figure 3.3E**). Only $GRAB_{NE}$ had a sustained and significantly increased tone for the rest of the session compared to baseline (**Supp Fig I**). In response to shock, there was a greater $GRAB_{DA3m}$ response than $GRAB_{NE2m}$ in the BLA and a greater $GRAB_{NE2m}$ response than $GRAB_{DA3m}$ in CA1. The BLA-DA response is also consistently higher than the CA1-DA response (**Figure 1G**, Kruskal-Wallis with Dunn's multiple comparison, $p=0.0095$). These data indicate DA is released in both CA1 and BLA in response to aversive stimuli.

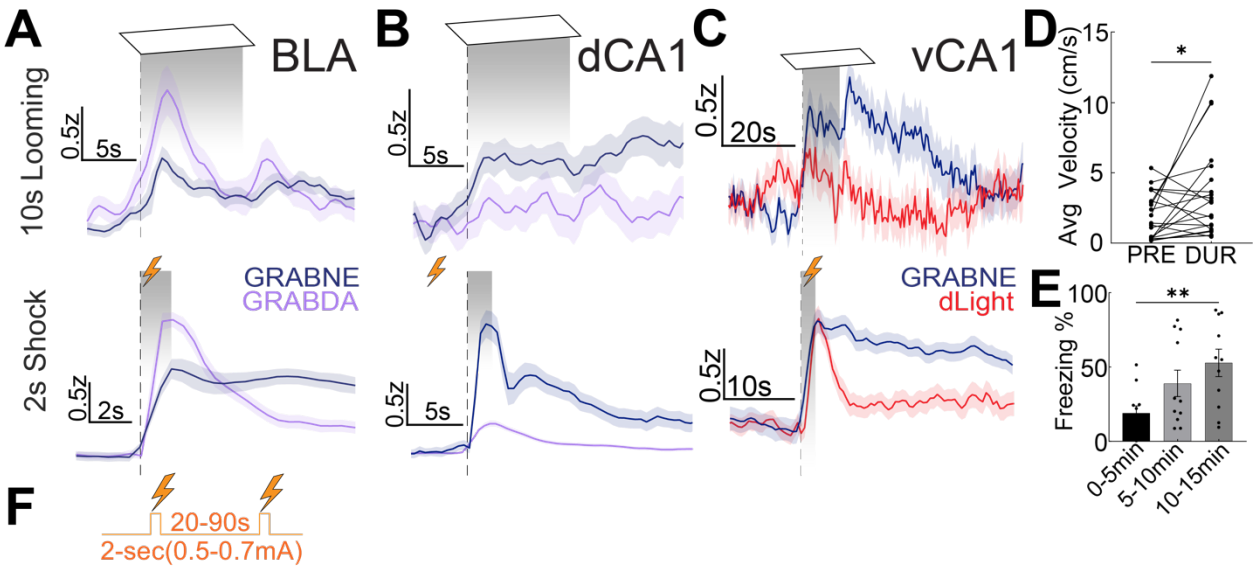

Figure 3.3 DA and NE dynamics to aversive stimuli: looming and shock
(**A-C**) $GRAB_{NE}$ and $GRAB_{rDA}$ or dLight photometry traces in (**A**) BLA, (**B**) dCA1, (**C**) vCA1 in response to 30s of exposure to looming (top) and shock (bottom). Looming: BLA, n_{NE}=7, n_{DA}=7; dCA1, n_{NE}=12, n_{DA}=7; vCA1, n_{NE}=7, n_{DA}=7. Shock: BLA, n_{NE}=6, n_{DA}=7; dCA1, n_{NE}=5, n_{DA}=7; vCA1, n_{NE}=7, n_{DA}=7. (**D**) Average velocity of mice increases during looming. One-way ANOVA, p=0.004, n=11. (**E**) Freezing behavior increases as mice are shocked. Paired t-test, p=0.036, n=21. (**F**) Paradigm of timing and shock intensity for shock experiment.

Next, we wanted to see the dynamics of NE and DA in response to a simple appetitive behavior. To do so, we randomly delivered sucrose pellets to food-restricted mice while recording $GRAB_{NE}$ or $GRAB_{DA}$ signal. Mice consumed nearly all presented rewards in each trial, and once trained, repeatedly entered their head to the hopper (**Fig 3.4C**). We found that as mice approached the hopper for reward, both NE and DA increased in the BLA, with DA having a much greater magnitude response than NE (**Fig 3.4A**). As mice consumed sucrose pellets there was a sustained increase in NE while DA response continued to decay. In the CA1, NE increased as mice approached the hopper, and as mice consumed, there was a subtle dip in the NE signal (**Fig 3.4B**). This decrease in $GRAB_{NE}$ signal corresponded with a decrease in the $GRAB_{DA}$ signal. These data taken

together suggest we see more DA is released in BLA than in CA1 in response to reward retrieval (Kruskal-Wallis with Dunn's multiple comparison, $p<0.0001$).

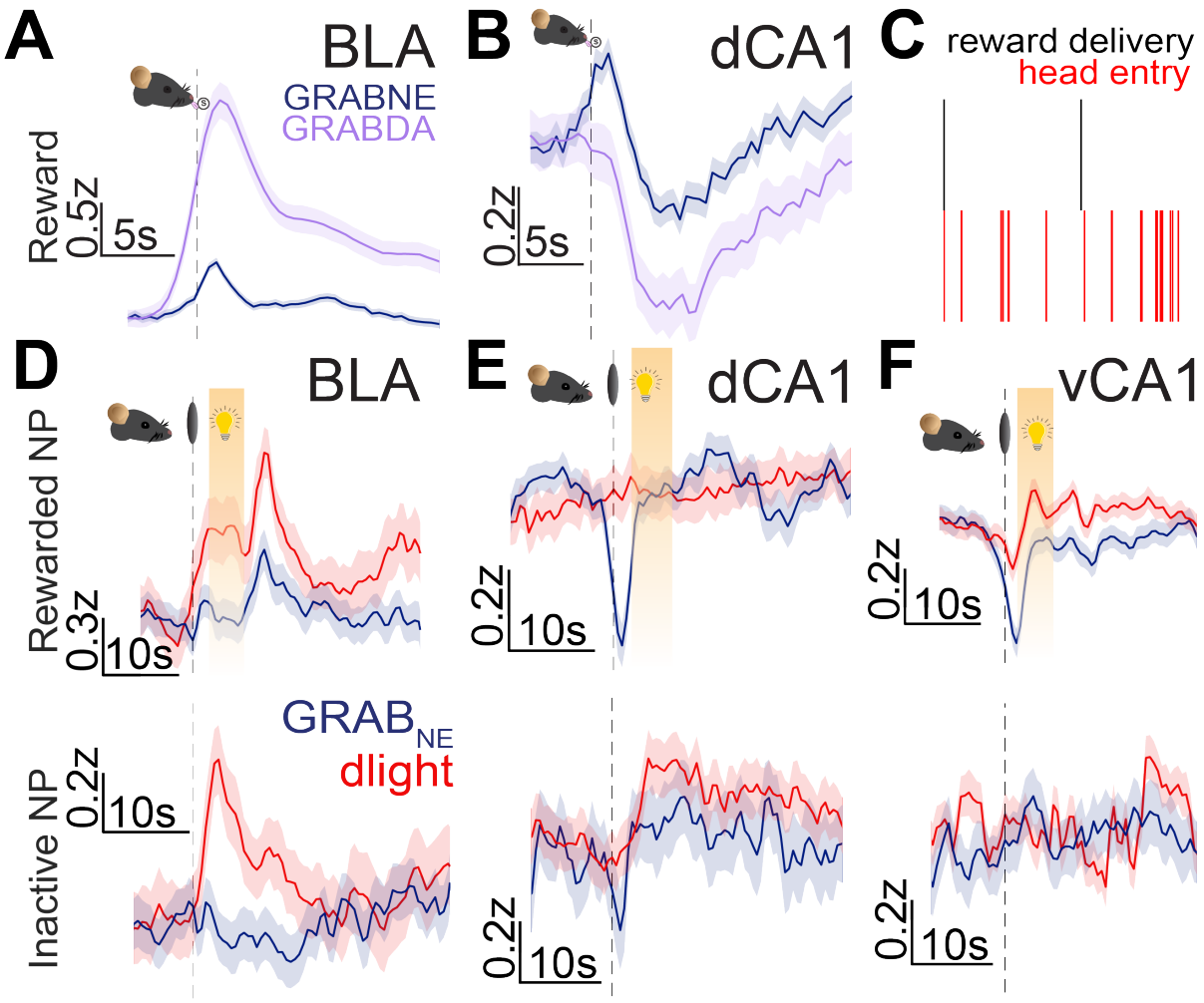

Figure 3.4 DA and NE dynamics to appetitive behavior: reward retrieval and nosepokes (**A-B**) $GRAB_{NE}$ and $GRAB_{rDA}$ photometry traces responding to reward retrieval in BLA (**A**, $GRAB_{NE}$ $GRAB_{rDA}$) or dCA1 (**B**). Reward: BLA, $n_{NE}=9$, $n_{DA}=12$; dCA1, $n_{NE}=9$, $n_{DA}=7$. (**C**) Representative raster of head entries (red) in response to reward deliveries (black) as mice retrieved reward. (**D-F**) $GRAB_{NE}$ and dLight photometry traces in response to rewarded nosepokes (top) and unrewarded nosepokes in the inactive port (bottom) in BLA (**D**), dCA1 (**E**), and vCA1 (**F**). Rewarded NP/inactive NP: BLA, $n_{NE}=8$, $n_{DA}=6$; dCA1, $n_{NE}=5$, $n_{DA}=8$; vCA1, $n_{NE}=5$, $n_{DA}=7$.

With clear increases in response to reward retrieval, we next wanted to understand how these behaviors differed across the hippocampus and in BLA in response to goal-directed behavior. In trained mice, we saw that as mice poked their nose for a reward, DA

in BLA increased rapidly, was unresponsive to the houselight, and then increased more at the delivery of the reward (**Fig 3.4D, top**). As mice then consumed the pellet, the DA signal in the BLA rapidly decreases over a few seconds. In trained mice, there is also a subtle increase in BLA-NE after poking for reward. When the light turns off and pellet is delivered, both NE and DA signal increase and decreases after initiating consumption. In dCA1, DA is unaffected throughout operant behavior (**Fig 3.4E, top**). Across the hippocampus, the NE signal decreases dramatically as mice approach the port to poke for reward and increases rapidly back to baseline after mice poke for reward (**Fig 3.4E-F, top**). In dCA1, there is a subtle increase in the NE signal after the reward is delivered (**Fig 3.4E, top**). In vCA1, there is a decrease in DA signal smaller in magnitude than the dramatic NE decrease, followed by a DA-specific increase in signal above baseline during the cue light (**Fig 3.4F, top**). There is a subtle increase in DA signal when the reward is delivered, and DA slowly returns to baseline. In BLA and dCA1, there are increases in DA signal when mice poke the inactive port that does not reward them (**Fig 3.4D-E, bottom**). In BLA, this increase comes back to baseline over 15s, while in dCA1, the increase is more subtle and is also sustained longer.

The peaks of these photometry data are summarized in **figure 3.5**. DA release in BLA is consistent across DA sensors and behaviors. We did not see the decrease in DA signal during reward retrieval in dLight that we saw in $GRAB_{DA}$ (**Fig 3.4B and Fig 3.5**).

dLight had a greater increase in some behaviors compared to $GRAB_{DA}$, such as shock in BLA and dCA1.

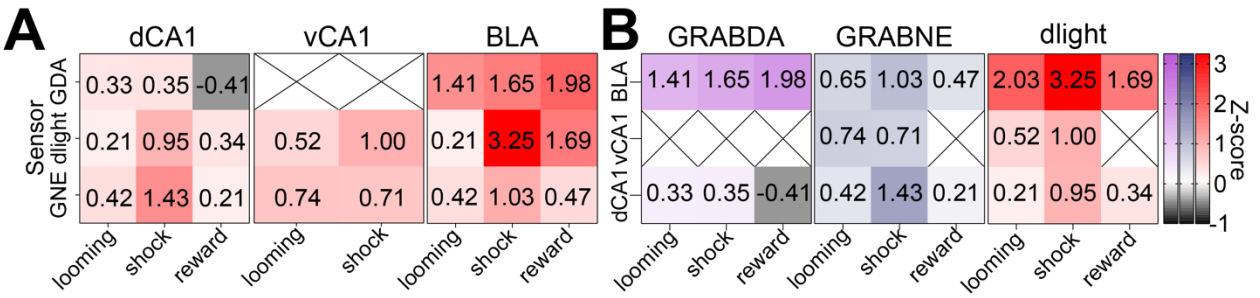

Figure 3.5 Heatmap summarizing peak z-score responses to looming, shock and reward (**A**) Within region comparison of peak z-scores across sensors in response to looming, shock, reward. (**B**) Within sensor comparison of peak z-scores across regions in response to looming, shock, reward.

3.4 Discussion

Here, we define the endogenous DA and NE responses to an array of stimuli that have varied salience and valence. Low-salience neutral stimuli like a low lux ambient light have subtle effects on NE and DA release in CA1 and BLA. A neutral salient stimuli like peppermint odor leads to an increase of NE and DA release in BLA, and more clear increases in NE exclusively across the hippocampus. In response to these neutral stimuli, we see a clear difference in the onset of DA signal in BLA and CA1. Specifically, DA and NE response initiated immediately in BLA and delayed in dCA1 in response to peppermint odor and house light exposure. This trend is somewhat followed in the highly aversive 2MT odor exposure, but the dLight response seems to not be as immediate. This may reflect flaws of the behavioral setup, because the onset of DA response is rapid after 5s of “exposure”. Because the LC and VTA strongly project to BLA, while LC has stronger innervation in CA1 than VTA, the DA delay we recorded might be the result of subtle neuromodulatory effects when these projections are activated. Because the BLA encodes valence of visual stimuli (J. Liu et al., 2021; Paton et al., 2006; Shan et al., 2023), and

dCA1 neurons tend to fire with salience and contextual cues independent of location (Barth et al., 2023), the DA delay observed might suggest the BLA registers the salience and valence of the event, and the dCA1 registers the contextual cues and valence after. The CA1 delay in DA release therefore might be through activation of other circuits, such as connections with the PFC. However, some studies suggest that the neutral cues do not activate dCA1 until valence is assigned (Yun et al., 2023), therefore, these modest DA signals may be the LC and VTA activated by stimuli, and reconfiguring their activity as the mouse determines the valence of the stimuli.

While the dCA1 is primarily known for its role in spatial memory and for its characteristic place cells, dCA1 pyramidal neurons do fire in response to aversive stimuli like tail shock and airpuff. In dCA1, NE clearly is released in response to shock, and more subtly to the onset and offset of looming stimuli. Salient features led to more consistent NE release in vCA1 than dCA1, which was reflected in the stronger NE release in vCA1 in response to looming stimuli compared to dCA1. Across regions we also see heightened NE tone after the first exposure to shock, which is in alignment with LC activity increasing after a stressful event and releasing NE (Curtis et al., 2012; McCall et al., 2017a), although there was no prolonged NE release in response to 2MT exposure.

In response to reward, the differing functions of CA1 and BLA were apparent in responses. BLA-DA activity was increased in response to the sounds of the coming reward, which matches past data suggesting that reward-associated cues increase BLA neuron activity (Paton et al., 2006; Tye & Janak, 2007). Previous data also suggests that LC-NE activity is suppressed during feeding (Sciolino et al., 2022). While this effect occurs in dCA1, as well as a complimentary dip in DA signal, there is a subtle increase in

BLA data in response to reward retrieval. These data are in contrast with LC-NE suppression during feeding or there are distinct LC-NE projections to BLA that are not suppressed. Another NE source may be projecting more to the BLA than dCA1 and is disinhibited while LC is inhibited during feeding. One such source of NE in this instance are A2 noradrenergic neurons, which project stronger to BLA than LC, and not to CA1 at all (Robertson et al., 2013).

Through the operant data, we can deconstruct neuromodulator activity at each . In trained mice, DA was released in BLA during motivated-behavior like poking for a reward, and NE and DA increased at the delivery of the reward. NE exclusively being delivered right before the reward was delivered (and preceding the start of the DA response, but not at any other point in the operant paradigm) may indicate LC activity increased only when as the mice anticipated the reward. BLA-DA also is increased during poking the port where no reward is associated, suggesting that even when mice are trained, unrewarded actions still may lead to DA release. The unrewarded noseport may represent some unexpected stimulus the mice interpret as significant, even without any clear outcome. While these findings are consistent with recent studies that show BLA-DA increases in response to cues for reward and reward delivery (Paton et al., 2006; Tye & Janak, 2007), this is the first reporting of NE release in BLA during reward retrieval and operant conditioning.

We hypothesized DA would be released in dCA1 during components of the task showing spatial memory components of the task, like approaching the rewarded noseport, as there are neurons that encode reward in CA1 (Gauthier & Tank, 2018). But in dCA1, we only saw a subtle increase in dopamine to the mouse poking its nose in the

unrewarded noseport. In vCA1, there was very modest DA increases to the cue and reward retrieval. We expected a stronger response because there is a spatial separation of neurons responding to appetitive cues (Shpokayte et al., 2022), and a greater portion of the cells this caudal in the vCA1 should be appetitive than aversive. To our knowledge, these are the first subsecond-resolution recordings of NE and DA in amygdala and hippocampus to a variety of stimuli that are often involved in circuit neuroscience studies.

Chapter 4: NE and DA during various appetitive and aversive behaviors (CA1 and BLA)

4.1 Introduction

The locus coeruleus-norepinephrine (LC-NE) system consists of a widespread projecting network of neurons that modulate a range of behaviors like arousal(Berridge, 2008; Carter et al., 2010), learning(Bouret & Sara, 2004; Kaufman et al., 2020; Seo et al., 2021), and stress-induced negative affect(Giustino et al., 2020; McCall, 2015; McCall et al., 2017b). As an obligate precursor for NE, dopamine (DA) is also produced in LC neurons. However, because tyrosine hydroxylase (TH; converts tyrosine to L-DOPA), not dopamine β-hydroxylase (DBH; converts DA to NE), is rate-limiting for catecholamine synthesis under normal circumstances(Udenfriend & Dairman, 1970), LC neurons were classically thought to release NE but not DA. Yet, the potential for DA release from noradrenergic neurons has been discussed since the early 2000s. Initially, microdialysis was used to detect neuromodulator release with autoreceptor antagonists (which disinhibit NE or DA neuron activity), and revealed the potential for noradrenergic release of DA. For example, α_2 adrenergic receptor (α_2ARs) antagonists, but not a D_2 dopamine receptor antagonist, upregulated DA release in the occipital cortex (OCC) and medial prefrontal cortex (mPFC), brain regions with very sparse dopaminergic innervation(Borgkvist et al., 2011; Devoto et al., 2003, 2004; Devoto, Flore, Saba, Fa, et al., 2005). Furthermore, LC stimulation increased the amount of extracellular DA in mPFC and in OCC, which was diminished after local tetrodotoxin administration in mPFC or OCC(Devoto, Flore, Saba, Fà, et al., 2005). Overall, these data suggest that α_2ARs on

LC axonal terminals regulate release of DA(Devoto et al., 2003; Devoto, Flore, Saba, Fa, et al., 2005).

While DA could be evoked from noradrenergic neurons through α_2AR antagonist administration, whether noradrenergic-sourced DA release affects behavior remained unclear. To investigate the role of LC-DA in behavior, studies employed LC terminal stimulation in the dorsal hippocampus (CA1) and found that spatial awareness and memory were enhanced(Kempadoo et al., 2016a; Takeuchi et al., 2016c). Infusion of high concentrations of D_1 receptor antagonists in CA1 reversed these enhanced spatial memory effects, while blocking β-adrenergic receptors (βARs) had no impact.

These studies implicate LC-evoked DA release in behavior for the first time, but the durations and intensities employed in optogenetics experiments(Gálvez-Márquez et al., 2022; Kempadoo et al., 2016a; Takeuchi et al., 2016c) do not reflect the LC's established neuronal activity during many of these tasks(Devilbiss & Waterhouse, 2011b; Kelberman et al., 2024). Pharmacological manipulations in these studies also do not preclude potential circuit level or non-selective effects of these manipulations. Moreover, a ventral tegmental area (VTA) to CA1 dopaminergic circuit controls persistent contextual memory(Lisman & Grace, 2005b) and contextual fear acquisition in the absence of noradrenergic signaling(Tsetsenis et al., 2021), affirming the need to determine the physiological and behavioral stimuli which evoke DA release from LC axons. There remains limited direct evidence for release of DA from LC terminals *in vivo* in response to appetitive, aversive, or neutral stimuli.

Previous studies detecting LC-evoked DA release utilized microdialysis, which while highly sensitive, lack temporal resolution(Kempadoo et al., 2016a; Takeuchi et al.,

2016c). In contrast, recently developed genetically-encoded biosensors have risen to prominence for neuromodulator detection due to their high temporal resolution and selectivity for target ligands. However, G protein-coupled receptors (GPCRs) have can have non-selective affinity for off-target neuromodulator-GPCRs of similar subclasses and derivatives, and off-target binding has been reported, specifically with NE and DA(López et al., 2024b). So while GPCR-based sensors have become widely-used for understanding behavior at relevant time-scales, studies must carefully consider the local innervation of their targeted circuit for off-target neuromodulator release that may inadvertently activate endogenous receptors and sensors(López et al., 2024b).

In this study, we consider the controversy surrounding LC-derived DA and how we may measure NE and DA dynamics in regions where there are some overlapping DA and NE inputs. Emerging evidence suggests LC neurons innervate regions with functional specificity and distinct subsets of neurons activate depending on behavioral state(Chandler et al., 2019b; Dupret et al., 2010b; Nakahara et al., 2004; Poe et al., 2020; Sinha et al., 1999; Uematsu et al., 2017b). For example, during early extinction of conditioned fear, LC projections to basolateral amygdala (BLA) are preferentially active. By contrast, during late extinction when mice exhibit diminished fear behavior, LC projections to mPFC are active(Uematsu et al., 2017b). The BLA is critical for cued fear(Campeau & Davis, 1995; Davis & Whalen, 2001; Fanselow & LeDoux, 1999b, 1999b; Maren, 2001; Matus-Amat et al., 20070730; Phillips & LeDoux, 1992) while CA1 is necessary in contextual fear conditioning(Anagnostaras et al., 1999; Maren et al., 1994; Matus-Amat et al., 20070730; Phillips & LeDoux, 1992), and both are also activated by salient stimuli(Barth et al., 2023; J. Liu et al., 2021; Schoenbaum et al., 1999; Shukla &

Chattarji, 2022; Uwano et al., 1995) and reward-associated cues(Ambroggi et al., 2008a; Gauthier & Tank, 2018; Martig & Mizumori, 2011; Paton et al., 2006; Tye & Janak, 2007; Uwano et al., 1995; Yun et al., 2023). Therefore, the BLA serves as a critical region alongside the hippocampus to further determine the specific nature of LC-evoked DA dynamics.

Since distinct subsets of LC neurons are activated in response to salient, aversive, and appetitive stimuli(Borodovitsyna et al., 2018b; Chandler et al., 2019b; Chen & Sara, 2007b; Curtis et al., 2012; de Medeiros et al., 2005b; Grimm et al., 2024; McCall et al., 2017b; Poe et al., 2020; Privitera et al., 2024; Silveira et al., 1993b) in different behavior states, we hypothesized that DA release from the LC would be greater in BLA than in CA1 during both aversive and appetitive stimuli, as salient stimuli are often associated with BLA activity(J. Liu et al., 2021; Uwano et al., 1995) and the CA1 receives little dopaminergic input(Tsetsenis et al., 2021). We first established the selectivity constraints and demonstrated high selectivity of the sensors we used. We next demonstrated that we can evoke DA release from LC-CA1 terminals in 2-photon *ex vivo* slice imaging and then found that LC-evoked DA signal follows an increasing linear trend with frequency *in vivo* in CA1 and BLA. We next established the NE and DA responses to appetitive and aversive stimuli in the BLA and CA1. Finally, we used chemogenetics to demonstrate that following appetitive and aversive stimuli, the LC contributes more to endogenous DA release in the BLA than in CA1. Together, we report that LC releases DA with both projection and stimulus specificity. As diminished DBH has been associated with increased vulnerability to psychosis(Cubells et al., 2000; Meltzer et al., 1976; Yamamoto et al., 2003) and neurodegeneration in Parkinson's disease(Lieberman et al., 1972;

Nagatsu et al., 1982), characterizing the ratio of DA/NE release by the LC may help determine the neural mechanisms behind these diseases.

4.2 Methods

4.2.1 Animals

Adult (20-35 g) male or female *Dbh*-cre or *Th*-cre mice and Cre (-) littermate control mice were used for *in vivo* experiments after backcrossing to C57BL/6J mice for at least 10 generations. Mice were group housed, given access to food pellets and water ad libitum, and maintained on a 12:12-hour dark/light cycle (lights off at 7:00 a.m.). Animals were held in a sound attenuated holding room facility in the lab starting at least one week prior to surgery, as well as post-surgery and throughout the duration of behavioral assays to minimize stress from transportation and disruption from foot traffic. All mice were handled and, where appropriate, connected to fiber optics two times a day for one week prior to behavioral experimental testing. All experimental procedures were approved by the Animal Care and Use Committee of Washington University and the Animal Care and Use Committee of University of Washington and conformed to NIH guidelines.

4.2.2 Stereotaxic surgery

Surgeries were performed under 2% isoflurane anesthesia (Piramal Healthcare, Maharashtra, India). All injections in BLA and CA1 were done using a Hamilton blunt syringe (Reno, NV), while injections into the LC were completed using a Hamilton beveled syringe (Reno, NV).

For detecting NE and DA dynamics in *ex-vivo* slice experiments, *Dbh*-cre mice were injected with 500nL of AAV1-hSyn-$GRAB_{NE2m}$-eGFP or AAV2/9-hSyn-WPRE-PA-$GRAB_{DA3m}$-eGFP into dorsal CA1 (AP: 1.9, ML: -1.4, DV: -1.65) (*Dbh*-cre::BLA or CA1: $GRAB_{DA}$ or $GRAB_{NE}$). To activate terminals while recording, Chrimson was injected into the LC (AP: -5.45, ML: -1.10, DV: -4.3 to -3.9) of the same mice (*Dbh*-cre::LC:Chrimson). Mice were allowed to recover and viruses to express for a minimum of 5 weeks.

For recording initial neural dynamics in response to behaviors, either 500nL of AAV2/9-hSyn-WPRE-PA-$GRAB_{DA3m}$-eGFP or AAV1-hSyn-$GRAB_{NE2m}$ (both prepared in the UW NAPE center Viral Core, Seattle, WA) were injected with a Hamilton blunt syringe (Reno, NV) into the BLA (AP: -1.4, ML: -3.15, DV: -4.8 to -4.55), dCA1 (AP: 1.9, ML: -1.4, DV: -1.65) of *Dbh*-cre mice (*Dbh*-cre::BLA or CA1:$GRAB_{DA}$ or $GRAB_{NE}$). For investigating the neuromodulator release in response to optogenetic activation of terminals, Chrimson was injected with a Hamilton beveled syringe (Reno, NV) into the LC (AP: -5.45, ML: -1.10, DV: -4.3 to -3.9) of the same mice as those which we were detecting behavioral neural dynamics. After injections, fiber optic ferrules (Doric) were chronically implanted above either the BLA or dCA1, and dental cement (Lang Dental, Wheeling, IL) or C&B Metabond was used to secure the implants. BLA and dCA1 implants and injections were done in the same mice. Mice were allowed to recover and viruses to express for a minimum of 5 weeks.

For investigating the neuromodulator release in response to optogenetic activation of terminals, the red-shifted channelrhodopsin ChrimsonR was injected with a Hamilton beveled syringe (Reno, NV) into the LC (AP: -5.45, ML: -1.10, DV: -4.3 to -3.9) of *Th*-cre mice (*Th*-cre::LC:Chrimson). To inhibit the VTA, the chemogenetic inhibitor AAV5-hSyn-

DIO-HA-hM4D(Gi) was injected bilaterally in the VTA of the same *Th*-cre mice (*Th*-cre::VTA^{bilat}:Gi-DREADDs). For detecting NE and DA dynamics in the same *Th*-cre mice, 500nL of AAV1-hSyn-GRAB$_{NE2m}$-eGFP or AAV2/9-hSyn-WPRE-PA-GRAB$_{DA3m}$-eGFP were injected into dorsal CA1 (AP: 1.9, ML: -1.4, DV: -1.65) and the BLA (AP: -1.4, ML: -3.15, DV: -4.8 to -4.55) (*Th*-cre::BLA or CA1:GRAB$_{DA}$ or GRAB$_{NE}$). After injections, fiber optic ferrules (Doric) were chronically implanted above the dCA1 (AP: 1.9, ML: -1.4, DV: -1.65) and the BLA (AP: -1.4, ML: -3.15, DV: -4.8 to -4.55), and C&B Metabond was used to secure the implants. We waited five weeks for viruses to express before initiation of stimulation experiments.

For dual-color neuromodulator recordings, 500nL of AAV9-hSyn-GRAB$_{rDA2m}$ and AAV1-hSyn-GRAB$_{NE2m}$-eGFP were injected into dorsal CA1 (AP: 1.9, ML: -1.4, DV: -1.65) and the BLA (AP: -1.4, ML: -3.15, DV: -4.8 to -4.55) (*Th*-cre::BLA or CA1:GRAB$_{rDA}$ and GRAB$_{NE}$). We injected the cre-dependent chemogenetic inhibitor AAV5-hSyn1-DIO-HA-hM4D(Gi) bilaterally in the LC or VTA of *Th*-cre mice (*Th*-cre::LC^{bilat}:Gi-DREADDs) or (*Th*-cre::VTA^{bilat}:Gi-DREADDs). After injections, fiber optic ferrules (Doric) were chronically implanted above the dCA1 (AP: 1.9, ML: -1.4, DV: -1.65), and C&B Metabond was used to secure the implants. We waited five weeks for viruses to express before initiation of stimulation experiments.

4.2.3 Tissue collection and immunohistochemistry

After the conclusion of behavioral testing, mice were anesthetized with sodium pentobarbital and transcardially perfused with ice-cold PBS, followed by 4% phosphate-buffered paraformaldehyde. Brains were removed, postfixed overnight in 4%

paraformaldehyde, and then saturated in 30% phosphate-buffered sucrose for 2–4 days at 4 °C. Brains were sectioned at 30 mM on a microtome and stored in a 0.01 M phosphate buffer at 4 °C prior to immunohistochemistry and tracing experiments. For behavioral cohorts, viral expression and optical fiber placements were confirmed before inclusion in the presented datasets. Viral expression and implant placements were verified using fluorescence and confocal (Leica Microsystems) microscopy. Images were produced with 10X, 20X, and 63X objectives and analyzed using ImageJ software (NIH) and Leica Application Suite Advanced Fluorescence software.

4.2.4 Looming stimulus

Adult mice were put in a custom-made open clear acrylic box, (50cm x 50cm) within a sound-attenuated room maintained at 23°C. The open box had white paper on all walls to limit outside stimuli. Mice were allowed to roam the box for 11 minutes prior to stimulus presentation to habituate to the box. At 11 minutes and in 60s intervals, a looming posterboard blocking overhead lighting was held over the arena for 10s. This was repeated 5 times. Fiber photometry was recorded for multiple biosensors detecting neural dynamics.

4.2.5 Reward retrieval and consumption

Mice were initially food deprived to 90% of their body weight. Prior to testing, we put multiple sucrose pellets per mouse in their home cage to extinguish neophobia of this reward. On testing days, we placed mice in a modular (17.8×15.2×18.4cm^3; Med Associates Inc.) arena where they were allowed to freely roam. Using MEDPC program,

we randomly delivered rewards at a pseudorandom ITI of 90-150s, with a total of 18 possible rewards in each session. Fiber photometry was recorded for multiple biosensors detecting neural dynamics.

4.2.6 Shock stimulus

Mice were placed in a modular arena and allowed to freely roam. After a baseline period of 180s in the arena, mice experienced the shock of a 0.5-0.7mA current run through the metal grating floor of the arena for 2s. There was a pseudorandom ITI of 20-90s, with 10 total shocks. Fiber photometry was recorded for multiple biosensors detecting neural dynamics. Video was recorded for the duration of the shock protocol and for 180s after. EzTrack(Pennington et al., 2019) was used to track and align freezing bouts for behavioral analysis.

4.2.7 In-vivo fiber photometry

An optic fiber was secured to implanted fibers on experimental mice with a ferrule sleeve (Doric, ZR_2.5). Two light-emitting diodes (LEDs) were driven by a real-time processor (TDT, either RZ5P or RZ10x) that recorded dynamics from optic fibers detecting biosensor activity expressed in the brain, with 531-Hz sinusoidal 470nm (465nm on the RZ5P) and 211-Hz sinusoidal 405nm light. The 470nm LED was used to record emitted light from green sensors ($GRAB_{NE}$, dLight, and $GRAB_{DA}$) while the 405nm LED served as an isosbestic control. In dual sensor recordings taken with the RZ10x, 311-Hz sinusoidal 535nm light was used to record red sensors ($GRAB_{rDA}$). LED power for each LED wavelength were measured at the tip and adjusted to 30uW before each day of

recording. For optogenetic stimulation, a 625nm LED was pulsed with 5ms pulse width for 3 or 30s. Laser power was adjusted to obtain 15mW transmittance into the brain.

4.2.8 Photometry analysis

A custom MATLAB script was developed for analysis of photometry recordings in the context of mouse behavior. For each photometry recording, a linear-least squares regression was used to find the projection of the isosbestic curve onto the 470 nm excitation photometry trace. The best fit isosbestic 405 nm excitation control signal was subtracted from the 470nm excitation signal to remove artifacts from intracellular NE-dependent sensor fluorescence(Lerner et al., 2015). Baseline drift was evident in the signal due to slow photobleaching artifacts, particularly the first several minutes of each recording session, and the linear least squares subtraction of the isosbestic control signal eliminated the drift seen in the 470nm excitation signal. After centering the signal around the first three minutes of the session, the photometry trace was z-scored relative to the mean and standard deviation of the test session. The post-processed fiber photometry signal was analyzed by time-locking each onset of behavior or stimulus, centering the data, and averaging the signal.

4.2.9 *Ex vivo* slice preparation

Mice were briefly anesthetized with isofluorane. Mice were perfused with cold N-methyl-d-glucamine (NMDG)–substituted artificial cerebrospinal fluid (aCSF) containing 93mM NMDG, 2.5mM KCl, 1.25mM NaH2PO4, 30mM NaHCO3, 20mM Hepes, 25mM glucose, 5mM ascorbic acid, 2mM thiourea, 3mM Na-pyruvate, 12mM N-acetyl-l-cysteine, 10mM MgSO4, and 0.5mM CaCl2. After perfusion, brains were extracted. Coronal

sections of the hippocampus were cut to a slice thickness of 250μm using a vibrating Leica VT1000S microtome in a bath of cold, oxygenated NMDG solution. The slices were then placed in hot NMDG aCSF solution (32-34 degrees C) for 10min. Then slices were placed in a room temperature holding chamber filled with HEPES solution consisting of: 92mM NaCl, 2.5mM KCl, 1.2 mM NaH2PO4, 30 mM NaHCO3, 20mM Hepes, 25 mM glucose, 2 mM CaCl2, 2mM MgCl2 (pH adjusted to 7.3 to 7.4 with NaOH). The samples were kept in the HEPES solution for at least 30min prior to 2-photon imaging and were covered to minimize photobleaching. For both HEPES and NMDG osmolality was confirmed to be between 300-310mOsm/kg, and pH was confirmed to be between 7.3-7.4.

4.2.10 2-photon slice imaging, optogenetic stimulation, and pharmacology

Flow rate of ACSF or drug was maintained at 2mL/min. Temperature of flowing ACSF was controlled at 31-34°C by the temperature controller TC-324C before any slice was added to the bath. An anchor was used to keep the brain slice stable while ACSF or ACSF and drug was washed on. A vacuum pump ensured a steady 2mL/s of flow. An Olympus 4x UPlanFL N lens was used to localize expression, and then an Olympus 20x XLPLN25XWMP lens 2mm working distance for water immersion, and we acquired images with Olympus FV31S-SW software. The 2-photon scope used was an FVMPE-RS Olympus 2p scope powered by a Mai Tai Ti-sapphire laser with dispersion compensation running at 920nm. Individual frames were acquired at 0.92hz using a Galvano scanner with a resolution of 512px x 512px.

After setting up a slice on the 2-photon rig, we ran a positive control trial by washing high concentration (100μM) reactive ligand over the sensor-expressing slice. Once reactivity to the reactive ligand was confirmed, we allowed oxygenated ACSF to flow for 5 minutes for ligand to unbind from sensor. We next initiated optogenetic stimulation of brain slices using a 615nm red LED (CoolLED) controlled by a master-9 stimulator, programmed for either 5hz or 20hz stimulation for 3s or 30s, with a pulse-width of 5ms and limited to power of 3mW. Ligand solutions were oxygenated for at least 5min prior to washing on slices. Ligands were prepared with concentrations of between 3nM to 100μM.

Following optogenetic stimulation trials, we allowed oxygenated ACSF to flow over slices for at least 5 minutes for ligand to unbind from sensors before initiating ligand washes for concentration response curves. In some washes, we pumped ligand for 60s and recorded for two additional minutes to capture sensor binding and unbinding. We waited one minute between sessions of low concentration and 3-5min for higher concentration washes. We confirmed fluorescence resembled baseline of the previous session before initiating another wash, and would alternate between high concentration ligand washes and low concentration washes (30μM, 10nM, 10μM, etc).

4.2.11 Pupillometry

Mice were anesthetized with 2% isofluorane. An infrared light was set up to record the mouse's pupil from a FLIR camera (1:1.4CCTV Lens, 9-22 mm lens with 1/3" focal length). Pupil contrast was carefully checked before recording session started. After 10min of recording for a baseline, we injected mice with either CNO (0.5 mg/kg i.p.) or saline vehicle. At least 45min after injection were recorded to track any changes in radii

due to inhibition of the LC. We used a pupillometry analysis toolbox developed and described in Privitera et al., 2020[79].

4.2.12 DBH-KO mice breeding and experiments

A total of 40 *Dbh*(-/-)mice, maintained on a mixed 129/SvEv and C57BL/6 J background as previously described(Thomas et al., 1995; Thomas & Palmiter, 1997), were used in this study. *Dbh*(-/-) males were bred to *Dbh*(+/-) females, and pregnant *Dbh*(+/-) dams were administered drinking water containing the β-adrenergic receptor (AR) agonist isoproterenol and the α_1AR agonist phenylephrine (20 μg/ml each; Sigma-Aldrich) with vitamin C (2 mg/ml) from E9.5E14.5, and the synthetic NE precursor L-3,4-dihydroxyphenylserine (DOPS; 2 mg/ml; Lundbeck, Deerfield, IL) + vitamin C (2 mg/ml) from E14.5-parturition to prevent embryonic lethality resulting from complete *Dbh* deficiency. *Dbh*(-/-) mice are easily distinguished from their NE-competent littermates by their visible delayed growth and bilateral ptosis phenotypes. *Dbh*(+/−) littermates were used as controls because their behavior and catecholamine levels 5 are indistinguishable from wild-type *Dbh*(+/+) mice(Bourdélat-Parks et al., 2005; Szot et al., 1999; Thomas & Palmiter, 1997). *Dbh*(-/-) males were bred to *Th*-cre females to produce *Th*-cre *Dbh*(-/-) mice.

All animal procedures and protocols were approved by the Emory University Animal Care and Use Committee, in accordance with the National Institutes of Health guidelines for the care and use of laboratory animals. Mice were maintained on a 12 h/12 h light/dark cycle (7:00/19:00 h) with access to food and water ad libitum, except during behavioral testing. Behavioral testing was conducted under standard lighting conditions

during the light cycle (14:00-17:00) in the same room where the mice were housed to minimize the stress of cage transport on test days.

To record NE or DA dynamics, 500nL of AAV1-hSyn-GRAB$_{NE2m}$ (prepared in the UW NAPE center Viral Core, Seattle, WA) or AAV2/9-hSyn-DA3m-WPRE-PA (Brain VTA) were injected with a Hamilton blunt syringe (Reno, NV) into CA1 (AP: 1.9, ML: -1.4, DV: -1.65) of *Dbh*(+/+)-cre, *Th*-cre *Dbh*(+/-), and *Th*-cre *Dbh*(-/-) mice. For inhibition experiments, AAV5-hSyn1-DIO-HA-hM4D (Gi) were injected bilaterally in the LC (AP: -5.45, ML: -1.10, DV: -4.3 to -3.9) or the VTA (15 degree angle, AP: -3.25, ML: -1.6, DV: -4.7 to -4.2). We waited five weeks for viruses to express before initiation of aversive and appetitive experiments.

For investigating the neuromodulator release in response to optogenetic activation of terminals, the red-shifted channelrhodopsin ChrimsonR was injected with a Hamilton beveled syringe (Reno, NV) into the LC (AP: -5.45, ML: -1.10, DV: -4.3 to -3.9). After injections, fiber optic ferrules (Doric) were chronically implanted above the dCA1 (AP: 1.9, ML: -1.4, DV: -1.65), and C&B Metabond was used to secure the implants. We waited five weeks for viruses to express before initiation of stimulation experiments, done in accordance with photometry methods.

4.2.13 Quantification and statistical analysis

All data are expressed as mean ± SEM. Behavioral data were analyzed with GraphPad Prism 10.0 (GraphPad, La Jolla, CA). Two-tailed student's t test, one-way or two-way ANOVAs were used to analyze between-subjects designs. Repeated-measures designs were analyzed using a mixed-effects restricted maximum likelihood (REML) model. Tukey

was used for post-hoc pairwise comparisons. The null hypothesis was rejected at the $p < 0.05$ level. Statistical significance was taken as *$p < 0.05$, **$p < 0.01$, ***$p < 0.005$, n.s. represents not significant. All statistical information is listed in Supplementary Table 1.

4.3 Results

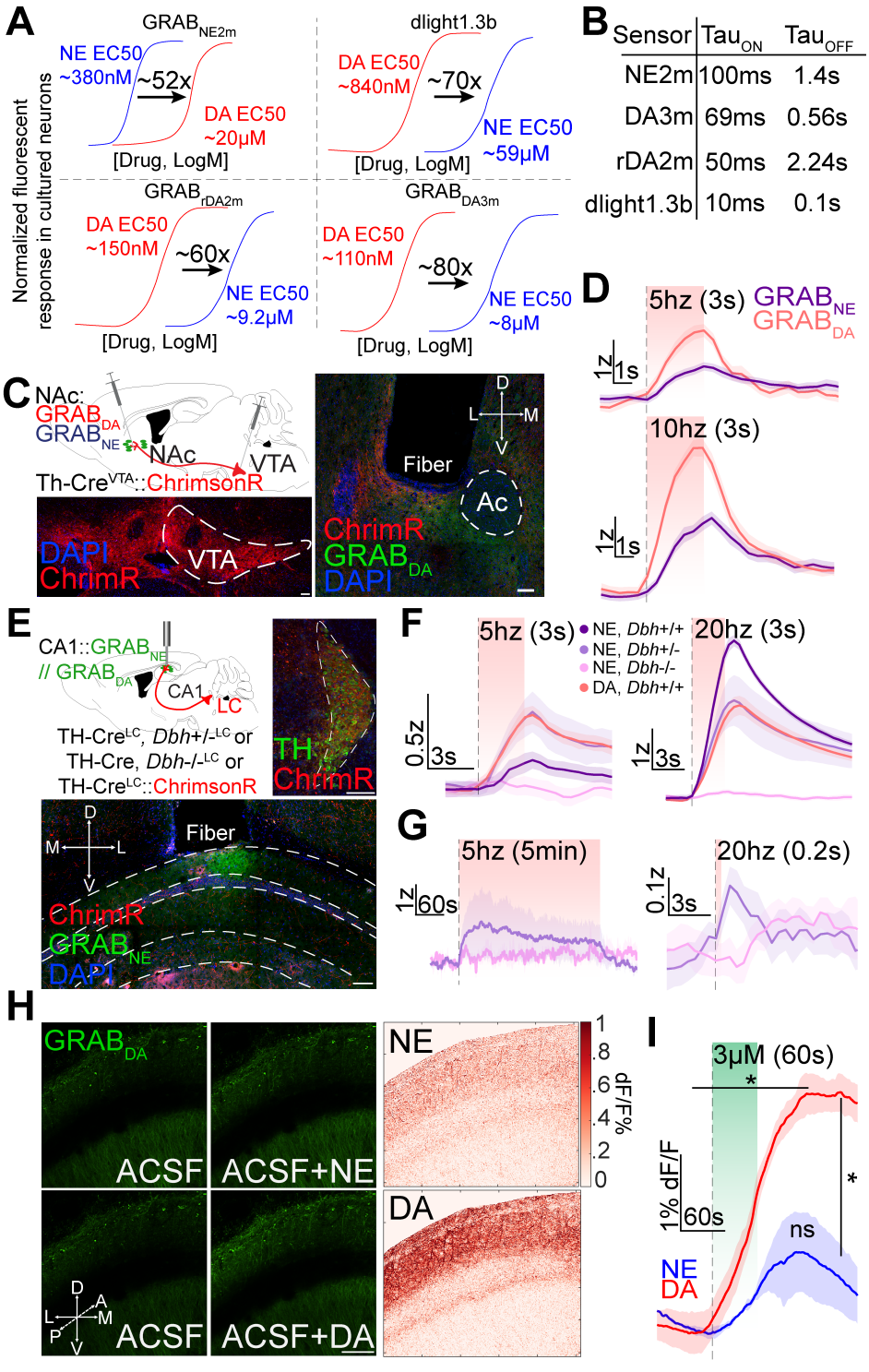

Figure 4.1. Biosensors are sufficiently selective for their respective ligand. A. Concentration response curves of various sensors used in this study for NE and DA. EC50s for both NE and DA and the fold differences are recorded. **B.** On and off kinetics of the sensors. **C.** Schematic depicts infection of VTA-DA cells with ChrimsonR (AAV5-hSyn-FLEX-ChrimsonR-tdTomato) and $GRAB_{NE}$ or $GRAB_{DA}$ in NAc**.** Representative image of ChrimsonR expression in VTA cell bodies (bottom) and terminals in NAc (right), with $GRAB_{DA}$ expression in NAc. Scale bar, 100μm. **D.** VTA-NAc^{TH} terminal stimulation at 5hz for 3s (top) or 10hz for 3s (bottom) **E.** Schematic of experimental approach for *Th*-cre, *Dbh*-/-, and control *Dbh*+/- heterozygous mice. ChrimsonR was injected into LC (right) and $GRAB_{NE}$ in CA1 (bottom). Scale bar, 100μm. **F.** Averaged $GRAB_{NE}$ and $GRAB_{DA}$ responses to LC-CA1 stimulation during different stimulation paradigms (left to right) 5hz (3s) and 20hz (3s). **G.** Averaged $GRAB_{NE}$ responses to tonic (left) and phasic (right) LC-CA1 stimulation during different stimulation paradigms 5hz 5min (left) and 20hz 200ms (right). *Dbh*(-/-) indicates *Dbh*-KO mice, n=3, while *Dbh*+/- indicate heterozygous controls, n=2, and *Dbh*+/+ are *Th*-cre mice, n=9 for $GRAB_{NE2m}$, n=3 for $GRAB_{DA3m}$. **H.** Representative images of baseline (left) and 3μM NE (middle top) or 3μM DA (middle bottom) washes, with heatmaps (right) showing change in fluorescence (ΔF/F). Scale bar, 100μm. **I.** Averaged traces of 3μM NE and 3μM DA washes. n=2.

4.3.1 Pharmacological selectivity does not account for biosensor detection differences in NE and DA release from LC axons

Because activation of catecholamine sensors by the off-target catecholamine (DA in the case of $GRAB_{NE2m}$) has been reported(López et al., 2024b), it is important to test the limitations of these sensors *in vivo*. If ligand selectivity of each biosensor is not considered, then the results of the stimuli-dependent release could be misconstrued, across any region where dual NE and DA innervation is present. We compiled the most updated EC50s generated *in vitro* (i.e. the presumed K_D due to lack of G-protein coupling) for DA and NE at each GPCR-based sensor for examining the difference in DA vs NE selectivity (**Figure 4.1A**)(Feng et al., 2019b, 2024; Patriarchi et al., 2018b; Sun et al., 2020). Among the available sensors, the most selective DA sensor is $GRAB_{DA3m}$, with an EC50 of 110nM for DA and 8μM for NE, representing an 80-fold difference in selectivity. The next most selective DA sensor at the time of this study was dLight1.3b, which has a 70-fold difference in selectivity, but also has a larger EC50 for NE than other sensors, at 59μM. $GRAB_{rDA2m}$ has a 60-fold difference in selectivity, and

similar EC50s for NE and DA compared to $GRAB_{DA3m}$. Compared to dLight, the $GRAB_{DA3m}$ sensors have a higher affinity for both the target catecholamine and for the non-targeted catecholamine. NE has less affinity at $GRAB_{NE2m}$ than DA has at $GRAB_{DA3m}$ sensors. Comparing on/off kinetics of these catecholamine biosensors is a powerful method of determining separability of recorded signals. The dLight1.3b sensor has a τ_{on} (10ms) 5-7 times faster than $GRAB_{DA3m}$ (69ms) and $GRAB_{rDA2m}$ (50ms) (**Figure 4.1B**). While they have a similar τ_{on} rate (50-69ms), the red $GRAB_{rDA2m}$ sensor has τ_{off} (2.24s) 4 times slower than the $GRAB_{DA3m}$ sensor (0.56s). Here, we use these kinetics to compare neuromodulator recordings during behavior and qualitatively explain the likely separability of simultaneously recorded signals.

4.3.2 $GRAB_{NE}$ does not detect DA *in vivo* in response to biologically relevant photostimulation

In this study, we employed several catecholamine sensors to understand DA release from LC. The rank order of selectivity (from highest to lowest) of DA sensors is $GRAB_{DA3m}$ (80x NE/DA, $EC50_{NE}$ = 8μM), dlight1.3b (70x, $EC50_{NE}$ = 59μM), $GRAB_{rDA2m}$ (60x, $EC50_{NE}$ = 9.2μM)(Feng et al., 2019b, 2024; Patriarchi et al., 2018b). $GRAB_{NE2m}$ has a 52-fold difference between NE and DA, with $EC50_{DA}$= 20μM. Because $GRAB_{NE2m}$ has the lowest fold-difference in selectivity, we tested $GRAB_{NE}$'s selectivity by stimulating VTA terminals in BLA and CA1 *in vivo*. We injected either $GRAB_{NE2m}$ or $GRAB_{DA3m}$ in the BLA or CA1 and Cre-dependent viral vectors containing the red-shifted excitatory opsin ChrimsonR, AAV5-hSyn-DIO-ChrimsonR-tdTmto, into the VTA of *Th*-cre mice (*Th*-cre::VTA:ChrimsonR) (**Figure S1A**).

To evoke DA release from VTA terminals, we mimicked sustained low tonic activation (5hz for 30s) and brief, phasic activation (20hz for 3s) that would not inherently be rewarding(Millard et al., 2024) to determine if DA release binds to $GRAB_{NE2m}$. First, we stimulated VTA terminals in BLA and found $GRAB_{NE2m}$ signal increased during both stimulation paradigms (**Figure S1B**). We found that when we stimulated VTA terminals in CA1, there were also subtle increases in $GRAB_{NE2m}$ fluorescence (**Figure S1C**). To assess these results further, we repeated this experiment in a region with substantially less NE innervation by stimulating VTA terminals in the nucleus accumbens (NAc) (**Figure 4.1C**), which we expected to produce a heightened $GRAB_{DA3m}$ signal. We detected increased $GRAB_{DA3m}$ fluorescence, but a modest $GRAB_{NE2m}$ signal was still detected in response to VTA-NAc stimulation (**Figure 4.1D**). Considering that the NAc contains a 1:10 ratio of NE to DA(Koob et al., 1975), we recognized the need to detect $GRAB_{NE2m}$ signal in a completely NE-deficient environment.

To do so, we stimulated LC-CA1 terminals in mice globally deficient in DBH, rendering them unable to produce NE. We expressed AAV5-hSyn-DIO-ChrimsonR-tdTmto in the LC of *Dbh*(+/+) mice (*Dbh*-cre::LC:ChrimsonR), *Dbh*(+/-) mice (*Th*-cre, *Dbh*(+/-)::LC:ChrimsonR) that have similar NE content to *Dbh*(+/+) mice, or *Dbh*(-/-) mice (*Th*-cre, *Dbh*(-/-)::LC:ChrimsonR), and $GRAB_{NE2m}$ in CA1 (**Figure 4.1E**). We found that *Dbh*(-/-) mice had no increase in $GRAB_{NE2m}$ fluorescence when photostimulating for 3 seconds at 5hz or 20hz (**Figure 4.1F**). In contrast, $GRAB_{NE2m}$ fluorescence increased in response to LC-CA1 photostimulation in both *Dbh*(+/+) and heterozygous *Dbh*(+/-) mice (**Figure 4.1F**). Similarly, in response to LC-CA1 photostimulation at both 5hz and 20hz, we detected robust increases in $GRAB_{DA3m}$ signal in *Dbh*(+/+) mice (**Figure 4.1F-G**).

These data suggest that in response to LC-CA1 stimulation in the absence of NE production, $GRAB_{NE2m}$ does not detect NE and $GRAB_{DA3m}$ is detecting DA.

The qualitative differences in $GRAB_{NE2m}$ signal between *Dbh*(+/+) and *Dbh*(-/-) mice is likely due to differences in strain background (C57Bl/6J and mixed C57Bl/6J;129SvEv, respectively). To simulate physiological LC activity at high tonic or phasic activation mimicking exposure to a novel-stimulus, we optogenetically stimulated LC terminals in CA1 at 5hz for 5min or at 20hz for 200ms while recording $GRAB_{NE2m}$ signal. We observed that in both activation paradigms, stimulating LC terminals in heterozygous *Dbh*(+/-) controls increased $GRAB_{NE2m}$ fluorescence, while the same experiment in *Dbh*(-/-) mice revealed no activation of $GRAB_{NE2m}$ (**Figure 4.1H**). These results indicate that the least selective catecholamine biosensor, $GRAB_{NE2m}$ (**Figure 4.1A**), does not detect appreciable increases in $GRAB_{DA3m}$ fluorescence at the upper boundary of stimulation parameters where we detect DA release from LC axon terminals (**Figure 4.1F**).

To further characterize the selectivity of sensors, we used *ex vivo* slice 2-photon imaging to record sensor activity while washing on high concentrations of ligands. We injected either $GRAB_{NE2m}$ or $GRAB_{DA3m}$ in the CA1 of WT mice. After waiting a minimum 5 weeks for expression, we recorded $GRAB_{NE2m}$ or $GRAB_{DA3m}$ fluorescence in coronal hippocampal slices in response to washes using 2-photon imaging (**Figure 4.1H**). When we washed 3μM of NE or DA on slices expressing $GRAB_{DA3m}$, respectively, we observed robust increases in $GRAB_{DA3m}$ fluorescence to DA (Sidak's multiple comparisons test, $p=0.0115$) compared to baseline, no significant change in fluorescence from baseline when NE was washed on ($p=0.23$), and a significant difference between NE and DA

(Sidak's multiple comparisons test, 0.0325). These data suggest $GRAB_{DA3m}$ is responding to DA and not NE in tissue slices at as high a concentration as 3μM.

4.3.3 *Ex vivo* photostimulation of LC terminals causes release of DA in a frequency-dependent manner

Having demonstrated $GRAB_{NE2m}$ and $GRAB_{DA3m}$'s selectivity over the potential cross-reactive catecholamine, we next sought to better describe the DA release evoked from the LC. To characterize LC-evoked DA release, we used *ex vivo* slice imaging which severs upstream circuit interactions while maintaining local, intact DA release from LC-$CA1^{Dbh}$ terminals. Imaging *ex vivo* also cuts off potential antidromic activation of LC cell bodies and subsequent VTA-DA neuron activation downstream. We injected either $GRAB_{NE2m}$ or $GRAB_{DA3m}$ in the CA1 and Cre-dependent viral vectors containing ChrimsonR, AAV5-hSyn-DIO-ChrimsonR-tdTmto, into the LC of *Dbh*-cre mice (*Dbh*-cre::LC:ChrimsonR). After waiting a minimum 5 weeks for expression, we recorded $GRAB_{NE2m}$ or $GRAB_{DA3m}$ fluorescence in coronal hippocampal slices in response to photostimulation of *Dbh*-cre::LC:ChrimsonR projections (615nm, 5 or 20hz, 5ms pulse width) using 2-photon imaging (**Figure 4.2A**). First, we established sensor expression with a positive control wash of 30μM NE or DA on slices expressing $GRAB_{NE2m}$ or $GRAB_{DA3m}$, respectively (**Figure 4.2B**). After establishing consistent sensor responses to either NE or DA, we photostimulated LC-$CA1^{Dbh}$ terminals over the full-field, pulsing a 615nm red LED at 5 or 20hz (3 or 30s duration, 5ms pulse width, 3mW) to determine evoked DA release across a range of LC activation intensities. In **Figure 4.2C**, an averaged $GRAB_{DA3m}$ trace during 20hz stimulation of LC-$CA1^{Dbh}$ terminals for 30s is provided, indicating robust $GRAB_{DA3m}$ responses to LC-$CA1^{Dbh}$ terminal stimulation.

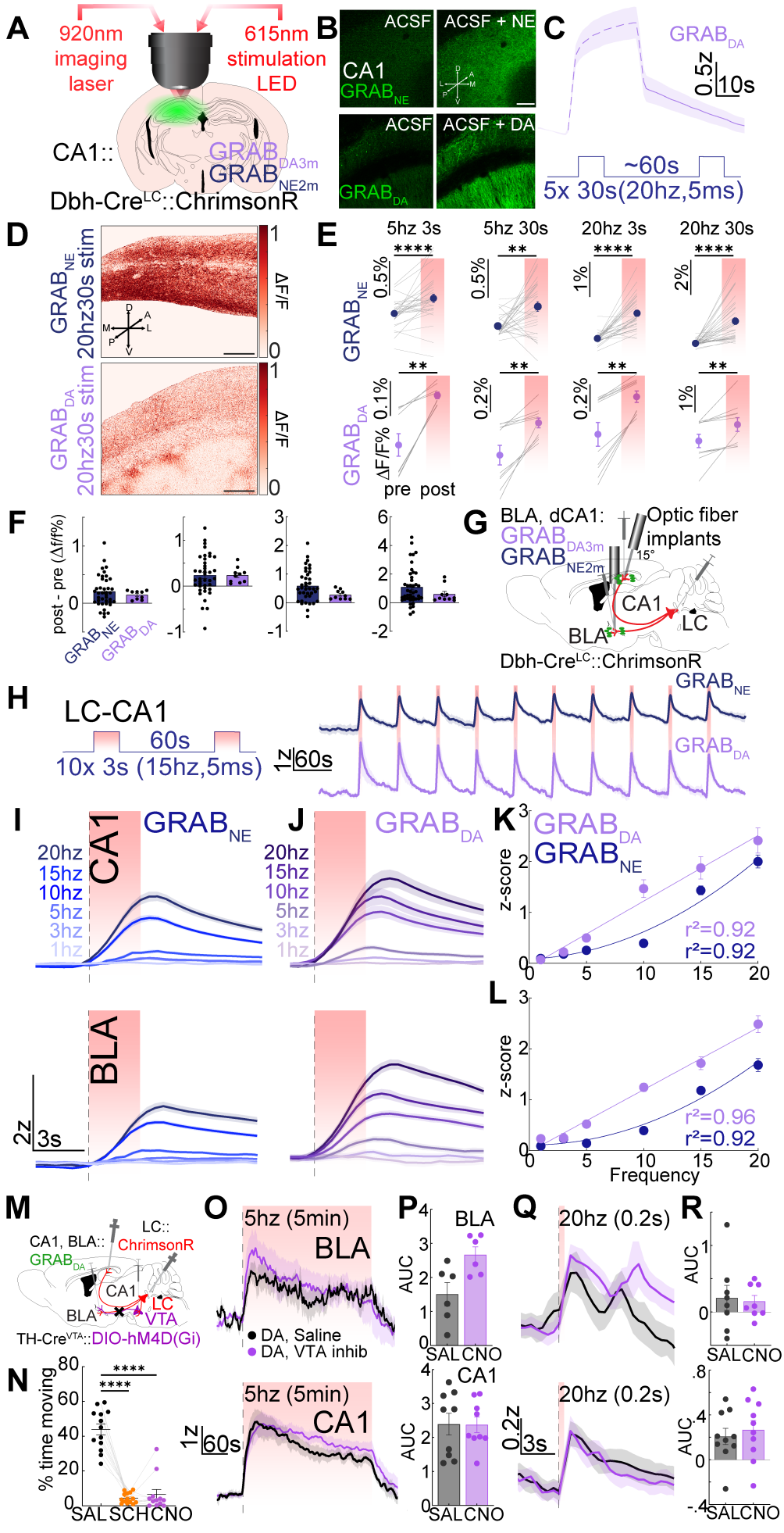
A
920nm imaging laser
615nm stimulation LED
CA1::
GRAB DA3m
GRAB NE2m
Dbh-Cre LC ::ChrimsonR
B
ACSF
ACSF + NE
CA1
GRAB NE
ACSF
ACSF + DA
GRAB DA
C
GRAB DA
0.5z
10s
~60s
5x 30s(20hz,5ms)
D
GRAB NE 20hz30s stim
GRAB DA 20hz30s stim
ΔF/F
E
5hz 3s
5hz 30s
20hz 3s
20hz 30s
GRAB NE
GRAB DA
ΔF/F%
pre post
F
post - pre (Δf/f%)
GRAB NE
GRAB DA
G
BLA, dCA1:
GRAB DA3m
GRAB NE2m
Optic fiber implants
15°
CA1
LC
BLA
Dbh-Cre LC ::ChrimsonR
H
LC-CA1
60s
10x 3s (15hz,5ms)
1z
60s
GRAB NE
GRAB DA
I
CA1
GRAB NE
20hz
15hz
10hz
5hz
3hz
1hz
BLA
2z
3s
J
GRAB DA
K
GRAB DA
GRAB NE
z-score
r²=0.92
r²=0.92
L
z-score
r²=0.96
r²=0.92
Frequency
M
CA1, BLA::
LC::
ChrimsonR
GRAB DA
CA1
BLA
LC
VTA
TH-Cre VTA ::DIO-hM4D(Gi)
N
% time moving
SAL SCH CNO
O
5hz (5min)
BLA
DA, Saline
DA, VTA inhib
5hz (5min)
CA1
1z
60s
P
BLA
AUC
SAL CNO
CA1
Q
20hz (0.2s)
20hz (0.2s)
0.2z
3s
R
AUC
SAL CNO

Figure 4.2. Evoked LC-DA axonal release *in vivo* follows a frequency-dependent linear relationship and is independent of VTA activity. A. Schematic of experimental approach of surgical injections and 2-photon imaging approach with optical stimulation. Schematic depicts infection of LC-NE cells with ChrimsonR (AAV5-hSyn-FLEX-ChrimsonR-tdTomato) and either $GRAB_{DA3m}$ or $GRAB_{NE2m}$ in CA1. **B.** Representative 2-p images. 30μM NE was washed on $GRAB_{NE}$ (top), and 30μM DA on $GRAB_{DA}$ (bottom), expressing slices. Rolling average of 5s, scale bar 100μm. **C.** Representative average of $GRAB_{DA}$ response to 20hz 30s pulses of optical stimulation of LC-CA1 terminals. Stimulation paradigm depicted below example trace. **D.** Heatmap of the $GRAB_{NE}$ (top) and $GRAB_{DA}$ (bottom). ΔF/F response to 20hz 30s stim of LC-CA1 terminals. Δ represents change from right before stimulation, gaussian filter applied to smooth baseline images. **E.** ΔF/F% change of pre to post in $GRAB_{NE}$ (top, n=4 biological replicates, 6 slices) and $GRAB_{DA}$ (bottom, n=2) in response to a range of stimulation paradigms: 5hz 3s, 5hz 30s, 20hz 3s, 20hz 30s (left to right). Wilcoxon matched-pairs signed rank test: $GRAB_{NE}$: 5hz 3s, $p<0.0001$; 5hz 30s, $p=0.0019$; 20hz 3s, $p<0.0001$; 20hz 30s, $p<0.0001$; $GRAB_{DA}$: 5hz 3s, $p=0.0039$; 5hz 30s, $p=0.002$; 20hz 3s, $p=0.002$; 20hz 30s, $p=0.002$. **F.** Schematic of surgical approach for in vivo photometry cohort. $GRAB_{DA}$ or $GRAB_{NE}$ were expressed in CA1 and BLA with fiber photometry implants, and ChrimsonR expressed in LC. Scale bar, 100μm. **G.** Comparison of the change in ΔF/F response for $GRAB_{NE}$ and $GRAB_{DA}$ in each stim trial from before to after stimulation across the same paradigms in **2E**. Mann-Whitney: 5hz 3s, n.s., $p=0.96$; 5hz 30s, n.s., $p=0.91$; 20hz 3s, n.s., $p=0.09$; 20hz 30s, n.s., $p=0.27$. **H.** Average photometry trace of LC-CA1 stimulation for 3s at 10hz, with a 5ms pulse width. n=5. **I.** Averaged in vivo photometry traces of $GRAB_{NE}$ responses to LC-CA1 (top) and LC-BLA (bottom) terminal stimulation. **J.** Averaged photometry traces of $GRAB_{DA}$ responses to LC-CA1 (top) and LC-BLA (bottom) terminal stimulation. **K.** Frequency response curves for LC-CA1 terminal stimulation for $GRAB_{NE}$ and $GRAB_{DA}$. Second-order curve fit to $GRAB_{NE}$, n=5-9, $r^2= 0.92$, and linear regression fit to $GRAB_{DA}$, n=3, $r^2= 0.92$. **L.** Frequency response curves for LC-BLA terminal stimulation for $GRAB_{NE}$, n=6, and $GRAB_{DA}$, n=3. Second-order curve fit to $GRAB_{NE}$, $r^2= 0.92$, and linear regression fit to $GRAB_{DA}$, $r^2= 0.96$. **M.** Schematic of experimental approach of surgical injections of LC-NE cells with ChrimsonR (AAV5-hSyn-FLEX-ChrimsonR-tdTomato), VTA-DA cells with Gi-DREADDs (AAV5-hSyn1-DIO-HA-hM4D(Gi)), and $GRAB_{DA3m}$ in CA1, of *Th*-cre mice. **N.** VTA inhibition decreased the time mice spent moving. SAL, n=7; SCH, n=7; CNO, n=6. **O.** Average trace of $GRAB_{DA}$ response to tonic stimulation (5hz, 5min) of LC terminals in BLA (top; n=8) and CA1 (bottom, n=10), with VTA inhibition (purple) or saline controls (black). **P.** AUC for 120s after start of 5hz stimulation for mice injected with saline or CNO (VTA Inhibition). **Q.** Average trace of $GRAB_{DA}$ response to phasic stimulation (20hz 200ms) of LC terminals in BLA (top; n=8), and CA1 (bottom, n=10). **R.** AUC for 3s after start of 20hz, 200ms stimulation for mice injected with saline or CNO (VTA Inhibition).

In both $GRAB_{DA3m}$ and $GRAB_{NE2m}$ expressing CA1 slices, we observed a significant increase in fluorescence across all stimulation paradigms tested (**Figure 4.2D-E**). We compared the change in ΔF/F% at each of the stimulation paradigms and found that none of the ΔF/F% changes between $GRAB_{NE2m}$ and $GRAB_{DA3m}$ response were significantly different (**Figure 4.2F**). To test the consistency of these results, we repeated these *ex vivo* experiments with dLight expressed in CA1, and ChrimsonR expressed in the LC of *Dbh*-cre mice (**Figure S2A-B, I**). We only observed significant increases in

fluorescence when we stimulated for 3s at 20hz, while other paradigms were more variable in their detected DA release (**Figure S2C**). These results indicate DA is released from LC-CA1^{Dbh} terminals *ex vivo,* regardless of any connections from LC to other dopaminergic nuclei.

4.3.4 Evoked LC-NE axonal release *in vivo* follows a frequency-dependent, non-linear relationship

Our *ex vivo* results demonstrate that photostimulating LC-CA1^{Dbh} axon terminals evokes DA release. We next determined how LC-evoked DA release varies across a range of photostimulation paradigms that parallel natural neuronal LC activity *in vivo*(Bourdélat-Parks et al., 2005; Devilbiss & Waterhouse, 2011b; Szot et al., 1999; Thomas et al., 1995, 1998) and examined two target regions. We injected either $GRAB_{NE2m}$ or $GRAB_{DA3m}$ in CA1 or BLA, and Cre-dependent viral vectors containing ChrimsonR, into the LC of *Dbh*-cre mice (*Dbh*-cre::LC:ChrimsonR; **Figure 4.2G**). We implanted optical fibers above injection sites in BLA and CA1 to record photometric signals during optogenetic stimulation of LC axon terminals.

During periods of low arousal, such as sleep, LC fires tonically at ~1-3hz. In high arousal states, like stress, elevated tonic LC-NE neuron firing rates are observed (between 5-10hz)(Aston-Jones & Cohen, 2005; Curtis et al., 2012; Devilbiss & Waterhouse, 2011b; Poe et al., 2020). Recent studies report release of DA from LC-CA1 projections in response to photostimulation at 20hz(Kempadoo et al., 2016a; Takeuchi et al., 2016c). Thus, we stimulated the LC-CA1^{Dbh} and LC-BLA^{Dbh} projections for 3s at 1, 3, 5, 10, 15, and 20hz with a 5ms pulse width and a total of 10 stimulation trains each session

with an interstimulation interval of 1min (**Figure 4.2H-L**). We depict a representative averaged response of $GRAB_{NE2m}$ and $GRAB_{DA3m}$ to the stimulation at 15hz for 3s in **Figure 4.2H**. We also depict the responses to LC-CA1 stimulation averaged across frequency in **Figure 4.2I** for $GRAB_{NE2m}$ recordings and **Figure 4.2J** for $GRAB_{DA3m}$ recordings. To characterize trends within each sensor and across regions, we plotted the peak responses across the frequencies tested in CA1 (**Figure 4.2K**) and in BLA (**Figure 4.2L**). LC-BLA^{NE} and LC-$CA1^{NE}$ release across frequencies strongly matched a second-order polynomial fit (adjusted R^2 values in CA1 was 0.92, BLA was 0.92). LC-$CA1^{DA}$ and LC-BLA^{DA} release across frequencies more closely followed a linear regression model, with adjusted R^2 values of 0.92 in CA1 and 0.96 in BLA (**Figure 4.2L**).

We repeated these experiments in mice expressing dLight in CA1 and BLA, with Cre-dependent ChrimsonR expressed in the LC of *Dbh*-cre mice (**Figure S2D, I**). We repeated *in vivo* stimulation for 3s across the same range of frequencies reported in **Figure 4.2H-L** (1-20hz) and depicted averaged responses in **Figure S2E, G**. We characterized trends in DA dynamics response across frequency and found that, a second-order polynomial was not appropriately fit in the BLA (adjusted R^2 values in BLA was 0.30), although in CA1, a second-order fit was moderately well-fit (R^2 values in CA1 was 0.84; **Figure S2F, S2H**). These data suggest that while NE release from LC follows a second-order relationship, LC evoked DA release follows a linear relationship. This points to likely differences in uptake, autoreceptor activity, metabolism, repletion, or sensor kinetics; the findings nevertheless indicate a potential separation of relevant LC firing properties and the relative NE and DA concentration in each. Further studies using

the newest high-resolution FLIM based sensors are needed to mechanistically quantify these findings(Díaz-García et al., 2019; Lee et al., 2019).

4.3.5 DA release from LC axons persists during VTA inhibition

In the 2-photon slice experiments (**Fig. 4.2D-H**), we severed connections from LC to CA1, preventing antidromic activation of the LC, but local DA neuron axon terminals may still be activated by interactions with evoked NE release via α_2AR or α_1AR expression on VTA neurons(Bernacka et al., 2022; Boyajian & Loughlin, 1987; Greene et al., 2005; Nicholas et al., 1993a, 1993b; Rosin et al., 1993). To remove VTA as a source of DA when LC terminals are stimulated, we inhibited the VTA while recording $GRAB_{DA}$ signal. We expressed the Cre-dependent inhibitory designer receptor exclusively activated by designer drugs (DREADD), virally delivered with AAV5-hSyn-DIO-HA-hM4D(Gi) bilaterally in the VTA of *Th*-cre mice (*Th*-cre::VTA:Gi-DREADDs), AAV5-hSyn-DIO-ChrimsonR-tdTmto in the LC (*Th*-cre::LC:Chrimson), and AAV2/9-hSyn-WPRE-PA-$GRAB_{DA3m}$ in CA1 or BLA (*Th*-cre::CA1 or BLA: $GRAB_{DA3m}$; **Figure 4.2M**). When we injected the DREADD agonist clozapine-N-oxide (CNO) (0.5 mg/kg, i.p.) 30min prior to exposing mice to a large open field chamber (50x50cm), we observed a significant decrease in the time the mice spent moving, which were mimicked by the effects of the D_1-antagonist SCH23390 (0.25 mg/kg, i.p.) (**Figure 4.2N**). D_1 dopamine receptors are involved in movement initiation and execution(Hauber, 1996; Heath et al., 2015), thus these data indicate that the hM4Di expressed is reliably suppressing DA transmission.

We next tested whether VTA-DA neurons were required for LC-evoked DA release and determined if VTA-DA neuronal involvement in LC-evoked DA release depends on

the mode of LC activity. To induce a range of LC activity, we simulated low tonic, high tonic, and phasic stimulation. For low tonic or high tonic stimulation, we stimulated terminals for 5min at either 1hz or 5hz. Photostimulation of LC-CA1Th and LC-BLATh terminals evoked DA release in response to 5hz (**Figure 4.2O-P**). To simulate phasic stimulation, we stimulated LC terminals in BLA and CA1 for 200ms at 20hz, which evoked DA release in both (**Figure 4.2Q-R**). When we inhibited the VTA using CNO, evoked DA did not decrease in either 5hz tonic stimulation (**Figure 4.2O-P**) or in 20hz phasic stimulation (**Figure 4.2Q-R**), indicating the VTA is not necessary for evoking DA release from LC axons. Taken all together, these results further establish that the LC releases DA independent of VTA activity.

4.3.6 Appetitive and aversive stimuli evoke more DA release in BLA compared to CA1

Previously, LC-evoked DA has been suggested to affect behavior, but there are no data that report endogenous DA release during behavior(Kempadoo et al., 2016a; Takeuchi et al., 2016c). To ascertain whether the LC releases DA endogenously in response to salient stimuli, we first investigated endogenous release of DA and NE in BLA and CA1 in response to simple aversive and appetitive stimuli. To detect NE or DA dynamics, we injected virally-delivered green NE or DA sensors, AAV1-hSyn-GRAB$_{NE2m}$ or AAV2/9-hSyn-WPRE-PA-GRAB$_{DA3m}$, respectively, into the BLA or CA1 (*Dbh*-cre::CA1 or BLA:GRAB$_{NE2m}$ or GRAB$_{DA3m}$; **Figure 4.3A**) of *Dbh-cre* mice we used in photostimulation experiments in Figure 2. We implanted optical fibers above injection

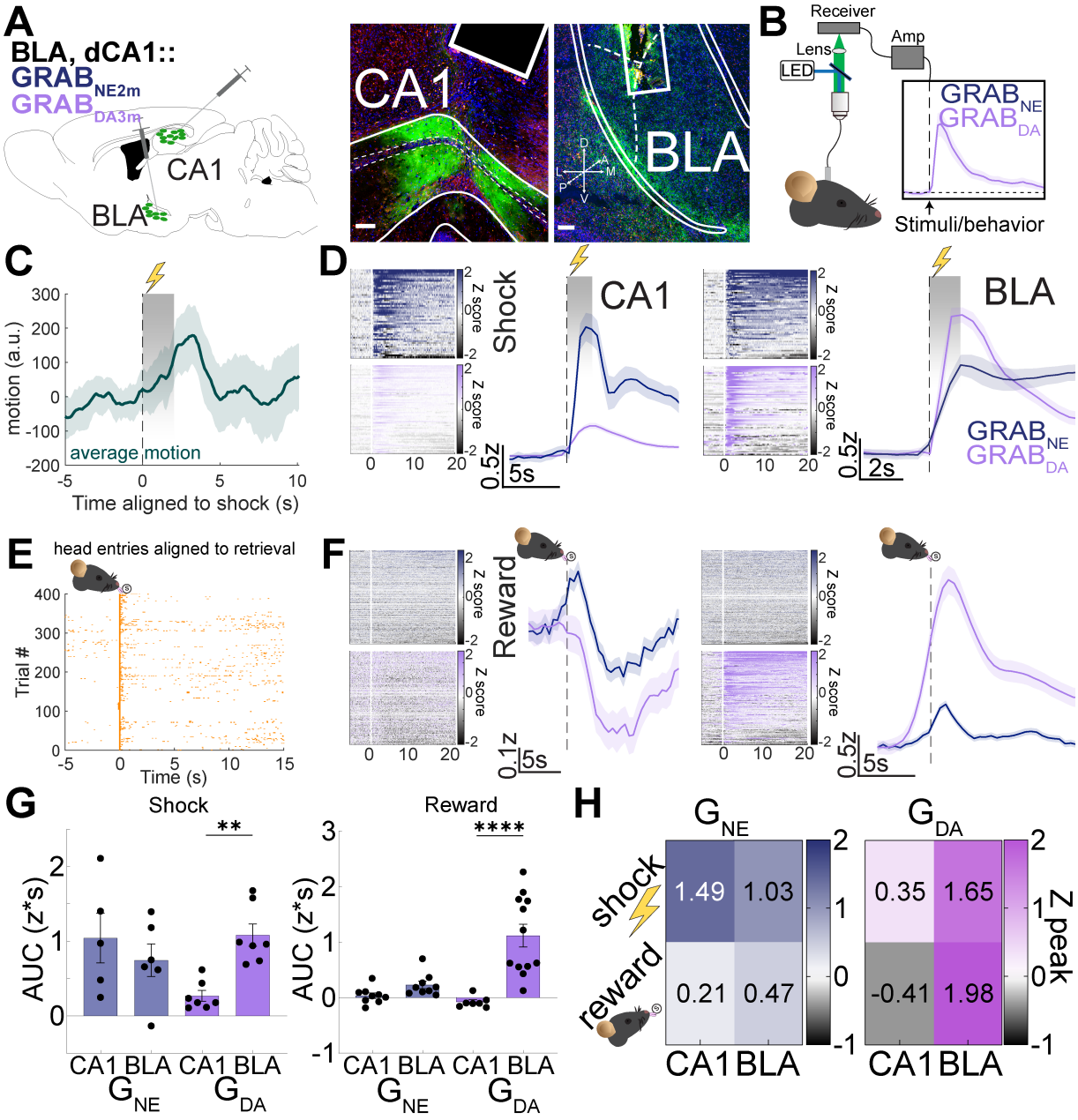

Figure 4.3. More NE than DA released in CA1, BLA releases DA across shock and reward.
A. Schematic of experimental approach depicts infection of cells with $GRAB_{DA}$ (AAV2/9-hSyn-WPRE-PA-DA3m) or $GRAB_{NE}$ (AAV1-hsyn-$GRAB_{NE2m}$) in CA1 and BLA with fiber photometry implants. Scale bar, 100μm. **B.** Schematic of photometry acquisition. **C.** Average motion aligned to shock in mice experessing $GRAB_{DA}$. **D.** $GRAB_{NE}$ and $GRAB_{DA}$ traces in response to 2s shock (0.5mA to 0.7mA) presented with a pseudorandom ITI of 20-90s in CA1 (left, n_{NE}=5, n_{DA}=7) and BLA (right, n_{NE}=6, n_{DA}=7). Heatmaps for $GRAB_{NE}$ and $GRAB_{DA}$ responses to shock with color axes from -2 to 2. **E.** Example rasterplot of reward delivery and subsequent head entries in trained mouse. **F.** $GRAB_{NE}$ and $GRAB_{DA}$ response to reward in CA1 (left, n_{NE}=9, n_{DA}=7) and BLA (right, n_{NE}=9, n_{DA}=12). Heatmaps for $GRAB_{NE}$ and $GRAB_{DA}$ responses to reward retrieval with color axes from -2 to 2. Sucrose pellets were delivered to hungry mice with a pseudorandom ITI of 30, 60, 90, 120s with an average of 90s. **G.** Quantification of the AUC of the average $GRAB_{NE}$ or $GRAB_{DA}$ response to shock (left) or reward (right). Post hoc P-values derived from Kruskal-Wallis with Dunn's multiple comparison. Shock, $GRAB_{DA}$-CA1 vs -BLA, p=0.0095. Reward, $GRAB_{DA}$-CA1 vs $GRAB_{DA}$-BLA, p<0.0001. **H.** Heatmap of peak z-scores during both experiments in **3D** and **3F**. All data are mean ± SEM.; n represents biologically independent mice.

sites in BLA and CA1 to record photometric signal during stimulus administration, including footshock, reward (**Figure 4.3B**).

First, mice were exposed to a 2s footshock, a highly salient and aversive stimulus. During the 2s shock, mice moved more than before each shock (**Figure 4.3C**). In CA1, $GRAB_{NE2m}$ and $GRAB_{DA3m}$ fluorescence increased at the onset of the shock, with the $GRAB_{DA3m}$ response lower than $GRAB_{NE2m}$ (**Figure 4.3D**, left, and **Figure S3A-B**). In BLA, the $GRAB_{DA3m}$ response was greater than $GRAB_{NE2m}$ in response to shock, but $GRAB_{NE2m}$ had a slow decay for over 30s, which was notably different to the decay in $GRAB_{NE2m}$ signal in response to other stimuli (**Figure 4.3D**, right, and **Figure S3C-D**). Only $GRAB_{NE2m}$ had a sustained and significantly increased signal for the rest of the session compared to baseline (**Figure S3I**). In response to shock, the BLA-DA response was higher than the CA1-DA response (**Figure 4.3G**, Kruskal-Wallis with Dunn's multiple comparison, p=0.0095). These data indicate NE and DA are released in both CA1 and BLA in response to aversive stimuli.

Next, we investigated baseline NE and DA dynamics in response to an appetitive stimulus, the retrieval and consumption of a sucrose reward. We recorded NE and DA dynamics as mice completed the task, and aligned photometry signals to the moment mice entered their heads in the hopper to retrieve sucrose pellets throughout the session (**Figure 4.3E**). We found that as mice approached the hopper for reward, NE was released in CA1, and as mice consumed, there was a subtle dip in the $GRAB_{NE2m}$ signal (**Figure 4.3F, left**). In the BLA, both NE and DA increased as mice approached the hopper to retrieve a sucrose pellet (**Figure 4.3F, right**). In response to shock and reward, $GRAB_{DA3m}$ signal increased in BLA greater than in CA1 (**Figure 4.3G,** shock: p=0.0095,

reward: $p<0.0001$), whereas $GRAB_{NE2m}$ signal was not significantly different within each behavior across regions. These data suggest more DA is released in BLA than in CA1 in response to salient stimuli (**Figure 4.3G-H**).

In addition to shock and reward delivery, we tested additional types of appetitive and aversive behaviors. First, we used a looming stimulus to simulate a less salient, aversive stimuli, and found that NE was released in CA1 and BLA to the onset of the looming stimulus (**Figure S3E**). Similar to the footshock, $GRAB_{DA3m}$ signal increased in BLA, but not in CA1, at the onset and offset of the looming stimulus (**Figure S3E**). Mice also exhibited darting behavior at the onset of the looming stimuli (**Figure S3F**). To assess a second appetitive behavior, mice were trained to poke their nose in a port for a reward predicted by a 2s light cue, while a second, inactive nose port, led to no reward delivery. When trained mice poked their nose in the correct port, dLight signal in BLA increased in anticipation of the cue-signaling reward (**Figure S3G**). While the dLight and $GRAB_{NE}$ signal in BLA did not increase to cue, the dLight and $GRAB_{NE}$ signals in BLA increased to reward retrieval and consumption (**Figure S3G**, top). There was no increase in dLight signal in CA1 during operant paradigm, but there was a decrease in $GRAB_{NE}$ signal to nosepoking for reward (**Figure S3G**, bottom). When mice poked their noses in the inactive nose port, there was a clear increase in dLight in BLA and a smaller increase in CA1, while there was no increase in $GRAB_{NE}$ signal in BLA or CA1 (**Figure S3H**). All together, these results establish that we can detect DA that is released in the BLA following both aversive and appetitive stimuli, and DA is only detected in CA1 during salient aversive stimuli.

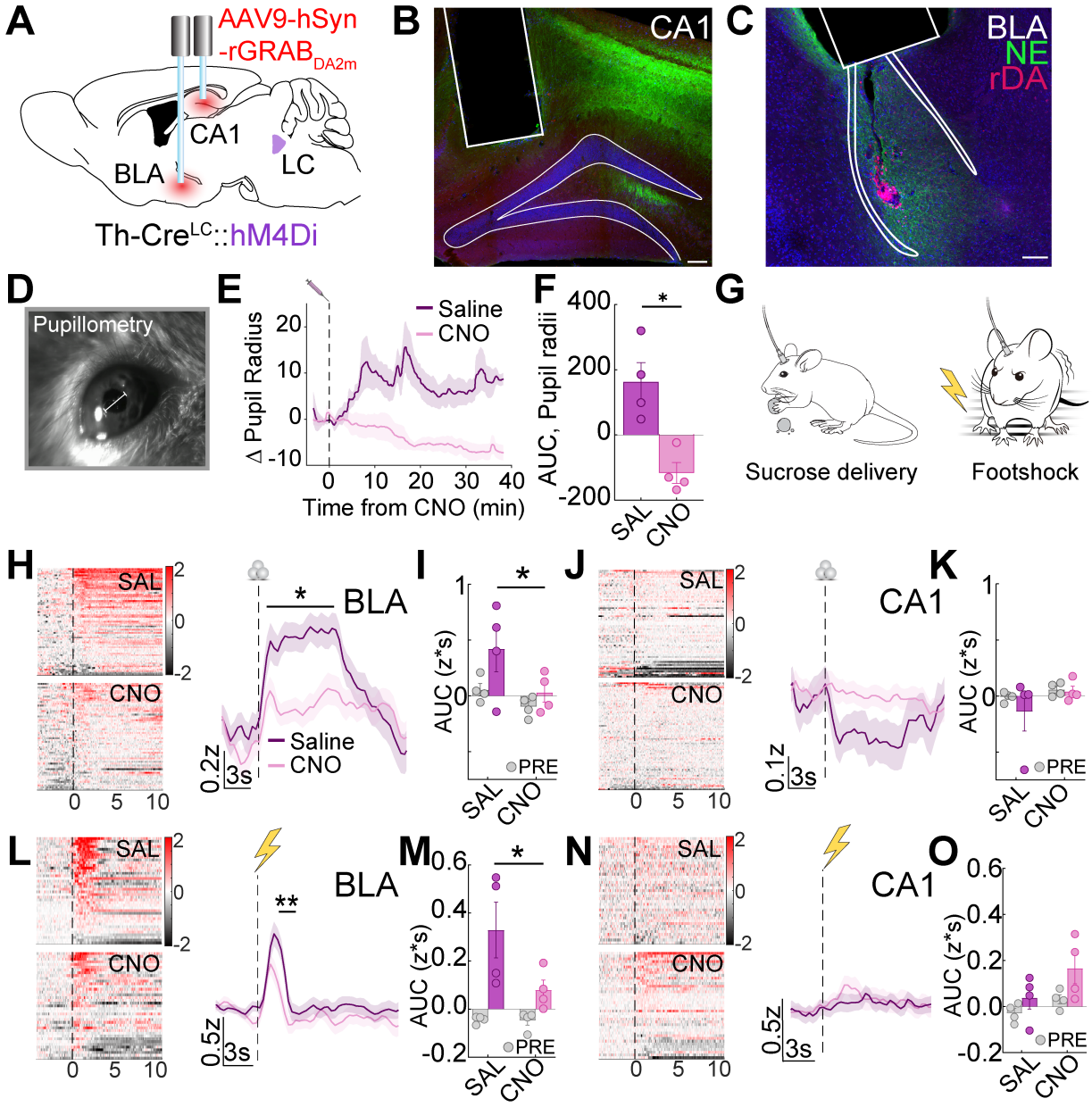

Figure 4.4. LC inhibition decreases DA release during reward and shock in BLA, and has no effect in CA1. A. Schematic of experimental approach of surgical injections. Schematic depicts infection of LC-NE cells with Gi-DREADDs (AAV5-hSyn1-DIO-HA-hM4D(Gi)) and expression of GRAB$_{rDA2m}$ in both BLA and CA1. **B.** Representative image of CA1 GRAB$_{rDA2m}$ expression and fiber placement. Scale bar, 100μm. **C.** Representative image of BLA GRAB$_{rDA2m}$ expression and fiber placement. **D.** Example of pupillometry recording with measurement depicted. **E.** Pupil radius measurements during LC inhibition. Gi-DREADDs were expressed bilaterally in LC. n=4. **F.** AUC for pupil radius measurements. (paired t-test, p=0.0223). **G.** Schematic of sucrose delivery (**H-K**) and footshock (**L-O**). **H.** Average traces and heatmaps for GRAB$_{rDA}$ response to reward retrieval in BLA during LC inhibition (pink) and saline controls (purple). Significance of 1s bins calculated using 2-way ANOVA, with Sidak test for multiple comparisons, p<0.05. n=4. **I.** AUC for 10s in SAL and CNO responses to reward in BLA. 2-way ANOVA, with Sidak test for multiple comparisons, p=0.0327. **J.** Average traces and heatmaps for GRAB$_{rDA}$ response to reward retrieval in CA1 during LC inhibition or saline. n=4. **K.** AUC for 10s in SAL and CNO responses to reward in CA1. **L.** Average traces and heatmaps for GRAB$_{rDA}$ response to shock in BLA during LC inhibition (pink) and saline (purple). Significance of 1s bins calculated using 2-way ANOVA, with Sidak test for multiple comparisons, p<0.05. n=4. **M.** AUC for 5s in SAL and CNO responses to reward in BLA. 2-way ANOVA, with Sidak test for multiple comparisons, p=0.025. **N.** Average traces and heatmaps for GRAB$_{rDA}$ response to shock in CA1 during LC inhibition or saline. n=4. **O.** AUC for 5s in SAL and CNO responses to reward in CA1.

4.3.7 LC inhibition decreases BLA DA release to appetitive stimuli

Next, we sought to conclusively demonstrate that DA released following appetitive stimulus presentation is from LC terminals. To accomplish this, we used chemogenetics to inhibit either LC or VTA activity. In contrast to our previous experiments, here we recorded both NE and DA signals simultaneously to assess the differential catecholamine release profiles in the same mice. We expressed $GRAB_{rDA2m}$ and $GRAB_{NE2m}$ and then recorded stimuli-evoked release dynamics using two-color fiber photometry. To accomplish this, we injected the Cre-dependent Gi-DREADD (AAV5-hSyn1-DIO-HA-hM4D(Gi)) bilaterally in the LC or VTA of *Th*-cre mice (*Th*-cre::LC^{bilat}:Gi-DREADDs) or (*Th*-cre::VTA^{bilat}:Gi-DREADDs) (**Figure 4.4A**), and both AAV9-hSyn-$GRAB_{rDA2m}$ and AAV1-hSyn-$GRAB_{NE2m}$ in the CA1 (**Figure 4.4B**) or BLA (**Figure 4.4C**).

Because increased pupil dilation is positively correlated with higher LC activity(Y. Liu et al., 2017; Murphy et al., 2014), we used pupillometry to establish the efficacy of Gi-DREADD inhibition of LC activity(Privitera et al., 2020) (**Figure 4.4D**). When we injected the DREADD agonist CNO (0.5 mg/kg, i.p.) in *Th*-cre mice expressing hM4D(Gi) in LC bilaterally (*Th*-cre::LC^{bilat}:Gi-DREADDs), we observed a consistent, significant decrease in pupil radii from baseline, as measured by comparing the “area under the curve” (AUC), suggesting that the LC was inhibited by this chemogenetic approach (**Figure 4.4E-F**, paired t-test, p=0.0223).

With DREADD inhibition of LC established, we next injected either CNO (0.5 mg/kg, i.p.) or saline 30 min prior to a session in which we delivered rewards at a pseudorandom ITI of 90-150s while recording $GRAB_{rDA2m}$ and $GRAB_{NE2m}$ simultaneously (**Figure 4.4I**). Following saline administration, as mice retrieved a reward and throughout

consumption, DA was released in the BLA before returning to baseline (**Figure 4.4H**). Relative to saline treatment, we observed a significant decrease in BLA DA release when mice retrieved and consumed a reward following CNO inhibition of LC (**Figure 4.4H**, 1s bins analyzed with 2-way ANOVA, Sidak test for multiple comparisons, $p<0.05$ for all bins). Comparing the total change in DA release (change in AUC), we found LC inhibition significantly reduced DA release in BLA during reward consumption relative to saline (**Figure 4.4I**, 2-way ANOVA, with Sidak test for multiple comparisons, $p=0.0327$). While mice retrieved and consumed the same number of rewards following saline and CNO injection (**Figure S4I**), we did not observe DA release in CA1 during reward consumption (**Figure 4.4J-K**). By contrast, in these same mice, LC inhibition decreased NE release in CA1 during reward consumption, establishing that the LC was inhibited, but there was no effect on the DA released (**Figure S4C**). Following saline administration in these mice, NE was released in BLA as mice retrieved the reward, whereas following CNO administration, surprisingly NE was elevated throughout consumption compared to saline sessions (**Figure S4B**). In summary, these data indicate that inhibiting the LC during reward retrieval leads to a decrease in NE release in CA1, a paradoxical increase in NE release in BLA, and a decrease in DA release in BLA. The NE increase we observed in the BLA is likely due to A2 cell cluster in the nucleus of the solitary tract, which more strongly projects to the BLA than CA1(Robertson et al., 2013) and may also inhibit the LC(Lopes et al., 2016; Van Bockstaele et al., 1999).

VTA activity and dopamine release is correlated with salient stimuli(Kutlu et al., 2021) and lesioning the LC or VTA disinhibits the activity of the other(Guiard, El Mansari, Merali, et al., 2008). Thus, VTA activity's influence on DA release to relevant stimuli is

important to understanding the LC's role in DA release. To determine the influence of VTA on dopamine release in response reward, we inhibited the VTA as mice retrieved rewards and recorded $GRAB_{rDA}$ and $GRAB_{NE}$ dynamics (**Figure S4G**). Following saline administration, NE and DA were released in BLA during reward retrieval, and $GRAB_{rDA}$ signal remained elevated during consumption while $GRAB_{NE}$ signal decreased (**Figure S4G, left**). In CA1, DA activity did not change, while NE activity decreased slightly during consumption (**Figure S4G, right**). In response to VTA inhibition, there was a decrease in DA that was released in the BLA during reward consumption compared to saline administration sessions, while there was no effect on DA activity in CA1 (**Figure S4G**). VTA inhibition during reward sessions also led to an increase in NE released in both BLA and CA1 compared to after saline administration (**Figure S4G**). The latency of mice to retrieve reward was significantly increased when the VTA was inhibited (**Figure S4I**), establishing that the VTA's activity was suppressed. The increase in NE release observed during VTA inhibition compared to saline administration support past data that found the LC and VTA cross-inhibit each other(Guiard, El Mansari, Merali, et al., 2008). Together, these data establish that the LC, with the VTA, are contributing DA in the BLA during reward retrieval.

To test if the $GRAB_{rDA2m}$ sensor is detecting NE, we recorded $GRAB_{rDA2m}$ and $GRAB_{NE2m}$ signal in the BLA simultaneously while mice retrieved a pellet for reward using dual-color photometry recordings. We found a clear separation in the onset of the sensors' signals (**Figure S4F**) that was greater than the reported on-times of the sensors (**Figure 4.1B**), suggesting these signals are likely to be separable and independent if carefully monitored using these considerations. Further, as mice consumed reward,

$GRAB_{rDA2m}$ sensor activity remained elevated for 20s after the $GRAB_{NE2m}$ activity returned to baseline. These recordings indicate we can reliably detect separable $GRAB_{NE2m}$ and $GRAB_{rDA2m}$ signals simultaneously during freely moving behaviors.

4.3.8 LC inhibition decreases DA release in BLA during aversive stimulus presentation

Prior studies implicate DA release from LC axons in spatial memory without VTA involvement(Kempadoo et al., 2016a; Takeuchi et al., 2016c), while other studies suggest DA from the VTA modulates aversive memory acquisition independent of the LC(Tsetsenis et al., 2021). To test whether LC-sourced DA is released in response to aversive stimuli, we again used chemogenetic inhibition of LC or VTA (*Th*^{Cre}::LC^{bilat} or VTA^{bilat}:Gi-DREADDs) prior to delivery of footshocks while recording $GRAB_{rDA2m}$ and $GRAB_{NE2m}$ dynamics in CA1 and BLA.

In the same mice as the appetitive stimulus experiments, we injected either CNO (0.5 mg/kg, i.p.) or saline 30min prior to a session in which we delivered footshocks at a pseudorandom ITI of 20-90s. Following saline administration, NE was released in BLA and CA1 at the onset of the shock (**Figure S4B**). NE remained elevated in BLA following cessation of the shock, and returned to baseline in CA1. When the LC was inhibited, there was only a significant increase in NE released in CA1 following cessation of the shock (**Figure S4C**), whereas there was no change in the NE released in the BLA during LC inhibition, suggesting other NE release from likely A1/A2 sources.

Following saline administration, DA was released in the BLA with the onset of a footshock, and the DA signal fell after the shock. In the CA1, surprisingly DA release was

not detected during footshock. Relative to saline treatment, inhibiting LC during shocks produced a significant decrease in DA released in BLA during the two seconds after shock cessation (comparing 1s bins, **Figure 4.4L**, 2-way ANOVA, $p<0.01$). LC inhibition also produced a significant decrease in the AUC of the $GRAB_{rDA2m}$ signal in BLA for 5s after shock onset compared to saline (**Figure 4.4M**, 2-way ANOVA, $p<0.05$). In CA1, LC inhibition did not affect the lack of release of DA (**Figure 4.4N-O**).

We next explored in the same cohort as reward experiments how VTA inhibition affected catecholamine release in response to an aversive stimulus. Following saline administration, NE was released in the BLA and in the CA1 in response to the onset of shock, and NE levels remained elevated after shock cessation in the BLA but not the CA1 (**Figure S4H, top**). Relative to saline controls, there was no change in NE release during shock in BLA or CA1. In the BLA, DA increased with the onset of shock and returned to baseline after cessation, while in the CA1, $GRAB_{rDA2m}$ signal did not change with the shock. When the VTA was inhibited during shock sessions, there were no clear changes in the $GRAB_{rDA2m}$ or the $GRAB_{NE2m}$ signal detected in BLA or CA1 relative to saline (**Figure S4H, bottom**). These results indicate that VTA inhibition does not affect catecholamine release in response to shock in both BLA and CA1 compared to saline controls, while during reward retrieval and consumption, VTA inhibition decreased DA release in BLA and increased NE release in both CA1 and BLA compared to saline trials. Contrary to the effects of LC inhibition on NE release in CA1 during reward, LC inhibition raised NE in CA1 at the cessation of shock compared to saline controls, indicating a possible phasic rebound in LC activity when the cells are under inhibitory constraint, something previously reported by our group and others(Kuo et al., 2020; Luskin et al.,

2025; Marzo et al., 2014). These data suggest LC inhibition decreases DA release in BLA during shock relative to saline treatment, while not impacting the weak DA release detected in CA1 during the same aversive stimuli.

4.4 Discussion

In summary, here we used optogenetics with photometry and 2-photon *ex vivo* imaging to demonstrate that stimulating LC terminals evokes DA release. We demonstrate that *in vivo,* LC-evoked NE release followed a second-order frequency response curve, while the LC-evoked DA release followed a linear trend in both BLA and CA1. We also established that LC inhibition diminished DA release in response to reward retrieval and shock in the BLA, while having minimal influence on DA release in the CA1. Together, we established that the LC has the capacity to release DA in both CA1 and BLA under physiologically meaningful conditions. We also determined that during appetitive and aversive stimuli, LC contributes DA release in BLA, but not appreciably in the CA1.

Recent studies have asserted that LC-NE neurons release DA in the hippocampus, enhancing contextual memory and plasticity independent of the VTA(Kempadoo et al., 2016a; Smith & Greene, 2012a; Takeuchi et al., 2016c). Some studies have used optogenetics and chemogenetics to evoke DA release from LC in dorsal CA1, but only over very long time scales(Kempadoo et al., 2016a; Wilmot et al., 2024). The present study optically stimulates brain slices at much lower stimulation duration (3s), more indicative of LC-NE neuron burst activity and frequency (as low as 1hz) to determine the lower limits of physiologically-relevant LC-evoked DA release. Although optogenetic

stimulation is inherently artificial, we use paradigms in this study which fall within the range of previously used and well-characterized optogenetic stimulation paradigms of LC(Carter et al., 2010; McCall, 2015), which were carefully matched to the natural range of LC activity(Carter et al., 2010; Devilbiss & Waterhouse, 2011b). In response to stimulation mimicking the natural range of LC activity, the evoked LC-NE signal followed a second-order trend while the evoked LC-DA signal followed a linear trend. These data suggest that NE and DA release from LC terminals are regulated differently, and that there are likely differences in uptake, autoreceptor activity, metabolism, or repletion. Future studies might characterize the differences in NE and DA release during various stimulation paradigms while altering transporter and vesicle activity, and use FLIM-based sensor technologies, now coming online for quantifying these differences with better resolution.

The present study particularly expands on previous work suggesting that LC releases DA by characterizing LC-evoked DA and NE release across a range of phasic and tonic activation profiles matched to physiologically relevant parameters (**Figure 4.1F, 4.2O-R**). Additionally, *in situ* RNA hybridization, autoradiography and immunohistochemistry have revealed varying degrees of α_1AR expression on VTA neurons(Boyajian & Loughlin, 1987; Greene et al., 2005; Mitrano et al., 2012; Nicholas et al., 1993a, 1993b; Rosin et al., 1993; Solecki et al., 2022). The expression of adrenergic receptors on VTA terminals suggests LC stimulation may amplify DA release from VTA-DA terminals via a Gq-mediated effect. However, by inhibiting VTA^{TH} neurons and stimulating LC terminals, we determined here that LC-evoked DA release does not rely on VTA in CA1 or BLA (**Figure 4.2O-R**).

While receptor pharmacology experiments have revealed the potential for DA release from noradrenergic terminals, electrical stimulation, lesions of LC, and genetic knockout of *Dbh* have been used to demonstrate the necessity of the LC for DA release. Selective lesioning of the LC leads to an increase in VTA-DA neuron activity, and VTA-DA lesions lead to an increase in LC-NE neuron activity(Grenhoff et al., 1993), suggesting that there are functional LC-VTA reciprocal projections(Deutch et al., 1986; Mejias-Aponte et al., 2009). These data would predict that in response to a stimulus that evokes VTA-BLA^{DA} release, the VTA may release more DA when the LC is inhibited compared to controls. However, our data suggest that either LC or VTA inhibition decrease the BLA-DA release during reward retrieval compared to controls (**Figure 4.4H-I, Figure S4F**). Furthermore, only LC inhibition decreased the BLA-DA release during shock compared to controls (**Figure 4.4L-M, Figure S4H**). Therefore, these findings taken together indicate that the LC is indeed likely contributing substantially to DA release in the BLA in response to both aversive and appetitive stimuli.

In our experiments, LC inhibition had unexpected effects on NE release. Whereas we would expect LC inhibition to decrease the NE release detected during behaviors, we found that during reward, NE decreased in CA1 (**Figure S4C**) and increased in BLA (**Figure S4B**). This result may be explained by the well-known A2 noradrenergic neurons in the nucleus tractus solitarius (NTS) which project more strongly to BLA than LC neurons do(Robertson et al., 2013; W. Zheng et al., 2022), and A2 neurons have been reported to be inhibited by LC neurons(Lopes et al., 2016; Van Bockstaele et al., 1999), such that inhibiting LC disinhibits A2 NE neurons, leading to the increased NE release in BLA seen in **Figure S4B**. These results contradict the increase in CA1-NE release while

mice experience shock under LC, and this increase in NE may be the result of a phasic rebound in LC activity when LC neurons are under inhibitory constraint. Additionally, inhibition of VTA led to increases in NE release to reward, but not in shock groups, compared to saline controls. Future studies should investigate how LC and VTA terminal activity differ across multi-region recordings in response to appetitive and aversive stimuli, to determine if circuit interactions between LC and VTA further help to explain these results.

Although we did not observe LC effects on CA1-DA release in response to aversive and appetitive stimuli with $GRAB_{rDA}$ (**Figure 4.4J, N**), we were able to evoke DA from LC terminals in CA1 through optogenetic stimulation *ex vivo* and *in vivo*, and we detected evoked LC-DA release in both CA1 and BLA. Combined with the decrease in DA release after LC inhibition in BLA and no release in CA1, these data suggest that the LC-CA1 innervation may release DA when these neurons experience elevated activation. More broadly, the data suggest that DA release from LC terminals in CA1 is dependent on behavioral states and neuronal activity.

There are also other sources of DA and NE than the LC and VTA that must be considered in how they may be involved in DA release in this study. Studies suggest that Dorsal Raphe nucleus (DRN) has either negligible(Sengupta & Holmes, 2019) or minor(Cho et al., 2017) DA innervation in BLA, and none in CA1. Substantia nigra (SN) projects to BLA, but not CA1, and these BLA projections are non-DAergic projections(Loughlin & Fallon, 1983). Further studies are needed to address if the DRN or SN inputs in BLA influence the interpretation of LC-BLA^{DA} release.

Biosensor selectivity relies on silencing cross-reactive neuromodulator sources (e.g. VTA-DA and LC-NE neurons both project to CA1 and BLA)(López et al., 2024b). To address these concerns with the sensors we used in this project, we employed genetic knockouts, inhibitory chemogenetics, and dual-color fiber photometry recordings. To address whether $GRAB_{NE}$ is binding DA at the stimulation paradigms we used in optogenetic experiments, we found no increase in NE signal when we stimulated LC-$CA1^{Dbh-/-}$ terminals for 3s at 20hz, which is the upper limit of stimulation intensities we employed. In addition, we see different $GRAB_{NE}$ and $GRAB_{DA}$ dynamics in response to reward retrieval and looming in CA1 (**Figure 4.3F, S3E**). This suggests that in our stimulation experiments, $GRAB_{NE}$ is sufficiently selective for NE over DA.

To address concerns that the red $GRAB_{rDA}$ sensor used in **Figure 4.4H-O** is detecting NE, we established that $GRAB_{rDA}$ dynamics are separable from $GRAB_{NE}$, considering sensor kinetics (**Figure 4.1B**). Given the known off-kinetics of these biosensors (< 3s), these data indicate $GRAB_{rDA}$ is detecting negligible binding of DA and NE on the cross-binding sensor at this level of endogenous release. Lastly, we plotted the AUC of the simultaneously recorded NE and DA dynamics for 10s after reward retrieval and saw no correlation in NE and DA detected (**Fig S4D**). These data taken together suggest the $GRAB_{rDA}$ and $GRAB_{NE}$ are sufficiently selective for endogenous detection of NE and DA at the expression levels in **Figure 4.4H-O**.

In our experiments, inhibiting the LC using a chemogenetic strategy decreased the DA response seen in response to shock and retrieving a reward in BLA, while VTA inhibition decreased the detected DA signal in response to reward but did not change the DA detected during shock. This suggests that in the BLA, only the LC is releasing DA in

response to aversive stimuli, while both the LC and VTA are releasing DA during appetitive stimuli in BLA. This bolsters past evidence that the VTA is necessary for making cue-reward associations and releases DA during reward retrieval(Sias et al., 2024).

Past studies have suggested that DA release in BLA is contributing to fear expression, and primarily acquisition, in BLA(Guarraci et al., 2000; Heath et al., 2015; Lamont & Kokkinidis, 1998; Nader & LeDoux, 1999), and BLA-projecting VTA neurons, specifically, have been shown to release DA and contribute to conditioned fear acquisition(W. Tang et al., 2020b). Another study demonstrated BLA projecting LC neurons contribute to fear memory formation(Uematsu et al., 2017b). Our data suggests the LC is contributing some portion of DA in BLA during an aversive conditioned stimulus (**Figure 4.4L**). Given both NE and DA are involved in fear acquisition in the amygdala(Giustino et al., 2020; Giustino & Maren, 2018; Heath et al., 2015; Pantoni et al., 2020), future studies should determine the how LC-sourced NE and DA released in the BLA may be critically involved in different aspects of acquisition behavior, and in regions with dual VTA and LC innervation investigators must take heed to consider non-VTA sources of DA in their result interpretations.

CA1 activity during aversive stimuli like tail shock and airpuff scales with salience and context independent of location(Barth et al., 2023), increases with the valence of a reward-predictive cue(Yun et al., 2023), and certain populations respond to reward(Gauthier & Tank, 2018). While DA has been suggested to be involved in enhancing memory persistence and spatial memory(Kempadoo et al., 2016a; Takeuchi et al., 2016c), the present study is among the first to look at dopamine's release in CA1 during aversive and appetitive stimuli. While DA was not detected in response to reward

in CA1, DA release was moderately present during shock in CA1, which may be sourced from the VTA and modulating the formation of aversive memories(Tsetsenis et al., 2021). Further, optically evoked LC-CA1^{DA} release *in vivo* was not significantly different from evoked LC-BLA^{DA} release (Kolmogorov-Smirnov test, n.s., p=0.93; **Figure 4.2K-L**). Together these data indicate that LC-CA1 projections have the capacity to release DA during behaviorally relevant epochs, but only do so under specific conditions. As hippocampal inputs to BLA are important for contextual conditioning, DA may signal the valence of contextual information in the CA1, which is then relayed to the BLA for consolidation.

While this study demonstrates the conditions for DA release from LC terminals, we do not address mechanisms of LC-DA release. DBH is not rate-limiting for NE synthesis thus how the LC may release DA has remained controversial even with emerging evidence of DA release from noradrenergic terminals. DBH is primarily localized to be inside of synaptic vesicles (Cimarusti et al., 1979b) although it has also been observed less-selectively throughout the somata and processes of LC neurons(Olschowka et al., 1981), while TH is localized in the cytoplasm(Pickel et al., 1975). For DA to be released from LC neurons endogenously as the present study suggests, there must be some population of synaptic vesicles in LC terminals that do not contain DBH or whole terminals that exclude DBH-containing vesicles. Future work should use electron microscopy to explore the distribution of vesicles and DBH within LC synapses in various regions throughout the brain.

LC contributing DA in BLA during reward suggests there must be some active process by which DA is endogenously released from LC terminals. In some human

populations, pharmacological(Gaval-Cruz & Weinshenker, 2009) (e.g. disulfiram) and genetic factors(Cubells & Zabetian, 2004) (e.g. *Dbh* deficiency, *Dbh* gene polymorphisms) will affect the ratio of DA/NE released by the LC, which may impact behavior especially with maladaptive comorbidities like addiction or ADHD. Due to the LC's characteristic functional activation of specific projections, the impact of the corelease of DA and NE from LC neurons on behavior requires an individual investigation in each circuit based on relevant behavior and function, and both NE and DA researchers should take caution before concluding definitive contributions in each case.

Appendix A: Supplemental figures

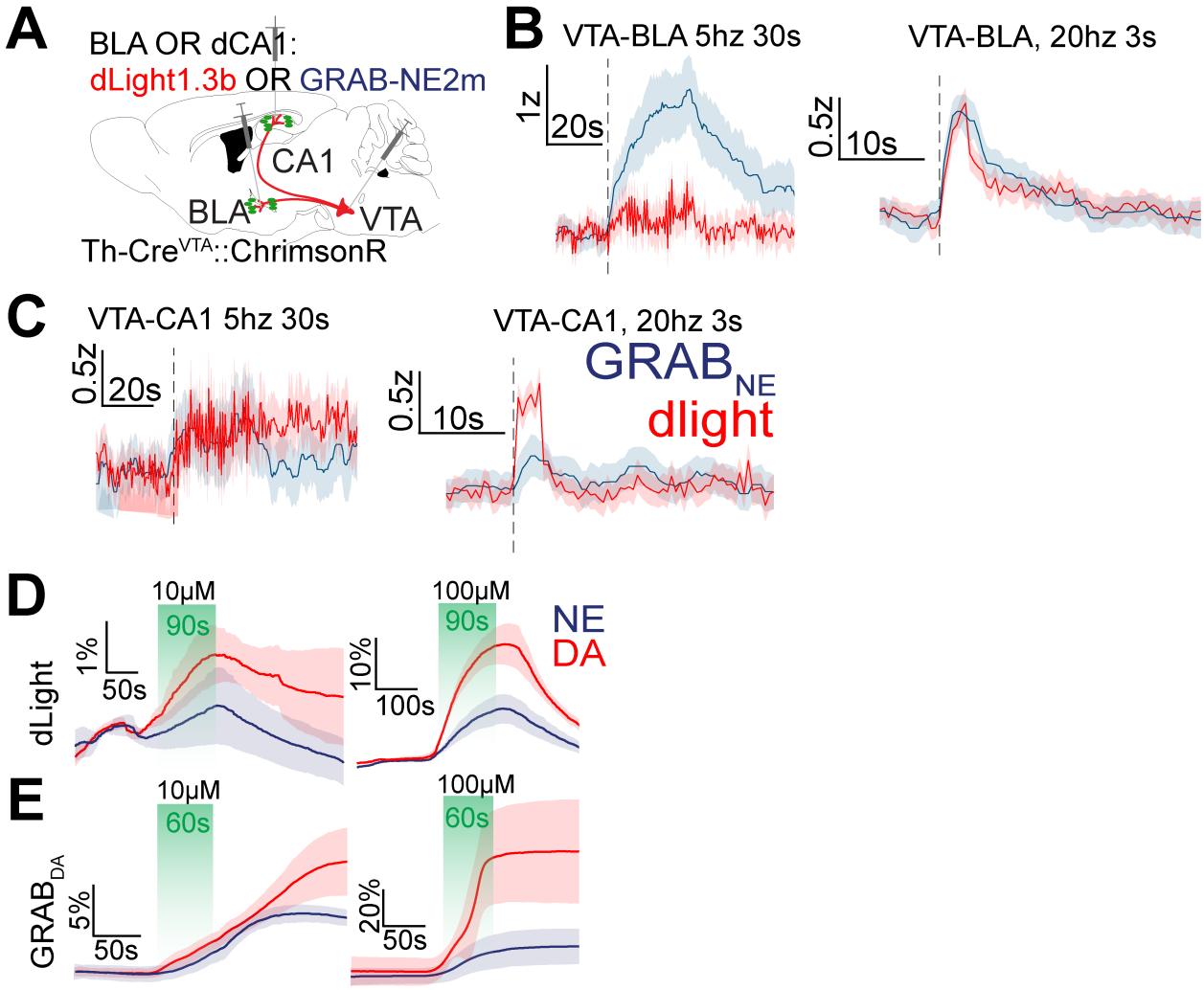

Figure S1- Controls for biosensor selectivity
A. Schematic of experimental approach of surgical injections for VTA terminal stimulation and recording photometric signals. Schematic depicts infection of VTA-DA cells with ChrimsonR (AAV5-hSyn-FLEX-ChrimsonR-tdTomato) and $GRAB_{NE}$ or dLight in BLA **(B)** or CA1 **(C)**. **B-C.** Stimulation of VTA terminals in BLA (**B**) and CA1 (**C**), at 5hz for 30s (left) or 20hz for 3s (right). **D-E.** ΔF/F% change during DA and NE washes on dlight **(G)** or GRABDA **(H)** expressing slices at either 10μM (left) or 100μM (right).

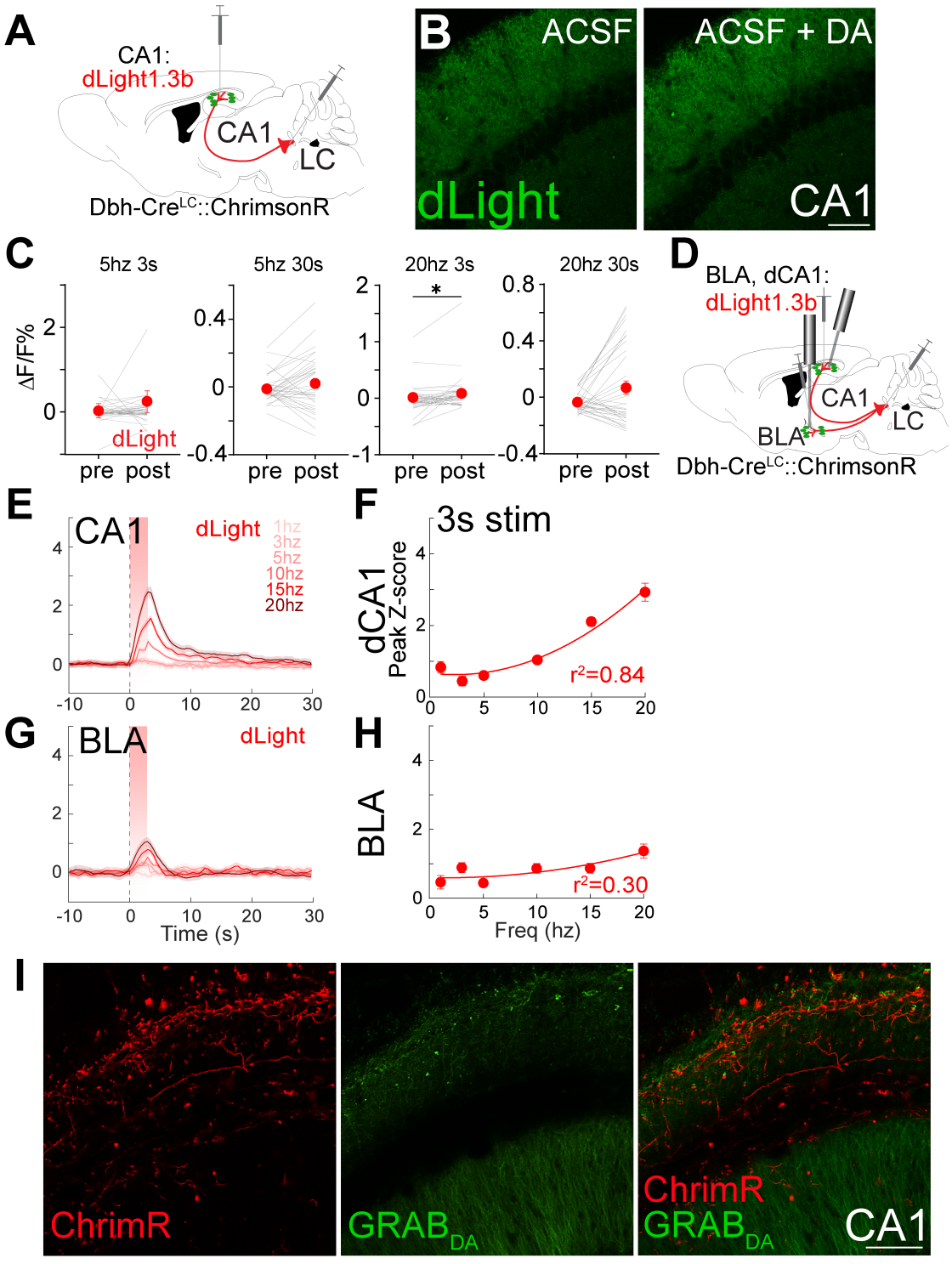

Figure S2- LC-evoked DA is detected by dLight *in vivo* and *ex vivo*

A. Schematic of surgeries for 2-photon experiments with dLight. Chrimson was expressed in LC, and dLight in CA1. **B.** Vehicle (left) and 30μM DA (right) washes on dLight expressing slices. Scale bar, 100μm. **C.** ΔF/F% change from before to after stim in dlight (n=4 biological replicates, 6 slices) in response to a range of stimulation paradigms: 5hz 3s, 5hz 30s, 20hz 3s, 20hz 30s (left to right). Wilcoxon test, p=0.027. **D.** Surgery schematic for *in vivo* optogenetic stimulation, with dLight expressed in CA1 and BLA and Chrimson expressed in LC. **E.** dLight response to LC-CA1 stimulation at a range of frequencies (1-20hz). **F.** Frequency response curves of dLight response when stimulating LC-CA1 terminals for 3s. Second-order curve fit to dLight, n=5-7, r^2= 0.84. **G.** dLight response to LC-BLA stimulation at a range of frequencies (1-20hz). **H.** Frequency response curves of dLight response when stimulating LC-BLA terminals for 3s. **I.** Representative 2-photon image of virus expression in a hippocampal slice expressing $GRAB_{DA}$ in CA1 and ChrimsonR in LC terminals in CA1. Scale bar, 100μm.

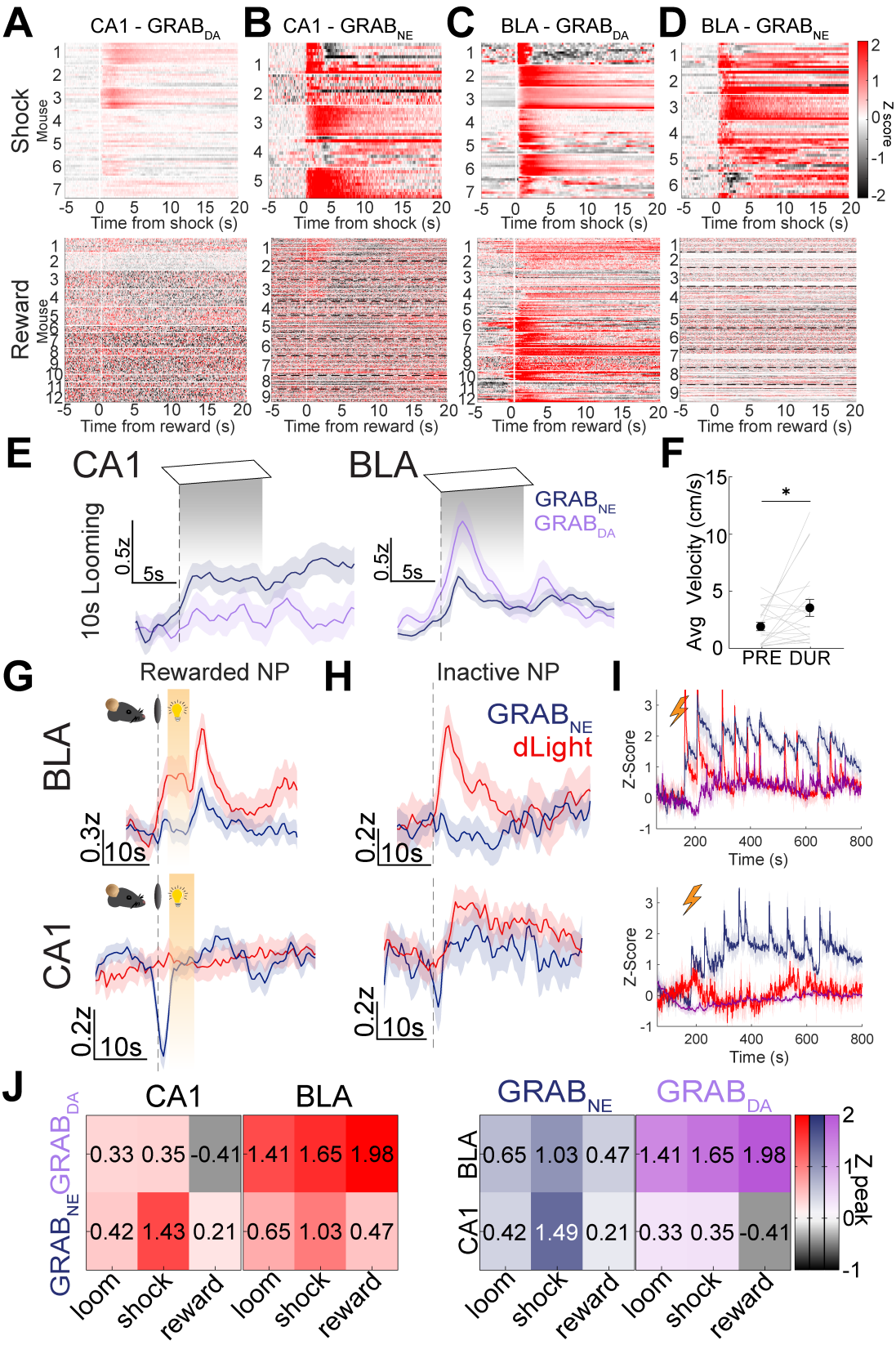

Figure S3- NE and DA dynamics during aversive and appetitive behaviors

A-B. Heatmaps of $GRAB_{DA}$ and $GRAB_{NE}$ response to shock (top) and reward (bottom) in BLA (**E**: $GRAB_{DA}$ in CA1, **F**: $GRAB_{NE}$ in CA1). **E-F.** Heatmaps of $GRAB_{DA}$ and $GRAB_{NE}$ response to shock (top) and reward (bottom) in BLA (**C**: $GRAB_{DA}$ in BLA, **D**: $GRAB_{NE}$ in BLA). **E.** NE and DA response to looming in CA1 (left) and BLA (right). **F.** Mice dart at the first three looming stimuli presentations. Paired t-test, p=0.0364. **G-H.** Response to nosepoking in the rewarded noseport (**G**), the unrewarded noseport (**H**) for BLA (top) or CA1 (bottom). **I.** Full session recording of $GRAB_{DA}$ (purple), $GRAB_{NE}$ (blue), or dLight (red) during shock in BLA (top) or CA1 (bottom). **J.** Heatmap of peak z-score in response to looming stimuli, shock, reward in CA1 and BLA.

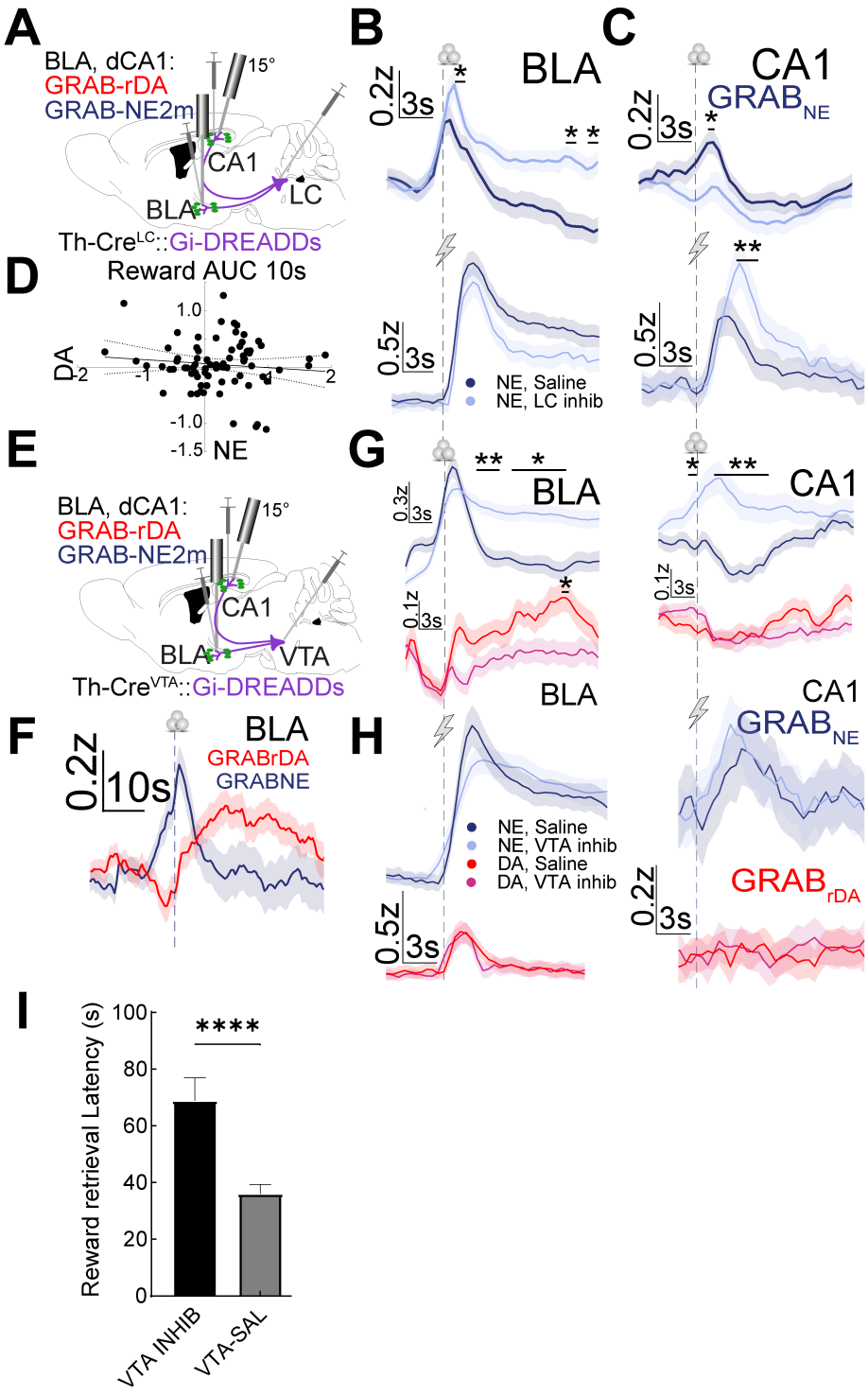

Supplemental Figure 4- VTA or LC inhibition effects on NE and DA release in reward and shock
A. Schematic of surgeries preparing for recording DA and NE dynamics while inhibiting LC. Cre-dependent Gi-DREADDs were expressed in LC (left) or VTA (right) of Th-cre mice, with $GRAB_{rDA}$ and $GRAB_{NE}$ expressed in CA1 and BLA. **B-C.** NE response to reward retrieval (top) or shock (bottom) in BLA (**B**) or CA1 (**C**) under LC inhibition (light blue) or vehicle (black). **D.** AUC for 10s of DA vs AUC for 10s of NE after reward retrieval in **Fig S4I**. R^2=0.01. **E.** Schematic of surgeries preparing for recording DA and NE dynamics while inhibiting VTA. **F.** Averaged, simultaneously recorded $GRAB_{rDA}$ and $GRAB_{NE}$ dynamics in BLA during reward retrieval prior to any neuromodulation. **G.** NE (top) and DA (bottom) response to reward in BLA (left) or CA1 (right) under VTA inhibition (NE: light blue; DA: magenta) or vehicle (NE: blue; DA: red). **H.** NE (top) and DA (bottom) response to shock in BLA (left) or CA1 (right) under VTA inhibition (NE: light blue; DA: magenta) or vehicle (NE: blue; DA: red). Significance of 1s bins for all traces calculated using 2-way ANOVA with Sidak test for multiple comparisons, $p<0.05$. **I.** Latency to retrieve rewards following either saline or CNO administration, in mice expressing hM4Di in VTA.

Chapter 5: Conclusions and Future Directions

Arousal and our ability to regulate attention are essential to survival. In the modern technological era, internet addiction is prevalent, especially with younger generations. Dysfunctional attention regulation impacts problem solving skills. The locus coeruleus (LC) is canonically known as the source of arousal and attention processing in the brain. During acute stress, heightened LC activity leads to norepinephrine release, which is important for directing attention towards performance in completing tasks. Chronic stress exposure may lead to long-term maladaptive attention processing disorders such as anxiety.

Our lab has recently reported that the LC-NE projections to BLA promote anxiety-like behavior. While data from the past 20 years suggest that noradrenergic circuitry may be involved in the release of DA, the specific extent to which the LC releases DA remains poorly understood. The heterogeneity of LC-NE projections' role in behavior obfuscates exactly how LC-DA release differs across the brain. My dissertation work addresses this gap in knowledge by establishing the extent of DA release evoked from the LC in the hippocampus and amygdala during appetitive and aversive stimuli.

5.1 Real-time detection of Neuromodulators

Our ability to understand the activity of neuromodulators has been limited by the technology used to sense them. While voltammetry has been useful in detecting neural activity at fast timescales, it relies on electro-active and structurally unique chemicals for detection (Park et al., 2010; Roberts & Sombers, 2018). Microdialysis has been useful in detecting concentrations of neuromodulators *in vivo* but is limited by the long timescale

for sample collection and analysis (Devoto et al., 2020; Gu et al., 2015; Wotjak et al., 2008). Over the past several years, our lab has been involved with technology development for manipulating circuit activity (Jeong et al., 2015; T. Kim et al., 2013), and throughout the course of my dissertation work, the lab has expanded our contributions in technology development to neurochemical detection (Cao et al., 2023; Stine et al., 2024; G. Wu et al., 2022) (**Chapter 2**). In my dissertation work, I have characterized and published the glial response to implantation of the gFET-aptamer DA device at different time points and depths and in response to the protective polymer, PDMS (Cao et al., 2023; G. Wu et al., 2022) (**Figure 2.1**). These findings contribute to a growing literature of techniques to mitigate the immune response which facilitates longer-term device efficacy.

Additionally, I characterized recently developed genetically-encoded neural indicators μMASS and dMASS to detect μ-opioid and DA dynamics in live brain slices (**Figure 2.2-2.3**). My work expands on our understanding of these sensors as they were originally characterized in HEK cells or cultured neurons. μMASS and dMASS sensors consistently respond to targeted ligand. With μMASS we saw responding to off-target ligands, that was greater than targeted ligands. While these sensors hold promise for *in vivo* implementation, these data exemplify the issue with selectivity and my own experimental design limitations including not reaching saturation points in washes.

With more widely used catecholamine sensors, we characterized selectivity for NE and DA in *ex vivo* 2-photon experiments for the first time. We found slices expressing DA sensors do respond to NE at high concentrations (**Figure 2.4**). These findings highlight

the importance of investigating the selectivity of all genetically-encoded sensors if there are off-target endogenous ligands that may bind to the sensor.

5.2 Catecholamine release to aversive and appetitive stimuli in amygdala and hippocampus

While we have long known that the hippocampus and amygdala are involved with processing aversive and appetitive cues and valence, our understanding of neuromodulator activity has been limited to microdialysis due to the selectivity challenges of voltammetry. With the development of catecholamine sensors, I characterized NE and DA dynamics to stimuli with a range of salience and valence.

We observed that the DA response to neutral, salient stimuli like an ambient light and odors was quicker in BLA than in dorsal and ventral CA1 (**Figure 3.2**). This delay in DA release may suggest that the BLA registers the salience and valence of the event, while dCA1 registers contextual cues and valence afterwards through DA signaling (Lisman & Grace, 2005b), however some studies suggest neutral cues do not activate dCA1 until valence is assigned (Yun et al., 2023). These studies contradict our findings that unrewarded nose pokes increased DA signal in the dCA1 (and BLA) of trained mice during operant conditioning.

The ventral CA1 had a stronger NE response to the onset and offset of a low salient looming stimulus than dorsal CA1 (**Figure 3.3**). We only saw DA released in hippocampus to more salient and negative-valence stimuli for mice like odor and shock, and in ventral hippocampus specifically, we saw DA release to cues associated to reward. Future studies should look at the NE and DA dynamics across the anterior to posterior axis in

vCA1, which shows functional separation to cues (Shpokayte et al., 2022). For dCA1, future studies should investigate the dynamics of DA release from LC during spatial memory, learning, and novelty.

5.3 LC-DA evoked release and LC sufficiency to release DA during appetitive and aversive stimuli

While noradrenergic sourced DA has been suggested by pharmacology and microdialysis experiments (Devoto et al., 2003; Devoto, Flore, Saba, Fa, et al., 2005), these studies have not been selective or specific enough to show direct projection-elicited release. More recent studies suggesting that the LC-NE system is the direct source of DA in spatial memory and plasticity rely on high concentration pharmacology and indirect, supraphysiological evidence of evoked LC-DA release (Kempadoo et al., 2016a; Smith & Greene, 2012a; Takeuchi et al., 2016a). Others suggest VTA is the source of DA in CA1 controlling persisting contextual memory(Lisman & Grace, 2005b) and contextual fear acquisition(Tsetsenis et al., 2021) in the absence of noradrenergic signaling. In this study, we aimed to establish the limitations of DA release from LC terminals in CA1 and BLA during appetitive and aversive conditions.

We address concerns of sensor selectivity through fiber photometry and optogenetic stimulation in DBH-KO mice. LC-CA1TH stimulation that typically produces a clear NE response produced no GRAB$_{NE}$ response in DBH-KO mice, indicating GRAB$_{NE}$ does not detect DA release in response to stimulation conditions we are using.

Using 2-photon imaging of live hippocampal slices, we reliably evoke DA release at frequencies and durations as low as 5hz 3s of stimulation. We characterize the LC-

evoked DA release and find that LC-DA across BLA and CA1 follows a linear trend of release with increasing frequency. This is in contrast with a second-order trend of release with LC-NE, suggesting there exists some limiting factor of LC-evoked DA release at higher phasic stimulation (**Figure 4.2**).

The VTA is not contributing to photo-stimulated LC-BLATH and LC-CA1TH release (**Figure 4.2**). VTA inhibition may be disinhibiting the LC, producing an increase in LC-evoked DA in some mice, which aligns with past data that the VTA and LC have inhibitory effects on each other (Guiard, El Mansari, & Blier, 2008). No DA release was detected in CA1 to reward and shock by GRAB$_{rDA}$. Importantly, in the BLA, LC inhibition decreased DA released during consumption of reward and shock. These data show for the first time that the LC is contributing DA in response to appetitive and aversive stimuli in BLA, but not in CA1. We hypothesize that this difference in DA released during reward is due to differences in LC firing in BLA and CA1 during both reward consumption and shock. To test these hypotheses, further work should establish VTA and LC activity during inhibition of the other respective source. Additionally, the mechanism for DA release from LC terminals is still unclear, and addressing this gap would be crucial for understanding the role of LC-DA in endogenous release. One potential way to test this hypothesis is to do electron microscopy in the LC to localization of DA, Dbh, and NE in the LC.

References

Abdalla, S. M., Cohen, G. H., Tamrakar, S., Koya, S. F., & Galea, S. (2021). Media Exposure and the Risk of Post-Traumatic Stress Disorder Following a Mass traumatic Event: An In-silico Experiment. *Frontiers in Psychiatry*, *12*, 674263. https://doi.org/10.3389/fpsyt.2021.674263

Adams, R. N. (1976). Probing brain chemistry with electroanalytical techniques. *Analytical Chemistry*, *48*(14), 1126A-1138A. https://doi.org/10.1021/ac50008a001

Ambroggi, F., Ishikawa, A., Fields, H. L., & Nicola, S. M. (2008a). Basolateral amygdala neurons facilitate reward-seeking behavior by exciting nucleus accumbens neurons. *Neuron*, *59*(4), Article 4. https://doi.org/10.1016/j.neuron.2008.07.004

Ambroggi, F., Ishikawa, A., Fields, H. L., & Nicola, S. M. (2008b). Basolateral amygdala neurons facilitate reward-seeking behavior by exciting nucleus accumbens neurons. *Neuron*, *59*(4), 648–661. https://doi.org/10.1016/j.neuron.2008.07.004

Anagnostaras, S. G., Maren, S., & Fanselow, M. S. (1999). Temporally Graded Retrograde Amnesia of Contextual Fear after Hippocampal Damage in Rats: Within-Subjects Examination. *Journal of Neuroscience*, *19*(3), 1106–1114. https://doi.org/10.1523/JNEUROSCI.19-03-01106.1999

Anderson, A. K., & Phelps, E. A. (2001). Lesions of the human amygdala impair enhanced perception of emotionally salient events. *Nature*, *411*(6835), 305–309. https://doi.org/10.1038/35077083

Armony, J. L., Servan-Schreiber, D., Cohen, J. D., & LeDoux, J. E. (1997). Computational modeling of emotion: Explorations through the anatomy and physiology of fear conditioning. *Trends in Cognitive Sciences*, *1*(1), 28–34. https://doi.org/10.1016/S1364-6613(97)01007-3

Ashwell, K. (2012). Chapter 26—The Olfactory System. In C. Watson, G. Paxinos, & L. Puelles (Eds.), *The Mouse Nervous System* (pp. 653–660). Academic Press. https://doi.org/10.1016/B978-0-12-369497-3.10026-3

Aston-Jones, G., & Cohen, J. D. (2005). AN INTEGRATIVE THEORY OF LOCUS COERULEUS-NOREPINEPHRINE FUNCTION: Adaptive Gain and Optimal Performance. *Annual Review of Neuroscience*, *28*(1), 403–450. https://doi.org/10.1146/annurev.neuro.28.061604.135709

Barnes, P. J. (1995). Beta-adrenergic receptors and their regulation. *American Journal of Respiratory and Critical Care Medicine*, *152*(3), 838–860. https://doi.org/10.1164/ajrccm.152.3.7663795

Barrett, L. F., Tugade, M. M., & Engle, R. W. (2004). Individual Differences in Working Memory Capacity and Dual-Process Theories of the Mind. *Psychological Bulletin*, *130*(4), 553–573. https://doi.org/10.1037/0033-2909.130.4.553

Barth, A. M., Jelitai, M., Vasarhelyi-Nagy, M. F., & Varga, V. (2023). Aversive stimulus-tuned responses in the CA1 of the dorsal hippocampus. *Nature Communications*, *14*(1), 6841. https://doi.org/10.1038/s41467-023-42611-w

Barton, B. A., Adams, K. S., Browne, B. L., & Arrastia-Chisholm, M. C. (2021). The effects of social media usage on attention, motivation, and academic performance. *Active Learning in Higher Education*, *22*(1), 11–22. https://doi.org/10.1177/1469787418782817

Bernacka, J., Kielbinski, M., Wawrzczak-Bargieła, A., Zajda, K., Maćkowiak, M., Przewlocki, R., & Solecki, W. (2022). Alpha-2A but not 2B/C noradrenergic receptors in ventral tegmental area regulate phasic dopamine release in nucleus

accumbens core. *Neuropharmacology*, *220*, 109258. https://doi.org/10.1016/j.neuropharm.2022.109258

Berridge, C. W. (2008). Noradrenergic modulation of arousal. *Brain Research Reviews*, *58*(1), 1–17. https://doi.org/10.1016/j.brainresrev.2007.10.013

Bethus, I., Tse, D., & Morris, R. G. M. (2010). Dopamine and Memory: Modulation of the Persistence of Memory for Novel Hippocampal NMDA Receptor-Dependent Paired Associates. *Journal of Neuroscience*, *30*(5), 1610–1618.

Biane, J. S., Ladow, M. A., Stefanini, F., Boddu, S. P., Fan, A., Hassan, S., Dundar, N., Apodaca-Montano, D. L., Zhou, L. Z., Fayner, V., Woods, N. I., & Kheirbek, M. A. (2023). Neural dynamics underlying associative learning in the dorsal and ventral hippocampus. *Nature Neuroscience*, *26*(5), 798–809. https://doi.org/10.1038/s41593-023-01296-6

Bird, C. M., & Burgess, N. (2008). The hippocampus and memory: Insights from spatial processing. *Nature Reviews Neuroscience*, *9*(3), 182–194. https://doi.org/10.1038/nrn2335

Borgkvist, A., Malmlöf, T., Feltmann, K., Lindskog, M., & Schilström, B. (2011). Dopamine in the hippocampus is cleared by the norepinephrine transporter. *The International Journal of Neuropsychopharmacology*, 1–10. https://doi.org/10.1017/S1461145711000812

Borodovitsyna, O., Flamini, M. D., & Chandler, D. J. (2018a). Acute Stress Persistently Alters Locus Coeruleus Function and Anxiety-like Behavior in Adolescent Rats. *Neuroscience*, *373*, 7–19. https://doi.org/10.1016/j.neuroscience.2018.01.020

Borodovitsyna, O., Flamini, M. D., & Chandler, D. J. (2018b). Acute Stress Persistently Alters Locus Coeruleus Function and Anxiety-like Behavior in Adolescent Rats. *Neuroscience*, *373*, 7–19. https://doi.org/10.1016/j.neuroscience.2018.01.020

Bourdélat-Parks, B. N., Anderson, G. M., Donaldson, Z. R., Weiss, J. M., Bonsall, R. W., Emery, M. S., Liles, L. C., & Weinshenker, D. (2005). Effects of dopamine β-hydroxylase genotype and disulfiram inhibition on catecholamine homeostasis in mice. *Psychopharmacology*, *183*(1), 72–80. https://doi.org/10.1007/s00213-005-0139-8

Bouret, S., & Sara, S. J. (2004). Reward expectation, orientation of attention and locus coeruleus-medial frontal cortex interplay during learning. *European Journal of Neuroscience*, *20*(3), Article 3. https://doi.org/10.1111/j.1460-9568.2004.03526.x

Boyajian, L., & Loughlin, E. (1987). *Anatomical Evidence for Alpha-2 Adrenoceptor Heterogeneity: Differential Autoradiographic Distributions of [3H]Rauwolscine and [3H]Idazoxan in Rat Brain*. *241*.

Brimijoin, S. (1974). LOCAL CHANGES IN SUBCELLULAR DISTRIBUTION OF DOPAMINE-β-HYDROXYLASE (EC 1.14.2.1) AFTER BLOCKADE OF AXONAL TRANSPORT. *Journal of Neurochemistry*, *22*(3), 347–353. https://doi.org/10.1111/j.1471-4159.1974.tb07599.x

Broussard, J. I., Yang, K., Levine, A. T., Tsetsenis, T., Jenson, D., Cao, F., Garcia, I., Arenkiel, B. R., Zhou, F.-M., Biasi, M. D., & Dani, J. A. (2016a). Dopamine Regulates Aversive Contextual Learning and Associated In Vivo Synaptic Plasticity in the Hippocampus. *Cell Reports*, *14*(8), 1930–1939. https://doi.org/10.1016/j.celrep.2016.01.070

Broussard, J. I., Yang, K., Levine, A. T., Tsetsenis, T., Jenson, D., Cao, F., Garcia, I., Arenkiel, B. R., Zhou, F.-M., Biasi, M. D., & Dani, J. A. (2016b). Dopamine Regulates Aversive Contextual Learning and Associated In Vivo Synaptic Plasticity in the Hippocampus. *Cell Reports*, *14*(8), Article 8. https://doi.org/10.1016/j.celrep.2016.01.070

Bruzsik, B., Biro, L., Sarosdi, K. R., Zelena, D., Sipos, E., Szebik, H., Török, B., Mikics, E., & Toth, M. (2021). Neurochemically distinct populations of the bed nucleus of stria terminalis modulate innate fear response to weak threat evoked by predator odor stimuli. *Neurobiology of Stress*, *15*, 100415. https://doi.org/10.1016/j.ynstr.2021.100415

Buffalari, D. M., & Grace, A. A. (2007). Noradrenergic Modulation of Basolateral Amygdala Neuronal Activity: Opposing Influences of α-2 and β Receptor Activation. *The Journal of Neuroscience*, *27*(45), 12358–12366. https://doi.org/10.1523/JNEUROSCI.2007-07.2007

Bunney, B. S., Walters, J. R., Roth, R. H., Stract, A. B., S, B., Walters, J. R., Roth, R. H., & K, G. (1973). *Dopaminergic Neurons: Effect of Antipsy- Chotic Drugs and Amphetamine Single Cell Activity' On*.

Campeau, S., & Davis, M. (1995). Involvement of the central nucleus and basolateral complex of the amygdala in fear conditioning measured with fear-potentiated startle in rats trained concurrently with auditory and visual conditioned stimuli. *Journal of Neuroscience*, *15*(3), 2301–2311. https://doi.org/10.1523/JNEUROSCI.15-03-02301.1995

Cao, Y., Chen, X., Matarasso, A., Wang, Z., Song, Y., Wu, G., Zhang, X., Sun, H., Wang, X., Bruchas, M. R., Li, Y., & Zhang, Y. (2023). Covalently Attached Slippery Surface Coatings to Reduce Protein Adsorptions on Poly(dimethylsiloxane) Planar Surfaces and 3D Microfluidic Channels. *ACS Applied Materials & Interfaces*, *15*(7), 9987–9995. https://doi.org/10.1021/acsami.2c20834

Carter, M. E., Yizhar, O., Chikahisa, S., Nguyen, H., Adamantidis, A., Nishino, S., Deisseroth, K., & de Lecea, L. (2010). Tuning arousal with optogenetic modulation of locus coeruleus neurons. *Nature Neuroscience*, *13*(12), 1526–1533. https://doi.org/10.1038/nn.2682

Chandler, D. J., Jensen, P., McCall, J. G., Pickering, A. E., Schwarz, L. A., & Totah, N. K. (2019a). Redefining Noradrenergic Neuromodulation of Behavior: Impacts of a Modular Locus Coeruleus Architecture. *The Journal of Neuroscience*, *39*(42), 8239–8249. https://doi.org/10.1523/JNEUROSCI.1164-19.2019

Chandler, D. J., Jensen, P., McCall, J. G., Pickering, A. E., Schwarz, L. A., & Totah, N. K. (2019b). Redefining Noradrenergic Neuromodulation of Behavior: Impacts of a Modular Locus Coeruleus Architecture. *The Journal of Neuroscience*, *39*(42), Article 42. https://doi.org/10.1523/JNEUROSCI.1164-19.2019

Chen, F.-J., & Sara, S. J. (2007a). Locus coeruleus activation by foot shock or electrical stimulation inhibits amygdala neurons. *Neuroscience*, *144*(2), 472–481. https://doi.org/10.1016/j.neuroscience.2006.09.037

Chen, F.-J., & Sara, S. J. (2007b). Locus coeruleus activation by foot shock or electrical stimulation inhibits amygdala neurons. *Neuroscience*, *144*(2), 472–481. https://doi.org/10.1016/j.neuroscience.2006.09.037

Cheng, C., & Li, A. Y. (2014). Internet addiction prevalence and quality of (real) life: A meta-analysis of 31 nations across seven world regions. *Cyberpsychology, Behavior and Social Networking*, *17*(12), 755–760. https://doi.org/10.1089/cyber.2014.0317

Cho, J. R., Treweek, J. B., Robinson, J. E., Xiao, C., Bremner, L. R., Greenbaum, A., & Gradinaru, V. (2017). Dorsal Raphe Dopamine Neurons Modulate Arousal and Promote Wakefulness by Salient Stimuli. *Neuron*, *94*(6), 1205-1219.e8. https://doi.org/10.1016/j.neuron.2017.05.020

Christopoulos, A. (2002). G Protein-Coupled Receptor Allosterism and Complexing. *Pharmacological Reviews*, *54*(2), Article 2. https://doi.org/10.1124/pr.54.2.323

Cimarusti, D. L., Saito, K., Vaughn, J. E., Barber, R., Roberts, E., & Thomas, P. E. (1979a). Immunocytochemical localization of dopamine-β-hydroxylase in rat locus coeruleus and hypothalamus. *Brain Research*, *162*(1), 55–67. https://doi.org/10.1016/0006-8993(79)90755-8

Cimarusti, D. L., Saito, K., Vaughn, J. E., Barber, R., Roberts, E., & Thomas, P. E. (1979b). Immunocytochemical localization of dopamine-β-hydroxylase in rat locus coeruleus and hypothalamus. *Brain Research*, *162*(1), 55–67. https://doi.org/10.1016/0006-8993(79)90755-8

Ciocchi, S., Passecker, J., Malagon-Vina, H., Mikus, N., & Klausberger, T. (2015). Brain computation. Selective information routing by ventral hippocampal CA1 projection neurons. *Science (New York, N.Y.)*, *348*(6234), 560–563. https://doi.org/10.1126/science.aaa3245

Cohen, J. Y., Haesler, S., Vong, L., Lowell, B. B., & Uchida, N. (2012). Neuron-type-specific signals for reward and punishment in the ventral tegmental area. *Nature*, *482*(7383), 85–88. https://doi.org/10.1038/nature10754

Cubells, J. F., Kranzler, H. R., McCance-Katz, E., Anderson, G. M., Malison, R. T., Price, L. H., & Gelernter, J. (2000). A haplotype at the DBH locus, associated with low plasma dopamine β-hydroxylase activity, also associates with cocaine-induced paranoia. *Molecular Psychiatry*, *5*(1), 56–63. https://doi.org/10.1038/sj.mp.4000657

Cubells, J. F., & Zabetian, C. P. (2004). Human genetics of plasma dopamine beta-hydroxylase activity: Applications to research in psychiatry and neurology. *Psychopharmacology*, *174*(4), 463–476. https://doi.org/10.1007/s00213-004-1840-8

Curtis, A. L., Leiser, S. C., Snyder, K., & Valentino, R. J. (2012). Predator stress engages corticotropin-releasing factor and opioid systems to alter the operating mode of locus coeruleus norepinephrine neurons. *Neuropharmacology*, *62*(4), Article 4. https://doi.org/10.1016/j.neuropharm.2011.11.020

Davis, M., & Whalen, P. J. (2001). The amygdala: Vigilance and emotion. *Molecular Psychiatry*, *6*(1), 13–34. https://doi.org/10.1038/sj.mp.4000812

de Lavilléon, G., Lacroix, M. M., Rondi-Reig, L., & Benchenane, K. (2015). Explicit memory creation during sleep demonstrates a causal role of place cells in navigation. *Nature Neuroscience*, *18*(4), 493–495. https://doi.org/10.1038/nn.3970

de Medeiros, M. A., Carlos Reis, L., & Eugênio Mello, L. (2005a). Stress-Induced c-Fos Expression is Differentially Modulated by Dexamethasone, Diazepam and

Imipramine. *Neuropsychopharmacology*, *30*(7), 1246–1256. https://doi.org/10.1038/sj.npp.1300694

de Medeiros, M. A., Carlos Reis, L., & Eugênio Mello, L. (2005b). Stress-Induced c-Fos Expression is Differentially Modulated by Dexamethasone, Diazepam and Imipramine. *Neuropsychopharmacology*, *30*(7), 1246–1256. https://doi.org/10.1038/sj.npp.1300694

de Oliveira, A. R., Reimer, A. E., de Macedo, C. E. A., de Carvalho, M. C., Silva, M. A. de S., & Brandão, M. L. (2011). Conditioned fear is modulated by D2 receptor pathway connecting the ventral tegmental area and basolateral amygdala. *Neurobiology of Learning and Memory*, *95*(1), 37–45. https://doi.org/10.1016/j.nlm.2010.10.005

Deutch, A. Y., Goldstein, M., & Roth, R. H. (1986). Activation of the locus coeruleus induced by selective stimulation of the ventral tegmental area. *Brain Research*, *363*(2), 307–314. https://doi.org/10.1016/0006-8993(86)91016-4

Devilbiss, D. M., & Waterhouse, B. D. (2000). Norepinephrine exhibits two distinct profiles of action on sensory cortical neuron responses to excitatory synaptic stimuli. *Synapse*, *37*(4), 273–282. https://doi.org/10.1002/1098-2396(20000915)37:4<273::AID-SYN4>3.0.CO;2-#

Devilbiss, D. M., & Waterhouse, B. D. (2011a). Phasic and Tonic Patterns of Locus Coeruleus Output Differentially Modulate Sensory Network Function in the Awake Rat. *Journal of Neurophysiology*, *105*(1), 69–87. https://doi.org/10.1152/jn.00445.2010

Devilbiss, D. M., & Waterhouse, B. D. (2011b). Phasic and Tonic Patterns of Locus Coeruleus Output Differentially Modulate Sensory Network Function in the Awake

Rat. *Journal of Neurophysiology*, *105*(1), Article 1. https://doi.org/10.1152/jn.00445.2010

Devoto, P., Flore, G., Longu, G., Pira, L., & Gessa, G. L. (2003). Origin of extracellular dopamine from dopamine and noradrenaline neurons in the medial prefrontal and occipital cortex. *Synapse*, *50*(3), 200–205. https://doi.org/10.1002/syn.10264

Devoto, P., Flore, G., Pira, L., Longu, G., & Gessa, G. L. (2004). Alpha2-adrenoceptor mediated co-release of dopamine and noradrenaline from noradrenergic neurons in the cerebral cortex. *Journal of Neurochemistry*, *88*(4), 1003–1009. https://doi.org/10.1046/j.1471-4159.2003.02239.x

Devoto, P., Flore, G., Saba, P., Fà, M., & Gessa, G. (2005). Co-release of noradrenaline and dopamine in the cerebral cortex elicited by single train and repeated train stimulation of the locus coeruleus. *BMC Neuroscience*, *6*(1), Article 1. https://doi.org/10.1186/1471-2202-6-31

Devoto, P., Flore, G., Saba, P., Fa, M., & Gessa, G. L. (2005). Stimulation of the locus coeruleus elicits noradrenaline and dopamine release in the medial prefrontal and parietal cortex. *Journal of Neurochemistry*, *92*(2), Article 2. https://doi.org/10.1111/j.1471-4159.2004.02866.x

Devoto, P., Flore, G., Saba, P., Scheggi, S., Mulas, G., Gambarana, C., Spiga, S., & Gessa, G. L. (2019). Noradrenergic terminals are the primary source of α2-adrenoceptor mediated dopamine release in the medial prefrontal cortex. *Progress in Neuro-Psychopharmacology and Biological Psychiatry*, *90*, 97–103. https://doi.org/10.1016/j.pnpbp.2018.11.015

Devoto, P., Sagheddu, C., Santoni, M., Flore, G., Saba, P., Pistis, M., & Gessa, G. L. (2020). Noradrenergic Source of Dopamine Assessed by Microdialysis in the Medial Prefrontal Cortex. *Frontiers in Pharmacology*, *11*, 588160. https://doi.org/10.3389/fphar.2020.588160

Dhiman, A., Kalra, P., Bansal, V., Bruno, John. G., & Sharma, T. K. (2017). Aptamer-based point-of-care diagnostic platforms. *Sensors and Actuators B: Chemical*, *246*, 535–553. https://doi.org/10.1016/j.snb.2017.02.060

Díaz-García, C. M., Lahmann, C., Martínez-François, J. R., Li, B., Koveal, D., Nathwani, N., Rahman, M., Keller, J. P., Marvin, J. S., Looger, L. L., & Yellen, G. (2019). Quantitative in vivo imaging of neuronal glucose concentrations with a genetically encoded fluorescence lifetime sensor. *Journal of Neuroscience Research*, *97*(8), 946–960. https://doi.org/10.1002/jnr.24433

Digital vs Traditional Media Consumption. (n.d.). Retrieved March 15, 2025, from https://www.gwi.com/hubfs/Digital_vs_Traditional_Media_Consumption.pdf

Dong, C., Gowrishankar, R., Jin, Y., He, X. J., Gupta, A., Wang, H., Sayar-Atasoy, N., Flores, R. J., Mahe, K., Tjahjono, N., Liang, R., Marley, A., Or Mizuno, G., Lo, D. K., Sun, Q., Whistler, J. L., Li, B., Gomes, I., Von Zastrow, M., … Tian, L. (2024). Unlocking opioid neuropeptide dynamics with genetically encoded biosensors. *Nature Neuroscience*, *27*(9), 1844–1857. https://doi.org/10.1038/s41593-024-01697-1

Dupret, D., O'Neill, J., Pleydell-Bouverie, B., & Csicsvari, J. (2010a). The reorganization and reactivation of hippocampal maps predict spatial memory performance. *Nature Neuroscience*, *13*(8), 995–1002. https://doi.org/10.1038/nn.2599

Dupret, D., O'Neill, J., Pleydell-Bouverie, B., & Csicsvari, J. (2010b). The reorganization and reactivation of hippocampal maps predict spatial memory performance. *Nature Neuroscience*, *13*(8), 995–1002. https://doi.org/10.1038/nn.2599

Engle, R. W. (2002). Working memory capacity as executive attention. *Current Directions in Psychological Science*, *11*(1), 19–23. https://doi.org/10.1111/1467-8721.00160

Fanselow, M. S., & Dong, H.-W. (2010). Are The Dorsal and Ventral Hippocampus functionally distinct structures? *Neuron*, *65*(1), Article 1. https://doi.org/10.1016/j.neuron.2009.11.031

Fanselow, M. S., & LeDoux, J. E. (1999a). Why We Think Plasticity Underlying Pavlovian Fear Conditioning Occurs in the Basolateral Amygdala. *Neuron*, *23*(2), 229–232. https://doi.org/10.1016/S0896-6273(00)80775-8

Fanselow, M. S., & LeDoux, J. E. (1999b). Why We Think Plasticity Underlying Pavlovian Fear Conditioning Occurs in the Basolateral Amygdala. *Neuron*, *23*(2), Article 2. https://doi.org/10.1016/S0896-6273(00)80775-8

Feng, J., Dong, H., Lischinsky, J. E., Zhou, J., Deng, F., Zhuang, C., Miao, X., Wang, H., Li, G., Cai, R., Xie, H., Cui, G., Lin, D., & Li, Y. (2024). Monitoring norepinephrine release in vivo using next-generation GRABNE sensors. *Neuron*, *112*(12), 1930-1942.e6. https://doi.org/10.1016/j.neuron.2024.03.001

Feng, J., Zhang, C., Lischinsky, J. E., Jing, M., Zhou, J., Wang, H., Zhang, Y., Dong, A., Wu, Z., Wu, H., Chen, W., Zhang, P., Zou, J., Hires, S. A., Zhu, J. J., Cui, G., Lin, D., Du, J., & Li, Y. (2019a). A Genetically Encoded Fluorescent Sensor for Rapid and Specific In Vivo Detection of Norepinephrine. *Neuron*, *102*(4), 745-761.e8. https://doi.org/10.1016/j.neuron.2019.02.037

Feng, J., Zhang, C., Lischinsky, J. E., Jing, M., Zhou, J., Wang, H., Zhang, Y., Dong, A., Wu, Z., Wu, H., Chen, W., Zhang, P., Zou, J., Hires, S. A., Zhu, J. J., Cui, G., Lin, D., Du, J., & Li, Y. (2019b). A Genetically Encoded Fluorescent Sensor for Rapid and Specific In Vivo Detection of Norepinephrine. *Neuron*, *102*(4), Article 4. https://doi.org/10.1016/j.neuron.2019.02.037

Gálvez-Márquez, D. K., Salgado-Ménez, M., Moreno-Castilla, P., Rodríguez-Durán, L., Escobar, M. L., Tecuapetla, F., & Bermudez-Rattoni, F. (2022). Spatial contextual recognition memory updating is modulated by dopamine release in the dorsal hippocampus from the locus coeruleus. *Proceedings of the National Academy of Sciences*, *119*(49), e2208254119. https://doi.org/10.1073/pnas.2208254119

Gao, N., Gao, T., Yang, X., Dai, X., Zhou, W., Zhang, A., & Lieber, C. M. (2016). Specific detection of biomolecules in physiological solutions using graphene transistor biosensors. *Proceedings of the National Academy of Sciences*, *113*(51), 14633–14638. https://doi.org/10.1073/pnas.1625010114

Gasbarri, A., Sulli, A., Innocenzi, R., Pacitti, C., & Brioni, J. D. (1996). Spatial memory impairment induced by lesion of the mesohippocampal dopaminergic system in the rat. *Neuroscience*, *74*(4), 1037–1044. https://doi.org/10.1016/0306-4522(96)00202-3

Gauthier, J. L., & Tank, D. W. (2018). A Dedicated Population for Reward Coding in the Hippocampus. *Neuron*, *99*(1), 179-193.e7. https://doi.org/10.1016/j.neuron.2018.06.008

Gaval-Cruz, M., & Weinshenker, D. (2009). mechanisms of disulfiram-induced cocaine abstinence: Antabuse and cocaine relapse. *Molecular Interventions*, *9*(4), 175–187. https://doi.org/10.1124/mi.9.4.6

Giustino, T. F., & Maren, S. (2018). Noradrenergic Modulation of Fear Conditioning and Extinction. *Frontiers in Behavioral Neuroscience*, *12*, 43. https://doi.org/10.3389/fnbeh.2018.00043

Giustino, T. F., Ramanathan, K. R., Totty, M. S., Miles, O. W., & Maren, S. (2020). Locus Coeruleus Norepinephrine Drives Stress-Induced Increases in Basolateral Amygdala Firing and Impairs Extinction Learning. *The Journal of Neuroscience*, *40*(4), Article 4. https://doi.org/10.1523/JNEUROSCI.1092-19.2019

Grace, A., & Onn, S. (1989). Morphology and electrophysiological properties of immunocytochemically identified rat dopamine neurons recorded in vitro. *The Journal of Neuroscience*, *9*(10), 3463–3481. https://doi.org/10.1523/JNEUROSCI.09-10-03463.1989

Greene, J. G., Dingledine, R., & Greenamyre, J. T. (2005). Gene expression profiling of rat midbrain dopamine neurons: Implications for selective vulnerability in parkinsonism. *Neurobiology of Disease*, *18*(1), 19–31. https://doi.org/10.1016/j.nbd.2004.10.003

Grenhoff, J., Nisell, M., Ferré, S., Aston-Jones, G., & Svensson, T. H. (1993). Noradrenergic modulation of midbrain dopamine cell firing elicited by stimulation of the locus coeruleus in the rat. *Journal of Neural Transmission / General Section JNT*, *93*(1), 11–25. https://doi.org/10.1007/BF01244934

Grimm, C., Duss, S. N., Privitera, M., Munn, B. R., Karalis, N., Frässle, S., Wilhelm, M., Patriarchi, T., Razansky, D., Wenderoth, N., Shine, J. M., Bohacek, J., & Zerbi, V. (2024). Tonic and burst-like locus coeruleus stimulation distinctly shift network activity across the cortical hierarchy. *Nature Neuroscience*, *27*(11), 2167–2177. https://doi.org/10.1038/s41593-024-01755-8

Gu, H., Varner, E. L., Groskreutz, S. R., Michael, A. C., & Weber, S. G. (2015). In Vivo Monitoring of Dopamine by Microdialysis with 1 min Temporal Resolution Using Online Capillary Liquid Chromatography with Electrochemical Detection. *Analytical Chemistry*, *87*(12), 6088–6094. https://doi.org/10.1021/acs.analchem.5b00633

Guarraci, F. A., Frohardt, R. J., Falls, W. A., & Kapp, B. S. (2000). The effects of intra-amygdaloid infusions of a D_2 dopamine receptor antagonist on Pavlovian fear conditioning. *Behavioral Neuroscience*, *114*(3), 647–651. https://doi.org/10.1037/0735-7044.114.3.647

Guiard, B. P., El Mansari, M., & Blier, P. (2008). Cross-Talk between Dopaminergic and Noradrenergic Systems in the Rat Ventral Tegmental Area, Locus Ceruleus, and Dorsal Hippocampus. *Molecular Pharmacology*, *74*(5), 1463–1475. https://doi.org/10.1124/mol.108.048033

Guiard, B. P., El Mansari, M., Merali, Z., & Blier, P. (2008). Functional interactions between dopamine, serotonin and norepinephrine neurons: An in-vivo electrophysiological study in rats with monoaminergic lesions. *International Journal of Neuropsychopharmacology*, *11*(5), 625–639. https://doi.org/10.1017/S1461145707008383

Guiard, B. P., & Gotti, G. (2024). The High-Precision Liquid Chromatography with Electrochemical Detection (HPLC-ECD) for Monoamines Neurotransmitters and Their Metabolites: A Review. *Molecules*, *29*(2), 496. https://doi.org/10.3390/molecules29020496

Hauber, W. (1996). Impairments of movement initiation and execution induced by a blockade of dopamine D1 OR D2 receptors are reversed by a blockade of *N*-methyl-d-aspartate receptors. *Neuroscience*, *73*(1), 121–130. https://doi.org/10.1016/0306-4522(96)00036-X

Heath, F. C., Jurkus, R., Bast, T., Pezze, M. A., Lee, J. L. C., Voigt, J. P., & Stevenson, C. W. (2015). Dopamine D1-like receptor signalling in the hippocampus and amygdala modulates the acquisition of contextual fear conditioning. *Psychopharmacology*, *232*(14), 2619–2629. https://doi.org/10.1007/s00213-015-3897-y

Hirata, H., & Aston-Jones, G. (1994). A novel long-latency response of locus coeruleus neurons to noxious stimuli: Mediation by peripheral C-fibers. *Journal of Neurophysiology*, *71*(5), 1752–1761. https://doi.org/10.1152/jn.1994.71.5.1752

Hock, B. J., & Bunsey, M. D. (1998). Differential Effects of Dorsal and Ventral Hippocampal Lesions. *The Journal of Neuroscience*, *18*(17), 7027–7032. https://doi.org/10.1523/JNEUROSCI.18-17-07027.1998

Ito, R., Everitt, B. J., & Robbins, T. W. (2005). The hippocampus and appetitive Pavlovian conditioning: Effects of excitotoxic hippocampal lesions on conditioned locomotor activity and autoshaping. *Hippocampus*, *15*(6), 713–721. https://doi.org/10.1002/hipo.20094

Itoi, K., & Sugimoto, N. (2010). The Brainstem Noradrenergic Systems in Stress, Anxiety and Depression. *Journal of Neuroendocrinology*, *22*(5), Article 5. https://doi.org/10.1111/j.1365-2826.2010.01988.x

Jacobsen, W. C., & Forste, R. (2011). The Wired Generation: Academic and Social Outcomes of Electronic Media Use Among University Students. *Cyberpsychology, Behavior, and Social Networking*, *14*(5), 275–280. https://doi.org/10.1089/cyber.2010.0135

Jeong, J.-W., McCall, J. G., Shin, G., Zhang, Y., Al-Hasani, R., Kim, M., Li, S., Sim, J. Y., Jang, K.-I., Shi, Y., Hong, D. Y., Liu, Y., Schmitz, G. P., Xia, L., He, Z., Gamble, P., Ray, W. Z., Huang, Y., Bruchas, M. R., & Rogers, J. A. (2015). Wireless Optofluidic Systems for Programmable In Vivo Pharmacology and Optogenetics. *Cell*, *162*(3), 662–674. https://doi.org/10.1016/j.cell.2015.06.058

Jimenez, J. C., Berry, J. E., Lim, S. C., Ong, S. K., Kheirbek, M. A., & Hen, R. (2020). Contextual fear memory retrieval by correlated ensembles of ventral CA1 neurons. *Nature Communications*, *11*(1), 3492. https://doi.org/10.1038/s41467-020-17270-w

Jimenez, J. C., Su, K., Goldberg, A. R., Luna, V. M., Biane, J. S., Ordek, G., Zhou, P., Ong, S. K., Wright, M. A., Zweifel, L., Paninski, L., Hen, R., & Kheirbek, M. A. (2018). Anxiety Cells in a Hippocampal-Hypothalamic Circuit. *Neuron*, *97*(3), Article 3. https://doi.org/10.1016/j.neuron.2018.01.016

Kapp, B. S., Whalen, P. J., Supple, W. F., & Pascoe, J. P. (1992). Amygdaloid contributions to conditioned arousal and sensory information processing. In *The*

amygdala: Neurobiological aspects of emotion, memory, and mental dysfunction (pp. 229–254). Wiley-Liss.

Karpinski, A. C., Kirschner, P. A., Ozer, I., Mellott, J. A., & Ochwo, P. (2013). An exploration of social networking site use, multitasking, and academic performance among United States and European university students. *Computers in Human Behavior*, *29*(3), 1182–1192. https://doi.org/10.1016/j.chb.2012.10.011

Kauer, J. A. (2004). Learning Mechanisms in Addiction: Synaptic Plasticity in the Ventral Tegmental Area as a Result of Exposure to Drugs of Abuse. *Annual Review of Physiology*, *66*(1), 447–475. https://doi.org/10.1146/annurev.physiol.66.032102.112534

Kaufman, A. M., Geiller, T., & Losonczy, A. (2020). A Role for the Locus Coeruleus in Hippocampal CA1 Place Cell Reorganization during Spatial Reward Learning. *Neuron*, *105*(6), Article 6. https://doi.org/10.1016/j.neuron.2019.12.029

Kelberman, M. A., Rodberg, E., Arabzadeh, E., Bair-Marshall, C. J., Berridge, C. W., Berrocoso, E., Breton-Provencher, V., Chandler, D. J., Che, A., Davy, O., Devilbiss, D. M., Downs, A. M., Drummond, G., Dvorkin, R., Fazlali, Z., Froemke, R. C., Glennon, E., Gold, J. I., Ito, H., … Totah, N. K. (2024). Diversity of ancestral brainstem noradrenergic neurons across species and multiple biological factors. *bioRxiv*, 2024.10.14.618224. https://doi.org/10.1101/2024.10.14.618224

Kempadoo, K. A., Mosharov, E. V., Choi, S. J., Sulzer, D., & Kandel, E. R. (2016a). Dopamine release from the locus coeruleus to the dorsal hippocampus promotes spatial learning and memory. *Proceedings of the National Academy of Sciences*, *113*(51), Article 51. https://doi.org/10.1073/pnas.1616515114

Kempadoo, K. A., Mosharov, E. V., Choi, S. J., Sulzer, D., & Kandel, E. R. (2016b). Dopamine release from the locus coeruleus to the dorsal hippocampus promotes spatial learning and memory. *Proceedings of the National Academy of Sciences*, *113*(51), 14835–14840. https://doi.org/10.1073/pnas.1616515114

Kentros, C. G., Agnihotri, N. T., Streater, S., Hawkins, R. D., & Kandel, E. R. (2004). Increased Attention to Spatial Context Increases Both Place Field Stability and Spatial Memory. *Neuron*, *42*(2), 283–295. https://doi.org/10.1016/S0896-6273(04)00192-8

Kim, J., Castro, L., Wasserman, E. A., & Freeman, J. H. (2018). Dorsal hippocampus is necessary for visual categorization in rats. *Hippocampus*, *28*(6), 392–405. https://doi.org/10.1002/hipo.22839

Kim, J. J., & Fanselow, M. S. (1992). Modality-Specific Retrograde Amnesia of Fear. *Science*, *256*(5057), 675–677. https://doi.org/10.1126/science.1585183

Kim, J. J., Rison, R. A., & Fanselow, M. S. (1993). Effects of amygdala, hippocampus, and periaqueductal gray lesions on short- and long-term contextual fear. *Behavioral Neuroscience*, *107*(6), 1093–1098. https://doi.org/10.1037/0735-7044.107.6.1093

Kim, T., McCall, J. G., Jung, Y. H., Huang, X., Siuda, E. R., Li, Y., Song, J., Song, Y. M., Pao, H. A., Kim, R.-H., Lu, C., Lee, S. D., Song, I.-S., Shin, G., Al-Hasani, R., Kim, S., Tan, M. P., Huang, Y., Omenetto, F. G., … Bruchas, M. R. (2013). Injectable, Cellular-Scale Optoelectronics with Applications for Wireless Optogenetics. *Science*, *340*(6129), 211–216. https://doi.org/10.1126/science.1232437

Kobayashi, K., Shikano, K., Kuroiwa, M., Horikawa, M., Ito, W., Nishi, A., Segi-Nishida, E., & Suzuki, H. (2022). Noradrenaline activation of hippocampal dopamine D1 receptors promotes antidepressant effects. *Proceedings of the National Academy of Sciences*, *119*(33), e2117903119. https://doi.org/10.1073/pnas.2117903119

Koob, G. F., Balcom, G. J., & Meyerhoff, J. L. (1975). Dopamine and norepinephrine levels in the nucleus accumbens, olfactory tubercle and corpus striatum following lesions in the ventral tegmental area. *Brain Research*, *94*(1), 45–55. https://doi.org/10.1016/0006-8993(75)90875-6

Kozai, T. D. Y., Jaquins-Gerstl, A. S., Vazquez, A. L., Michael, A. C., & Cui, X. T. (2015). Brain Tissue Responses to Neural Implants Impact Signal Sensitivity and Intervention Strategies. *ACS Chemical Neuroscience*, *6*(1), 48–67. https://doi.org/10.1021/cn500256e

Kozai, T. D. Y., Langhals, N. B., Patel, P. R., Deng, X., Zhang, H., Smith, K. L., Lahann, J., Kotov, N. A., & Kipke, D. R. (2012). Ultrasmall implantable composite microelectrodes with bioactive surfaces for chronic neural interfaces. *Nature Materials*, *11*(12), 1065–1073. https://doi.org/10.1038/nmat3468

Kroning, K. E., Li, M., Petrescu, D. I., & Wang, W. (2021). A genetically encoded sensor with improved fluorescence intensity for opioid detection at cellular resolution. *Chemical Communications*, *57*(81), 10560–10563. https://doi.org/10.1039/D1CC04524E

Kuo, C.-C., Hsieh, J.-C., Tsai, H.-C., Kuo, Y.-S., Yau, H.-J., Chen, C.-C., Chen, R.-F., Yang, H.-W., & Min, M.-Y. (2020). Inhibitory interneurons regulate phasic activity

of noradrenergic neurons in the mouse locus coeruleus and functional implications. *The Journal of Physiology*, *598*(18), 4003–4029. https://doi.org/10.1113/JP279557

Kutlu, M. G., Zachry, J. E., Melugin, P. R., Cajigas, S. A., Chevee, M. F., Kelly, S. J., Kutlu, B., Tian, L., Siciliano, C. A., & Calipari, E. S. (2021). Dopamine release in the nucleus accumbens core signals perceived saliency. *Current Biology*, *31*(21), 4748-4761.e8. https://doi.org/10.1016/j.cub.2021.08.052

Lamont, E. W., & Kokkinidis, L. (1998). Infusion of the dopamine D1 receptor antagonist SCH 23390 into the amygdala blocks fear expression in a potentiated startle paradigm. *Brain Research*, *795*(1), 128–136. https://doi.org/10.1016/S0006-8993(98)00281-9

Lategan, A. J., Marien, M. R., & Colpaert, F. C. (1990). Effects of locus coeruleus lesions on the release of endogenous dopamine in the rat nucleus accumbens and caudate nucleus as determined by intracerebral microdialysis. *Brain Research*, *523*(1), 134–138. https://doi.org/10.1016/0006-8993(90)91646-X

Lategan, A. J., Marien, M. R., & Colpaert, F. C. (1992). Suppression of nigrostriatal and mesolimbic dopamine release in vivo following noradrenaline depletion by DSP-4: A microdialysis study. *Life Sciences*, *50*(14), 995–999. https://doi.org/10.1016/0024-3205(92)90093-5

Leach, J., & Ansell, L. (2008). Impairment in attentional processing in a field survival environment. *Applied Cognitive Psychology*, *22*(5), 643–652. https://doi.org/10.1002/acp.1385

Lee, S. J., Chen, Y., Lodder, B., & Sabatini, B. L. (2019). Monitoring Behaviorally Induced Biochemical Changes Using Fluorescence Lifetime Photometry. *Frontiers in Neuroscience*, *13*. https://doi.org/10.3389/fnins.2019.00766

LeGates, T. A., Kvarta, M. D., Tooley, J. R., Francis, T. C., Lobo, M. K., Creed, M. C., & Thompson, S. M. (2018). Reward behaviour is regulated by the strength of hippocampus–nucleus accumbens synapses. *Nature*, *564*(7735), 258–262. https://doi.org/10.1038/s41586-018-0740-8

Lerner, T. N., Shilyansky, C., Davidson, T. J., Evans, K. E., Beier, K. T., Zalocusky, K. A., Crow, A. K., Malenka, R. C., Luo, L., Tomer, R., & Deisseroth, K. (2015). Intact-Brain Analyses Reveal Distinct Information Carried by SNc Dopamine Subcircuits. *Cell*, *162*(3), 635–647. https://doi.org/10.1016/j.cell.2015.07.014

Li, S., Cullen, W. K., Anwyl, R., & Rowan, M. J. (2003). Dopamine-dependent facilitation of LTP induction in hippocampal CA1 by exposure to spatial novelty. *Nature Neuroscience*, *6*(5), 526–531. https://doi.org/10.1038/nn1049

Lieberman, AbrahamN., Freedman, LewisS., & Goldstein, M. (1972). SERUM DOPAMINE-β-HYDROXYLASE ACTIVITY IN PATIENTS WITH HUNTINGTON'S CHOREA AND PARKINSON'S DISEASE. *The Lancet*, *299*(7742), 153–154. https://doi.org/10.1016/S0140-6736(72)90725-8

Liprando, L. A., Miner, L. H., Blakely, R. D., Lewis, D. A., & Sesack, S. R. (2004). Ultrastructural interactions between terminals expressing the norepinephrine transporter and dopamine neurons in the rat and monkey ventral tegmental area. *Synapse*, *52*(4), 233–244. https://doi.org/10.1002/syn.20023

Lisman, J. E., & Grace, A. A. (2005a). The Hippocampal-VTA Loop: Controlling the Entry of Information into Long-Term Memory. *Neuron*, *46*(5), 703–713. https://doi.org/10.1016/j.neuron.2005.05.002

Lisman, J. E., & Grace, A. A. (2005b). The Hippocampal-VTA Loop: Controlling the Entry of Information into Long-Term Memory. *Neuron*, *46*(5), Article 5. https://doi.org/10.1016/j.neuron.2005.05.002

Liu, J., Lin, L., & Wang, D. V. (2021). Representation of Fear of Heights by Basolateral Amygdala Neurons. *Journal of Neuroscience*, *41*(5), 1080–1091. https://doi.org/10.1523/JNEUROSCI.0483-20.2020

Liu, Y., Rodenkirch, C., Moskowitz, N., Schriver, B., & Wang, Q. (2017). Dynamic Lateralization of Pupil Dilation Evoked by Locus Coeruleus Activation Results from Sympathetic, Not Parasympathetic, Contributions. *Cell Reports*, *20*(13), 3099–3112. https://doi.org/10.1016/j.celrep.2017.08.094

Livingston, K. E., Mahoney, J. P., Manglik, A., Sunahara, R. K., & Traynor, J. R. (2018). Measuring ligand efficacy at the mu-opioid receptor using a conformational biosensor. *eLife*, *7*, e32499. https://doi.org/10.7554/eLife.32499

Llorca-Torralba, M., Suárez-Pereira, I., Bravo, L., Camarena-Delgado, C., Garcia-Partida, J. A., Mico, J. A., & Berrocoso, E. (2019). Chemogenetic Silencing of the Locus Coeruleus–Basolateral Amygdala Pathway Abolishes Pain-Induced Anxiety and Enhanced Aversive Learning in Rats. *Biological Psychiatry*, *85*(12), 1021–1035. https://doi.org/10.1016/j.biopsych.2019.02.018

Lopes, L. T., Patrone, L. G. A., Li, K.-Y., Imber, A. N., Graham, C. D., Gargaglioni, L. H., & Putnam, R. W. (2016). Anatomical and functional connections between the locus

coeruleus and the nucleus tractus solitarius in neonatal rats. *Neuroscience*, *324*, 446–468. https://doi.org/10.1016/j.neuroscience.2016.03.036

López, R. C., Noble, N., Özçete, Ö. D., Cai, X., Handy, G. E., Andersen, J. W., Patriarchi, T., Li, Y., & Kaeser, P. S. (2024a). Innervation density governs crosstalk of GPCR-based norepinephrine and dopamine sensors. *bioRxiv*, 2024.11.23.624963. https://doi.org/10.1101/2024.11.23.624963

López, R. C., Noble, N., Özçete, Ö. D., Cai, X., Handy, G. E., Andersen, J. W., Patriarchi, T., Li, Y., & Kaeser, P. S. (2024b). *Innervation density governs crosstalk of GPCR-based norepinephrine and dopamine sensors* (p. 2024.11.23.624963). bioRxiv. https://doi.org/10.1101/2024.11.23.624963

Loughlin, S. E., & Fallon, J. H. (1983). Dopaminergic and non-dopaminergic projections to amygdala from substantia nigra and ventral tegmental area. *Brain Research*, *262*(2), 334–338. https://doi.org/10.1016/0006-8993(83)91029-6

Luskin, A. T., Li, L., Fu, X., Martin, M. M., Barcomb, K., Girven, K. S., Blackburn, T., Wells, B. A., Thai, S. T., Li, E. M., Rana, A. N., Simon, R. C., Sun, L., Gao, L., Murry, A. D., Golden, S. A., Stuber, G. D., Ford, C. P., Gu, L., & Bruchas, M. R. (2025). Heterogeneous pericoerulear neurons tune arousal and exploratory behaviours. *Nature*, *643*(8071), 437–447. https://doi.org/10.1038/s41586-025-08952-w

Maren, S. (2001). Neurobiology of Pavlovian Fear Conditioning. *Annual Review of Neuroscience*, *24*(Volume 24, 2001), 897–931. https://doi.org/10.1146/annurev.neuro.24.1.897

Maren, S., De Oca, B., & Fanselow, M. S. (1994). Sex differences in hippocampal long-term potentiation (LTP) and Pavlovian fear conditioning in rats: Positive correlation

between LTP and contextual learning. *Brain Research*, *661*(1), Article 1. https://doi.org/10.1016/0006-8993(94)91176-2

Maren, S., & Fanselow, M. S. (1995). Synaptic plasticity in the basolateral amygdala induced by hippocampal formation stimulation in vivo. *Journal of Neuroscience*, *15*(11), 7548–7564. https://doi.org/10.1523/JNEUROSCI.15-11-07548.1995

Maren, S., & Holt, W. G. (2004). Hippocampus and Pavlovian Fear Conditioning in Rats: Muscimol Infusions Into the Ventral, but Not Dorsal, Hippocampus Impair the Acquisition of Conditional Freezing to an Auditory Conditional Stimulus. *Behavioral Neuroscience*, *118*(1), 97–110. https://doi.org/10.1037/0735-7044.118.1.97

Martig, A. K., & Mizumori, S. J. Y. (2011). Ventral tegmental area disruption selectively affects CA1/CA2 but not CA3 place fields during a differential reward working memory task. *Hippocampus*, *21*(2), Article 2. https://doi.org/10.1002/hipo.20734

Marzo, A., Totah, N. K., Neves, R. M., Logothetis, N. K., & Eschenko, O. (2014). Unilateral electrical stimulation of rat locus coeruleus elicits bilateral response of norepinephrine neurons and sustained activation of medial prefrontal cortex. *Journal of Neurophysiology*, *111*(12), 2570–2588. https://doi.org/10.1152/jn.00920.2013

Masana, M., Bortolozzi, A., & Artigas, F. (2011). Selective enhacement of mesocortical dopaminergic transmission by noradrenergic drugs: Therapeutic opportunities in schizophrenia. *International Journal of Neuropsychopharmacology*, *14*(1), 53–68. https://doi.org/10.1017/S1461145710000908

Matejuk, A., & Ransohoff, R. M. (2020). Crosstalk Between Astrocytes and Microglia: An Overview. *Frontiers in Immunology*, *11*. https://doi.org/10.3389/fimmu.2020.01416

Matus-Amat, P., Higgins, E. A., Sprunger, D., Wright-Hardesty, K., & Rudy, J. W. (20070730). The role of dorsal hippocampus and basolateral amygdala NMDA receptors in the acquisition and retrieval of context and contextual fear memories. *Behavioral Neuroscience*, *121*(4), Article 4. https://doi.org/10.1037/0735-7044.121.4.721

McCall, J. G. (n.d.). *CRH Engagement of the Locus Coeruleus Noradrenergic System Mediates Stress-Induced Anxiety*. 36.

McCall, J. G. (2015). *CRH Engagement of the Locus Coeruleus Noradrenergic System Mediates Stress-Induced Anxiety*. 36.

McCall, J. G., Siuda, E. R., Bhatti, D. L., Lawson, L. A., McElligott, Z. A., Stuber, G. D., & Bruchas, M. R. (2017a). Locus coeruleus to basolateral amygdala noradrenergic projections promote anxiety-like behavior. *eLife*, *6*, e18247. https://doi.org/10.7554/eLife.18247

McCall, J. G., Siuda, E. R., Bhatti, D. L., Lawson, L. A., McElligott, Z. A., Stuber, G. D., & Bruchas, M. R. (2017b). Locus coeruleus to basolateral amygdala noradrenergic projections promote anxiety-like behavior. *eLife*, *6*, e18247. https://doi.org/10.7554/eLife.18247

McNamara, C. G., Tejero-Cantero, Á., Trouche, S., Campo-Urriza, N., & Dupret, D. (2014). Dopaminergic neurons promote hippocampal reactivation and spatial memory persistence. *Nature Neuroscience*, *17*(12), 1658–1660. https://doi.org/10.1038/nn.3843

Mejias-Aponte, C. A. (2016). Specificity and impact of adrenergic projections to the midbrain dopamine system. *Brain Research*, *1641*(Pt B), 258–273. https://doi.org/10.1016/j.brainres.2016.01.036

Mejias-Aponte, C. A., Drouin, C., & Aston-Jones, G. (2009). Adrenergic and Noradrenergic Innervation of the Midbrain Ventral Tegmental Area and Retrorubral Field: Prominent Inputs from Medullary Homeostatic Centers. *Journal of Neuroscience*, *29*(11), 3613–3626. https://doi.org/10.1523/JNEUROSCI.4632-08.2009

Meltzer, H. Y., Cho, H. W., & Carroll, B. J. (1976). Serum Dopamine-βHydroxylase Activity in the Affective Psychoses and Schizophrenia: Decreased Activity in Unipolar Psychotically Depressed Patients. *Archives of General Psychiatry*, *33*(5), 585–591. https://doi.org/10.1001/archpsyc.1976.01770050047007

Millard, S. J., Hoang, I. B., Sherwood, S., Taira, M., Reyes, V., Greer, Z., O'Connor, S. L., Wassum, K. M., James, M. H., Barker, D. J., & Sharpe, M. J. (2024). Cognitive representations of intracranial self-stimulation of midbrain dopamine neurons depend on stimulation frequency. *Nature Neuroscience*, *27*(7), 1253–1259. https://doi.org/10.1038/s41593-024-01643-1

Mitrano, D. A., Schroeder, J. P., Smith, Y., Cortright, J. J., Bubula, N., Vezina, P., & Weinshenker, D. (2012). Alpha-1 Adrenergic Receptors are Localized on Presynaptic Elements in the Nucleus Accumbens and Regulate Mesolimbic Dopamine Transmission. *Neuropsychopharmacology*, *37*(9), 2161–2172. https://doi.org/10.1038/npp.2012.68

Morel, C., Montgomery, S. E., Li, L., Durand-de Cuttoli, R., Teichman, E. M., Juarez, B., Tzavaras, N., Ku, S. M., Flanigan, M. E., Cai, M., Walsh, J. J., Russo, S. J., Nestler, E. J., Calipari, E. S., Friedman, A. K., & Han, M.-H. (2022). Midbrain projection to the basolateral amygdala encodes anxiety-like but not depression-like behaviors. *Nature Communications*, *13*(1), Article 1. https://doi.org/10.1038/s41467-022-29155-1

Moreno-Castilla, P., Pérez-Ortega, R., Violante-Soria, V., Balderas, I., & Bermúdez-Rattoni, F. (2017). Hippocampal release of dopamine and norepinephrine encodes novel contextual information. *Hippocampus*, *27*(5), Article 5. https://doi.org/10.1002/hipo.22711

Morris, J. S., Friston, K. J., Büchel, C., Frith, C. D., Young, A. W., Calder, A. J., & Dolan, R. J. (1998). A neuromodulatory role for the human amygdala in processing emotional facial expressions. *Brain*, *121*(1), 47–57. https://doi.org/10.1093/brain/121.1.47

Mouradian, R. D., Sessler, F. M., & Waterhouse, B. D. (1991). Noradrenergic potentiation of excitatory transmitter action in cerebrocortical slices: Evidence for mediation by an α1 receptor-linked second messenger pathway. *Brain Research*, *546*(1), 83–95. https://doi.org/10.1016/0006-8993(91)91162-T

Murphy, P. R., O'Connell, R. G., O'Sullivan, M., Robertson, I. H., & Balsters, J. H. (2014). Pupil diameter covaries with BOLD activity in human locus coeruleus. *Human Brain Mapping*, *35*(8), 4140–4154. https://doi.org/10.1002/hbm.22466

Nader, K., & LeDoux, J. (1999). Inhibition of the mesoamygdala dopaminergic pathway impairs the retrieval of conditioned fear associations. *Behavioral Neuroscience*, *113*(5), 891–901. https://doi.org/10.1037/0735-7044.113.5.891

Nagatsu, T., Wakui, Y., Kato, T., Fujita, K., Kondo, T., Yokochi, F., & Narabayashi, H. (1982). Dopamine beta-hydroxylase activity in cerebrospinal fluid of Parkinsonian patients. *Biomedical Research*, *3*(1), 95–98. https://doi.org/10.2220/biomedres.3.95

Nakahara, H., Itoh, H., Kawagoe, R., Takikawa, Y., & Hikosaka, O. (2004). Dopamine Neurons Can Represent Context-Dependent Prediction Error. *Neuron*, *41*(2), Article 2. https://doi.org/10.1016/S0896-6273(03)00869-9

Nestler, E. J., & Aghajanian, G. K. (1997). Molecular and Cellular Basis of Addiction. *Science*, *278*(5335), 58–63. https://doi.org/10.1126/science.278.5335.58

Nicholas, A. P., Pieribone, V. A., & Hökfelt, T. (1993a). Cellular localization of messenger RNA for beta-1 and beta-2 adrenergic receptors in rat brain: An in situ hybridization study. *Neuroscience*, *56*(4), 1023–1039. https://doi.org/10.1016/0306-4522(93)90148-9

Nicholas, A. P., Pieribone, V., & Hökfelt, T. (1993b). Distributions of mRNAs for alpha-2 adrenergic receptor subtypes in rat brain: An in situ hybridization study. *Journal of Comparative Neurology*, *328*(4), 575–594. https://doi.org/10.1002/cne.903280409

O'Brien, C. P., Testa, T., O'Brien, T. J., Brady, J. P., & Wells, B. (1977). Conditioned narcotic withdrawal in humans. *Science (New York, N.Y.)*, *195*(4282), Article 4282. https://doi.org/10.1126/science.841320

O'Carroll, C. M., Martin, S. J., Sandin, J., Frenguelli, B., & Morris, R. G. M. (2006). Dopaminergic modulation of the persistence of one-trial hippocampus-dependent memory. *Learning & Memory*, *13*(6), 760–769. https://doi.org/10.1101/lm.321006

Okuyama, T., Kitamura, T., Roy, D. S., Itohara, S., & Tonegawa, S. (2016). Ventral CA1 neurons store social memory. *Science*, *353*(6307), 1536–1541. https://doi.org/10.1126/science.aaf7003

Oliveira, A. R. de, Reimer, A. E., & Brandão, M. L. (2009). Role of dopamine receptors in the ventral tegmental area in conditioned fear. *Behavioural Brain Research*, *199*(2), 271–277. https://doi.org/10.1016/j.bbr.2008.12.004

Olschowka, J. A., Molliver, M. E., Grzanna, R., Rice, F. L., & Coyle, J. T. (1981). Ultrastructural demonstration of noradrenergic synapses in the rat central nervous system by dopamine-beta-hydroxylase immunocytochemistry. *The Journal of Histochemistry and Cytochemistry: Official Journal of the Histochemistry Society*, *29*(2), 271–280. https://doi.org/10.1177/29.2.7019303

Padilla-Coreano, N., Canetta, S., Mikofsky, R. M., Alway, E., Passecker, J., Myroshnychenko, M. V., Garcia-Garcia, A. L., Warren, R., Teboul, E., Blackman, D. R., Morton, M. P., Hupalo, S., Tye, K. M., Kellendonk, C., Kupferschmidt, D. A., & Gordon, J. A. (2019). Hippocampal-Prefrontal Theta Transmission Regulates Avoidance Behavior. *Neuron*, *104*(3), 601-610.e4. https://doi.org/10.1016/j.neuron.2019.08.006

Pantoni, M. M., Carmack, S. A., Hammam, L., & Anagnostaras, S. G. (2020). Dopamine and norepinephrine transporter inhibition for long-term fear memory enhancement.

Behavioural Brain Research, *378*, 112266. https://doi.org/10.1016/j.bbr.2019.112266

Park, J., Aragona, B. J., Kile, B. M., Carelli, R. M., & Wightman, R. M. (2010). In vivo voltammetric monitoring of catecholamine release in subterritories of the nucleus accumbens shell. *Neuroscience*, *169*(1), 132–142. https://doi.org/10.1016/j.neuroscience.2010.04.076

Park, J., Kile, B. M., & Mark Wightman, R. (2009). In vivo voltammetric monitoring of norepinephrine release in the rat ventral bed nucleus of the stria terminalis and anteroventral thalamic nucleus. *European Journal of Neuroscience*, *30*(11), 2121–2133. https://doi.org/10.1111/j.1460-9568.2009.07005.x

Paton, J. J., Belova, M. A., Morrison, S. E., & Salzman, C. D. (2006). The primate amygdala represents the positive and negative value of visual stimuli during learning. *Nature*, *439*(7078), 865–870. https://doi.org/10.1038/nature04490

Patriarchi, T., Cho, J. R., Merten, K., Howe, M. W., Marley, A., Xiong, W.-H., Folk, R. W., Broussard, G. J., Liang, R., Jang, M. J., Zhong, H., Dombeck, D., von Zastrow, M., Nimmerjahn, A., Gradinaru, V., Williams, J. T., & Tian, L. (2018a). Ultrafast neuronal imaging of dopamine dynamics with designed genetically encoded sensors. *Science*, *360*(6396), eaat4422. https://doi.org/10.1126/science.aat4422

Patriarchi, T., Cho, J. R., Merten, K., Howe, M. W., Marley, A., Xiong, W.-H., Folk, R. W., Broussard, G. J., Liang, R., Jang, M. J., Zhong, H., Dombeck, D., von Zastrow, M., Nimmerjahn, A., Gradinaru, V., Williams, J. T., & Tian, L. (2018b). Ultrafast neuronal imaging of dopamine dynamics with designed genetically encoded

sensors. *Science*, *360*(6396), Article 6396. https://doi.org/10.1126/science.aat4422

Pennington, Z. T., Dong, Z., Feng, Y., Vetere, L. M., Page-Harley, L., Shuman, T., & Cai, D. J. (2019). ezTrack: An open-source video analysis pipeline for the investigation of animal behavior. *Scientific Reports*, *9*(1), 19979. https://doi.org/10.1038/s41598-019-56408-9

Perez, D. M. (2020). A1-Adrenergic Receptors in Neurotransmission, Synaptic Plasticity, and Cognition. *Frontiers in Pharmacology*, *11*. https://www.frontiersin.org/articles/10.3389/fphar.2020.581098

Phelps, E. A., & LeDoux, J. E. (2005). Contributions of the Amygdala to Emotion Processing: From Animal Models to Human Behavior. *Neuron*, *48*(2), 175–187. https://doi.org/10.1016/j.neuron.2005.09.025

Phillips, R. G., & LeDoux, J. E. (1992). Differential contribution of amygdala and hippocampus to cued and contextual fear conditioning. *Behavioral Neuroscience*, *106*(2), 274–285. https://doi.org/10.1037/0735-7044.106.2.274

Pickel, V. M., Joh, T. H., & Reis, D. J. (1975). Ultrastructural localization of tyrosine hydroxylase in noradrenergic neurons of brain. *Proceedings of the National Academy of Sciences*, *72*(2), 659–663. https://doi.org/10.1073/pnas.72.2.659

Poe, G. R., Foote, S., Eschenko, O., Johansen, J. P., Bouret, S., Aston-Jones, G., Harley, C. W., Manahan-Vaughan, D., Weinshenker, D., Valentino, R., Berridge, C., Chandler, D. J., Waterhouse, B., & Sara, S. J. (2020). Locus coeruleus: A new look at the blue spot. *Nature Reviews Neuroscience*, *21*(11), Article 11. https://doi.org/10.1038/s41583-020-0360-9

Privitera, M., Ferrari, K. D., von Ziegler, L. M., Sturman, O., Duss, S. N., Floriou-Servou, A., Germain, P.-L., Vermeiren, Y., Wyss, M. T., De Deyn, P. P., Weber, B., & Bohacek, J. (2020). A complete pupillometry toolbox for real-time monitoring of locus coeruleus activity in rodents. *Nature Protocols*, *15*(8), 2301–2320. https://doi.org/10.1038/s41596-020-0324-6

Privitera, M., Ziegler, L. M. von, Floriou-Servou, A., Duss, S. N., Zhang, R., Waag, R., Leimbacher, S., Sturman, O., Roessler, F. K., Heylen, A., Vermeiren, Y., Dam, D. V., Deyn, P. P. D., Germain, P.-L., & Bohacek, J. (2024). Noradrenaline release from the locus coeruleus shapes stress-induced hippocampal gene expression. *eLife*, *12*. https://doi.org/10.7554/eLife.88559.2

Rappleye, M., Wait, S. J., Lee, J. D., Siebart, J. C., Torp, L., Smith, N., Muster, J., Matreyek, K. A., Fowler, D. M., & Berndt, A. (2023). Optogenetic Microwell Array Screening System: A High-Throughput Engineering Platform for Genetically Encoded Fluorescent Indicators. *ACS Sensors*, *8*(11), 4233–4244. https://doi.org/10.1021/acssensors.3c01573

Roberts, J. G., & Sombers, L. A. (2018). Fast Scan Cyclic Voltammetry: Chemical Sensing in the Brain and Beyond. *Analytical Chemistry*, *90*(1), 490–504. https://doi.org/10.1021/acs.analchem.7b04732

Robertson, S. D., Plummer, N. W., de Marchena, J., & Jensen, P. (2013). Developmental origins of central norepinephrine neuron diversity. *Nature Neuroscience*, *16*(8), Article 8. https://doi.org/10.1038/nn.3458

Rosenbaum, D. M., Rasmussen, S. G. F., & Kobilka, B. K. (2009). The structure and function of G-protein-coupled receptors. *Nature*, *459*(7245), 356–363. https://doi.org/10.1038/nature08144

Rosin, D. L., Zeng, D., Stornetta, R. L., Norton, F. R., Riley, T., Okusa, M. D., Guyenet, P. G., & Lynch, K. R. (1993). Immunohistochemical localization ofα2a-adrenergic receptors in catecholaminergic and other brainstem neurons in the rat. *Neuroscience*, *56*(1), 139–155. https://doi.org/10.1016/0306-4522(93)90569-2

Rossato, J. I., Bevilaqua, L. R. M., Izquierdo, I., Medina, J. H., & Cammarota, M. (2009). Dopamine Controls Persistence of Long-Term Memory Storage. *Science*, *325*(5943), 1017–1020. https://doi.org/10.1126/science.1172545

Sara, S. J., & Bouret, S. (2012). Orienting and Reorienting: The Locus Coeruleus Mediates Cognition through Arousal. *Neuron*, *76*(1), Article 1. https://doi.org/10.1016/j.neuron.2012.09.011

Sayegh, F. J. P., Mouledous, L., Macri, C., Pi Macedo, J., Lejards, C., Rampon, C., Verret, L., & Dahan, L. (2024). Ventral tegmental area dopamine projections to the hippocampus trigger long-term potentiation and contextual learning. *Nature Communications*, *15*(1), 4100. https://doi.org/10.1038/s41467-024-47481-4

Schank, J. R., Ventura, R., Puglisi-Allegra, S., Alcaro, A., Cole, C. D., Liles, L. C., Seeman, P., & Weinshenker, D. (2006). Dopamine β-Hydroxylase Knockout Mice have Alterations in Dopamine Signaling and are Hypersensitive to Cocaine. *Neuropsychopharmacology*, *31*(10), Article 10. https://doi.org/10.1038/sj.npp.1301000

Schoenbaum, G., Chiba, A. A., & Gallagher, M. (1999). Neural Encoding in Orbitofrontal Cortex and Basolateral Amygdala during Olfactory Discrimination Learning. *Journal of Neuroscience*, *19*(5), 1876–1884. https://doi.org/10.1523/JNEUROSCI.19-05-01876.1999

Sciolino, N. R., Hsiang, M., Mazzone, C. M., Wilson, L. R., Plummer, N. W., Amin, J., Smith, K. G., McGee, C. A., Fry, S. A., Yang, C. X., Powell, J. M., Bruchas, M. R., Kravitz, A. V., Cushman, J. D., Krashes, M. J., Cui, G., & Jensen, P. (2022). Natural locus coeruleus dynamics during feeding. *Science Advances*, *8*(33), eabn9134. https://doi.org/10.1126/sciadv.abn9134

Sengupta, A., & Holmes, A. (2019). A Discrete Dorsal Raphe to Basal Amygdala 5-HT Circuit Calibrates Aversive Memory. *Neuron*, *103*(3), 489-505.e7. https://doi.org/10.1016/j.neuron.2019.05.029

Sengupta, A., Yau, J. O. Y., Jean-Richard-Dit-Bressel, P., Liu, Y., Millan, E. Z., Power, J. M., & McNally, G. P. (2018). Basolateral Amygdala Neurons Maintain Aversive Emotional Salience. *Journal of Neuroscience*, *38*(12), 3001–3012. https://doi.org/10.1523/JNEUROSCI.2460-17.2017

Sensing at the Surface of Graphene Field-Effect Transistors—Fu—2017—Advanced Materials—Wiley Online Library. (n.d.). Retrieved March 24, 2025, from https://advanced.onlinelibrary.wiley.com/doi/10.1002/adma.201603610

Seo, D., Zhang, E. T., Piantadosi, S. C., Marcus, D. J., Motard, L. E., Kan, B. K., Gomez, A. M., Nguyen, T. K., Xia, L., & Bruchas, M. R. (2021). A locus coeruleus to dentate gyrus noradrenergic circuit modulates aversive contextual processing. *Neuron*, *109*(13), Article 13. https://doi.org/10.1016/j.neuron.2021.05.006

Shan, L., Yuan, L., Zhang, B., Ma, J., Xu, X., Gu, F., Jiang, Y., & Dai, J. (2023). Neural Integration of Audiovisual Sensory Inputs in Macaque Amygdala and Adjacent Regions. *Neuroscience Bulletin*, *39*(12), 1749–1761. https://doi.org/10.1007/s12264-023-01043-8

Shi, Y.-W., Fan, B.-F., Xue, L., Wen, J.-L., & Zhao, H. (2017). Regulation of Fear Extinction in the Basolateral Amygdala by Dopamine D2 Receptors Accompanied by Altered GluR1, GluR1-Ser845 and NR2B Levels. *Frontiers in Behavioral Neuroscience*, *11*. https://doi.org/10.3389/fnbeh.2017.00116

Shpokayte, M., McKissick, O., Guan, X., Yuan, B., Rahsepar, B., Fernandez, F. R., Ruesch, E., Grella, S. L., White, J. A., Liu, X. S., & Ramirez, S. (2022). Hippocampal cells segregate positive and negative engrams. *Communications Biology*, *5*(1), 1–15. https://doi.org/10.1038/s42003-022-03906-8

Shukla, A., & Chattarji, S. (2022). Stressed rats fail to exhibit avoidance reactions to innately aversive social calls. *Neuropsychopharmacology*, *47*(6), 1145–1155. https://doi.org/10.1038/s41386-021-01230-z

Sias, A. C., Jafar, Y., Goodpaster, C. M., Ramírez-Armenta, K., Wrenn, T. M., Griffin, N. K., Patel, K., Lamparelli, A. C., Sharpe, M. J., & Wassum, K. M. (2023). *Dopamine projections to the basolateral amygdala drive the encoding of identity-specific reward memories* (p. 2022.09.26.509602). bioRxiv. https://doi.org/10.1101/2022.09.26.509602

Sias, A. C., Jafar, Y., Goodpaster, C. M., Ramírez-Armenta, K., Wrenn, T. M., Griffin, N. K., Patel, K., Lamparelli, A. C., Sharpe, M. J., & Wassum, K. M. (2024). Dopamine projections to the basolateral amygdala drive the encoding of identity-specific

reward memories. *Nature Neuroscience*, *27*(4), 728–736. https://doi.org/10.1038/s41593-024-01586-7

Silveira, M. C. L., Sandner, G., & Graeff, F. G. (1993a). Induction of Fos immunoreactivity in the brain by exposure to the elevated plus-maze. *Behavioural Brain Research*, *56*(1), 115–118. https://doi.org/10.1016/0166-4328(93)90028-O

Silveira, M. C. L., Sandner, G., & Graeff, F. G. (1993b). Induction of Fos immunoreactivity in the brain by exposure to the elevated plus-maze. *Behavioural Brain Research*, *56*(1), Article 1. https://doi.org/10.1016/0166-4328(93)90028-O

Sinha, R., Catapano, D., & O'Malley, S. (1999). Stress-induced craving and stress response in cocaine dependent individuals. *Psychopharmacology*, *142*(4), Article 4. https://doi.org/10.1007/s002130050898

Smith, C. C., & Greene, R. W. (2012a). CNS Dopamine Transmission Mediated by Noradrenergic Innervation. *Journal of Neuroscience*, *32*(18), Article 18. https://doi.org/10.1523/JNEUROSCI.6486-11.2012

Smith, C. C., & Greene, R. W. (2012b). CNS Dopamine Transmission Mediated by Noradrenergic Innervation. *Journal of Neuroscience*, *32*(18), 6072–6080. https://doi.org/10.1523/JNEUROSCI.6486-11.2012

Solecki, W. B., Kielbinski, M., Bernacka, J., Gralec, K., Klasa, A., Pradel, K., Rojek-Sito, K., & Przewłocki, R. (2022). Alpha1-adrenergic receptor blockade in the ventral tegmental area attenuates acquisition of cocaine-induced pavlovian associative learning. *Frontiers in Behavioral Neuroscience*, *16*, 969104. https://doi.org/10.3389/fnbeh.2022.969104

Steffensen, S. C., Svingos, A. L., Pickel, V. M., & Henriksen, S. J. (1998). Electrophysiological Characterization of GABAergic Neurons in the Ventral Tegmental Area. *The Journal of Neuroscience*, *18*(19), 8003–8015. https://doi.org/10.1523/JNEUROSCI.18-19-08003.1998

Stine, C., Zhou, X., Achanta, A., Johnson, J., Patriarchi, T., & Bruchas, M. (2024). Modulation of Stress-Induced Deficits in Approach-Avoidance Behavior by a Ventral Tegmental Area Nociceptin Opioid Peptide Circuit. *Biological Psychiatry*, *95*(10), S26. https://doi.org/10.1016/j.biopsych.2024.02.069

Sun, F., Zhou, J., Dai, B., Qian, T., Zeng, J., Li, X., Zhuo, Y., Zhang, Y., Wang, Y., Qian, C., Tan, K., Feng, J., Dong, H., Lin, D., Cui, G., & Li, Y. (2020). Next-generation GRAB sensors for monitoring dopaminergic activity in vivo. *Nature Methods*, *17*(11), Article 11. https://doi.org/10.1038/s41592-020-00981-9

Szot, P., Weinshenker, D., White, S. S., Robbins, C. A., Rust, N. C., Schwartzkroin, P. A., & Palmiter, R. D. (1999). Norepinephrine-Deficient Mice Have Increased Susceptibility to Seizure-Inducing Stimuli. *Journal of Neuroscience*, *19*(24), 10985–10992. https://doi.org/10.1523/JNEUROSCI.19-24-10985.1999

Takeuchi, T., Duszkiewicz, A. J., Sonneborn, A., Spooner, P. A., Yamasaki, M., Watanabe, M., Smith, C. C., Fernández, G., Deisseroth, K., Greene, R. W., & Morris, R. G. M. (2016a). Locus coeruleus and dopaminergic consolidation of everyday memory. *Nature*, *537*(7620), 357–362. https://doi.org/10.1038/nature19325

Takeuchi, T., Duszkiewicz, A. J., Sonneborn, A., Spooner, P. A., Yamasaki, M., Watanabe, M., Smith, C. C., Fernández, G., Deisseroth, K., Greene, R. W., &

Morris, R. G. M. (2016b). Locus coeruleus and dopaminergic consolidation of everyday memory. *Nature*, *537*(7620), Article 7620. https://doi.org/10.1038/nature19325

Takeuchi, T., Duszkiewicz, A. J., Sonneborn, A., Spooner, P. A., Yamasaki, M., Watanabe, M., Smith, C. C., Fernández, G., Deisseroth, K., Greene, R. W., & Morris, R. G. M. (2016c). Locus coeruleus and dopaminergic consolidation of everyday memory. *Nature*, *537*(7620), Article 7620. https://doi.org/10.1038/nature19325

Tang, J., & Dani, J. A. (2009). Dopamine enables in vivo synaptic plasticity associated with the addictive drug nicotine. *Neuron*, *63*(5), 673–682. https://doi.org/10.1016/j.neuron.2009.07.025

Tang, W., Kochubey, O., Kintscher, M., & Schneggenburger, R. (2020a). A VTA to Basal Amygdala Dopamine Projection Contributes to Signal Salient Somatosensory Events during Fear Learning. *Journal of Neuroscience*, *40*(20), 3969–3980.

Tang, W., Kochubey, O., Kintscher, M., & Schneggenburger, R. (2020b). A VTA to Basal Amygdala Dopamine Projection Contributes to Signal Salient Somatosensory Events during Fear Learning. *Journal of Neuroscience*, *40*(20), Article 20.

Thomas, S. A., Marck, B. T., Palmiter, R. D., & Matsumoto, A. M. (1998). Restoration of norepinephrine and reversal of phenotypes in mice lacking dopamine beta-hydroxylase. *Journal of Neurochemistry*, *70*(6), 2468–2476. https://doi.org/10.1046/j.1471-4159.1998.70062468.x

Thomas, S. A., Matsumoto, A. M., & Palmiter, R. D. (1995). Noradrenaline is essential for mouse fetal development. *Nature*, *374*(6523), 643–646. https://doi.org/10.1038/374643a0

Thomas, S. A., & Palmiter, R. D. (1997). Impaired Maternal Behavior in Mice Lacking Norepinephrine and Epinephrine. *Cell*, *91*(5), 583–592. https://doi.org/10.1016/S0092-8674(00)80446-8

Titulaer, J., Björkholm, C., Feltmann, K., Malmlöf, T., Mishra, D., Bengtsson Gonzales, C., Schilström, B., & Konradsson-Geuken, Å. (2021). The Importance of Ventral Hippocampal Dopamine and Norepinephrine in Recognition Memory. *Frontiers in Behavioral Neuroscience*, *15*, 667244. https://doi.org/10.3389/fnbeh.2021.667244

Trivedi, M. A., & Coover, G. D. (2004). Lesions of the ventral hippocampus, but not the dorsal hippocampus, impair conditioned fear expression and inhibitory avoidance on the elevated T-maze. *Neurobiology of Learning and Memory*, *81*(3), 172–184. https://doi.org/10.1016/j.nlm.2004.02.005

Tsetsenis, T., Badyna, J. K., Wilson, J. A., Zhang, X., Krizman, E. N., Subramaniyan, M., Yang, K., Thomas, S. A., & Dani, J. A. (2021). Midbrain dopaminergic innervation of the hippocampus is sufficient to modulate formation of aversive memories. *Proceedings of the National Academy of Sciences*, *118*(40), e2111069118. https://doi.org/10.1073/pnas.2111069118

Tye, K. M., & Janak, P. H. (2007). Amygdala Neurons Differentially Encode Motivation and Reinforcement. *Journal of Neuroscience*, *27*(15), 3937–3945. https://doi.org/10.1523/JNEUROSCI.5281-06.2007

Udenfriend, S., & Dairman, W. (1970). Regulation of norepinephrine synthesis. *Advances in Enzyme Regulation*, *9*, 145–165. https://doi.org/10.1016/s0065-2571(71)80042-0

Udenfriend, S., & Dairman, W. (1971). Regulation of norepinephrine synthesis. *Advances in Enzyme Regulation*, *9*, 145–165. https://doi.org/10.1016/S0065-2571(71)80042-0

Uematsu, A., Tan, B. Z., Ycu, E. A., Cuevas, J. S., Koivumaa, J., Junyent, F., Kremer, E. J., Witten, I. B., Deisseroth, K., & Johansen, J. P. (2017a). Modular organization of the brainstem noradrenaline system coordinates opposing learning states. *Nature Neuroscience*, *20*(11), 1602–1611. https://doi.org/10.1038/nn.4642

Uematsu, A., Tan, B. Z., Ycu, E. A., Cuevas, J. S., Koivumaa, J., Junyent, F., Kremer, E. J., Witten, I. B., Deisseroth, K., & Johansen, J. P. (2017b). Modular organization of the brainstem noradrenaline system coordinates opposing learning states. *Nature Neuroscience*, *20*(11), Article 11. https://doi.org/10.1038/nn.4642

Uwano, T., Nishijo, H., Ono, T., & Tamura, R. (1995). Neuronal responsiveness to various sensory stimuli, and associative learning in the rat amygdala. *Neuroscience*, *68*(2), 339–361. https://doi.org/10.1016/0306-4522(95)00125-3

Valentini, V., Frau, R., & Di Chiara, G. (2004). Noradrenaline transporter blockers raise extracellular dopamine in medial prefrontal but not parietal and occipital cortex: Differences with mianserin and clozapine. *Journal of Neurochemistry*, *88*(4), 917–927. https://doi.org/10.1046/j.1471-4159.2003.02238.x

Van Bockstaele, E. J., Peoples, J., & Telegan, P. (1999). Efferent projections of the nucleus of the solitary tract to peri-locus coeruleus dendrites in rat brain: Evidence

for a monosynaptic pathway. *The Journal of Comparative Neurology*, *412*(3), 410–428. https://doi.org/10.1002/(sici)1096-9861(19990927)412:3<410::aid-cne3>3.0.co;2-f

Vazdarjanova, A., & McGaugh, J. L. (1998). Basolateral amygdala is not critical for cognitive memory of contextual fear conditioning. *Proceedings of the National Academy of Sciences*, *95*(25), 15003–15007. https://doi.org/10.1073/pnas.95.25.15003

Vuilleumier, P., Richardson, M. P., Armony, J. L., Driver, J., & Dolan, R. J. (2004). Distant influences of amygdala lesion on visual cortical activation during emotional face processing. *Nature Neuroscience*, *7*(11), 1271–1278. https://doi.org/10.1038/nn1341

Walker, D. L., & Davis, M. (2002). The role of amygdala glutamate receptors in fear learning, fear-potentiated startle, and extinction. *Pharmacology Biochemistry and Behavior*, *71*(3), 379–392. https://doi.org/10.1016/S0091-3057(01)00698-0

Wang, C., Zhang, Y., Shao, S., Cui, S., Wan, Y., & Yi, M. (2019). Ventral Hippocampus Modulates Anxiety-Like Behavior in Male But Not Female C57BL/6 J Mice. *Neuroscience*, *418*, 50–58. https://doi.org/10.1016/j.neuroscience.2019.08.032

Weiskrantz, L. (1956). Behavioral changes associated with ablation of the amygdaloid complex in monkeys. *Journal of Comparative and Physiological Psychology*, *49*(4), 381–391. https://doi.org/10.1037/h0088009

Whalen, P. J., Rauch, S. L., Etcoff, N. L., McInerney, S. C., Lee, M. B., & Jenike, M. A. (1998). Masked Presentations of Emotional Facial Expressions Modulate

Amygdala Activity without Explicit Knowledge. *Journal of Neuroscience*, *18*(1), 411–418. https://doi.org/10.1523/JNEUROSCI.18-01-00411.1998

Wilmot, J. H., Diniz, C. R. A. F., Crestani, A. P., Puhger, K. R., Roshgadol, J., Tian, L., & Wiltgen, B. J. (2024). Phasic locus coeruleus activity enhances trace fear conditioning by increasing dopamine release in the hippocampus. *eLife*, *12*, RP91465. https://doi.org/10.7554/eLife.91465

Wise, R. A., & Rompre, P.-P. (1989). Brain Dopamine and Reward. *Annual Review of Psychology*, *40*(1), Article 1. https://doi.org/10.1146/annurev.ps.40.020189.001203

Wotjak, C. T., Landgraf, R., & Engelmann, M. (2008). Listening to neuropeptides by microdialysis: Echoes and new sounds? *Pharmacology Biochemistry and Behavior*, *90*(2), 125–134. https://doi.org/10.1016/j.pbb.2008.03.017

Wu, G., Zhang, N., Matarasso, A., Heck, I., Li, H., Lu, W., Phaup, J. G., Schneider, M. J., Wu, Y., Weng, Z., Sun, H., Gao, Z., Zhang, X., Sandberg, S. G., Parvin, D., Seaholm, E., Islam, S. K., Wang, X., Phillips, P. E. M., … Zhang, Y. (2022). Implantable Aptamer-Graphene Microtransistors for Real-Time Monitoring of Neurochemical Release in Vivo. *Nano Letters*, *22*(9), 3668–3677. https://doi.org/10.1021/acs.nanolett.2c00289

Wu, J., Liu, P., Chen, F., Ge, L., Lu, Y., & Li, A. (2020). Excitability of Neural Activity is Enhanced, but Neural Discrimination of Odors is Slightly Decreased, in the Olfactory Bulb of Fasted Mice. *Genes*, *11*(4), 433. https://doi.org/10.3390/genes11040433

Wu, Z., Lin, D., & Li, Y. (2022). Pushing the frontiers: Tools for monitoring neurotransmitters and neuromodulators. *Nature Reviews Neuroscience*, *23*(5), 257–274. https://doi.org/10.1038/s41583-022-00577-6

Yamamoto, K., Cubells, J. F., Gelernter, J., Benkelfat, C., Lalonde, P., Bloom, D., Lal, S., Labelle, A., Turecki, G., Rouleau, G. A., & Joober, R. (2003). Dopamine Beta-Hydroxylase (DBH) gene and schizophrenia phenotypic variability: A genetic association study. *American Journal of Medical Genetics Part B: Neuropsychiatric Genetics*, *117B*(1), 33–38. https://doi.org/10.1002/ajmg.b.10011

Yun, M., Hwang, J. Y., & Jung, M. W. (2023). Septotemporal variations in hippocampal value and outcome processing. *Cell Reports*, *42*(2). https://doi.org/10.1016/j.celrep.2023.112094

Zhao, C., Cheung, K. M., Huang, I.-W., Yang, H., Nakatsuka, N., Liu, W., Cao, Y., Man, T., Weiss, P. S., Monbouquette, H. G., & Andrews, A. M. (2021). Implantable aptamer-field-effect transistor neuroprobes for in vivo neurotransmitter monitoring. *Science Advances*, *7*(48), eabj7422. https://doi.org/10.1126/sciadv.abj7422

Zheng, J., Anderson, K. L., Leal, S. L., Shestyuk, A., Gulsen, G., Mnatsakanyan, L., Vadera, S., Hsu, F. P. K., Yassa, M. A., Knight, R. T., & Lin, J. J. (2017). Amygdala-hippocampal dynamics during salient information processing. *Nature Communications*, *8*(1), 14413. https://doi.org/10.1038/ncomms14413

Zheng, W., Wu, C., Du, W.-J., Li, Y., Shen, F., Haghparast, A., Liang, J., Sui, N., & Zhang, J.-J. (2022). Differential involvement of nucleus tractus solitarius projections and locus coeruleus projections to the basolateral amygdala in morphine-associated

memory destabilization. *Progress in Neuro-Psychopharmacology and Biological Psychiatry*, *115*, 110496. https://doi.org/10.1016/j.pnpbp.2021.110496

Zhong, J., Liu, Q., Yang, X., Su, J., Li, X., Luo, M., & Wang, L. (2023). Mice learn from the predator-attack experience to accelerate flight behavior via optimizing the strategy of environment exploration. *Biochemical and Biophysical Research Communications*, *665*, 26–34. https://doi.org/10.1016/j.bbrc.2023.04.060

Zhou, K., Xu, H., Lu, S., Jiang, S., Hou, G., Deng, X., He, M., & Zhu, Y. (2022). Reward and aversion processing by input-defined parallel nucleus accumbens circuits in mice. *Nature Communications*, *13*(1), 6244. https://doi.org/10.1038/s41467-022-33843-3

Zhou, T., Li, Y., Li, X., Zeng, F., Rao, Y., He, Y., Wang, Y., Liu, M., Li, D., Xu, Z., Zhou, X., Du, S., Niu, F., Peng, J., Mei, X., Ji, S.-J., Shu, Y., Lu, W., Guo, F., … Peng, B. (2022). Microglial debris is cleared by astrocytes via C4b-facilitated phagocytosis and degraded via RUBICON-dependent noncanonical autophagy in mice. *Nature Communications*, *13*, 6233. https://doi.org/10.1038/s41467-022-33932-3

Zhuo, Y., Luo, B., Yi, X., Dong, H., Miao, X., Wan, J., Williams, J. T., Campbell, M. G., Cai, R., Qian, T., Li, F., Weber, S. J., Wang, L., Li, B., Wei, Y., Li, G., Wang, H., Zheng, Y., Zhao, Y., … Li, Y. (2024). Improved green and red GRAB sensors for monitoring dopaminergic activity in vivo. *Nature Methods*, *21*(4), 680–691. https://doi.org/10.1038/s41592-023-02100-w